UNIVERSIDADE DA CORUÑA
GRUPO DE POLÍMEROS
DEPARTAMENTO DE FÍSICA

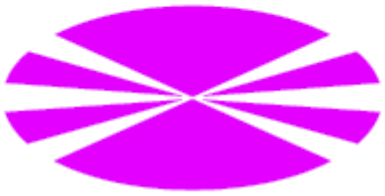

Supervisors:

Dra. Ana Isabel Ares Pernas, Dr. Senentxu Lanceros-Méndez and Dr. Ferrie Wander Joseph van Hattum

A study of the physical properties of carbon nanofiber reinforced polypropylene composites

Antonio J. Paleo Vieito

July 2012

UNIVERSIDADE DA CORUÑA

Dª. Ana Isabel Ares Pernas, Profesora Titular de Universidad en el área de Física Aplicada perteneciente al Departamento de Física de la Universidad de A Coruña.

D. Senentxu Lanceros Méndez, Profesor Asociado Doctor en Física perteneciente al departamento de Física de la Escuela de Ciencias de la Universidade do Minho, (Portugal).

y

D. Ferrie W. J. Van Hattum, Profesor Auxiliar Doctor en Ciencia e Ingeniería de Polímeros perteneciente al IPC – Instituto de Polímeros e Compósitos de la Universidade do Minho, (Portugal).

AUTORIZAN:

A D. Antonio J. Paleo Vieito a presentar la memoria titulada: "A study of the physical properties of carbon nanofiber reinforced polypropylene composites", que ha realizado bajo nuestra dirección para optar al grado de Doctor por la Universidad de A Coruña con Mención Internacional.

A Coruña, Julio de 2012

Fdo.: Dra. Ana I. Ares Pernas	**Fdo.: Dr. Senentxu Lanceros Méndez**	**Fdo.: Dr. Ferrie W.J. Van Hattum Instituto de Polímeros e Compósitos Universidade do Minho**
Departamento de Física	**Departamento de Física**	
Universidad de A Coruña	**Universidade do Minho**	

To my aunt Aurelia

Acknowledgments

First and most of all, I should like to thank all my supervisors. Prof. Ferrie van Hattum for offering me the possibility to work as a research holder at the University of Minho, UM (Portugal). I wish also to express my gratitude to him because of his open-mind and availability to share results and knowledge generated within the project with the Electroactive Smart Materials group led by Prof. Senentxu Lanceros-Mendez of the University of Minho, and with the Group of Polymers of the University of A Coruña, UDC (Spain). In this regard, I can firmly state that this thesis would not also be possible without this triple - collaboration. I wish to thank Prof. Senentxu for their relevant and continuous support and guidance. I cannot forget Prof. Gerardo Rocha for his important scientific contribution and last but not least I am indebted to my friend Prof. Ana Isabel Ares, this thesis would be no more than wishful thinking without her help, motivation and interest since the first moment.

I would like to sincerely thank all my colleagues and friends of Polymers and Physic Departments at the UM, Carla Leer, Eva Barroso, Jorge Silva and Marcin Bilewicz. They made my first months in Portugal were a very pleasant and like-home experience. I also want to thank very much Vitor Sencadas for his first-level scientific vision and friendship, Jaime Silva for his friendship and patient for answering all of my questions. I cannot forget all my colleagues of Physic Department, especially, I would like to thank Paulo Cardoso, Armando Ferreira, Marcos Silva and Pedro Costa for their friendship and fun times shared at Lab. I also want to thank very much João Paulo Gomes Peixoto, Carla Leer and Patrick Lake, Mauricio Malheiros and Natalia López for their important scientific, technical and collaborative assistance.

I am especially thankful to my family, my mom Hersi, dad Antonio, my brother Juan and my sister Ana and brother-in-law Chevi and their beautiful daughter Alba, without their loving care and understanding, I would not have been able to complete this work.

Table of Contents

List of Tables

Chapter 2 - Carbon nanofiber type and content dependence of the physical properties of carbon nanofiber reinforced polypropylene composites

Chapter 3 - Rheological and electrical analysis in carbon nanofibre reinforced polypropylene composites

Chapter 4 - Piezoresistive effect in polypropylene - carbon nanofiber composites obtained by shear extrusion

Chapter 5 - Piezoresistive polypropylene-carbon nanofiber composites as mechanical transducers

List of Figures

Chapter 1 - Introduction

Chapter 2 - Carbon nanofiber type and content dependence of the physical properties of carbon nanofiber reinforced polypropylene composites

Chapter 3 - Rheological and electrical analysis in carbon nanofibre reinforced polypropylene composites

Chapter 4 - Piezoresistive effect in polypropylene - carbon nanofiber composites obtained by shear extrusion

Chapter 5 - Piezoresistive polypropylene-carbon nanofiber composites as mechanical transducers

List of abbreviations

AC – Alternating current

AFM - Atomic force microscopy

AR – Aspect Ratio

CB - Carbon black

CNFs - Carbon nanofibers

CNTs - Carbon nanotubes

CPICs - Conducting particle-reinforced insulating matrix composites

CR - Coats-Redfern method

CSCNT - Cup-stacked carbon nanotubes

CVD - Chemical vapor deposition

DC- Direct current

DSC - Differential scanning calorimetry

DTGA - Derivative thermogravimetric analysis

Ea - Activation energy

EACs - Electroactive ceramics

EAPs - Electroactive polymers

ECPNs – Electrically conductive polymer nanocomposites

EM – Electron microscopy

EMI - Electromagnetic interference shielding

ESD - Electrostatic dissipative materials

GF – Gauge factor

GF_L – Gauge factor along longitudinal direction

GF_T - Gauge factor along transversal direction

GSA - Greyscale analysis

HIPS - High impact polystyrene

HRTEM - High resolution transmission electron microscopy

IVP – Initial value problem

LOM - Transmitted light optical microscopy

LVE - Linear viscoelastic region

MR – Magnetoresistance

MWCNT - Multi wall carbon nanotube

NGPs - Nanographene platelets

OM – Optical microscopy

PE – Polyethylene

PNCs - Polymer nanocomposites

PP – Polypropylene

PS – Polystyrene

RFI - Radio frequency interference

RPSD - Radial power spectral density

SEM - Scanning electron microscope

SMAs - Shape memory alloys

SSE - Single screw extruder

SWCNT - Single wall carbon nanotube

TEC - Thermal expansion coefficient

TEM - Transmission electron microscopy

TGA - Thermogravimetric analysis

TSE - Twin screw extruder

VGCFs - Vapor grown carbon fibers

VGCNFs - Vapor grown carbon nanofibers

List of symbols

A – Pre-exponential factor

C – Energy storage

cm^2 – Centimetre squared

d – Distance

$d_i(t)$ – Variable displacement

ΔH_m - Melting enthalpy

ΔH_o - Melting enthalpy of the 100 % crystalline polypropylene

$\Delta R/R$ – Resistance change

ΔX_c – Degree of crystallinity

e - Electron charge

ε – Mechanical strain

η^* - Complex viscosity

G – Conductance

G' - Storage modulus

G'' – Loss modulus

G'/G'' - Inverse of loss tangent

g/cm^3 – Grams per centimeter cubic

GPa – Giga Pascals

h - Planck constant

I - Electrical current densities

I-V - Current-voltage

$J\ g^{-1}$- Joules per grams

KJ/mol – Kilo joules per mole

MPa – Mega Pascals

mm – Milimeter

mm min^{-1} - Milimeters per minute

μA - Micro amperes

μm- Micro meter

N – Newton

nm – Nanometer

ν or t- Critical exponent

$^{o}\ C$ - Degrees Celsius

ω – Frequency

$\Omega\ cm$ – Ohms per centimetre

$\Omega\ m$ – Ohms per metre

Pa – Pascal

Φ – Concentration (filler)

Φ_c - Percolation threshold

R – Electrical resistance

R_1 – Fixed electrical resistance

R_2 – Variable electrical resistance

Rg - Radius of gyration

R or R^2 – Standard deviation

rad/s – Radians per second

ρ_V – Volume resistivity

σ - Electrical conductivity / Mechanical Stress

σ_0 - Polymer conductivity

S cm^{-1} - Siemens per centimetre

T_c – Crystallization temperature

$T_{initial}$ – Initial temperature

T_m – Melting temperature

T_{onset} – Onset temperature

vol % - Volume percentage

V_e - Average excluded volume

V(t) – Variable voltage

wt % - Weight percentage

z – Displacement

Resumo

Os polímeros termoplásticos son coñecidos, en xeral, pola súa ampla empregabilidade en extrusión e moldeamento, cunha gran variedade de aplicacións tales como a embalaxe, os téxtiles e os compoñentes para a industria do automóbil.

Unha tentativa de aumentar a súa aplicabilidade implica a incorporación de partículas nanométricas con propiedades eléctricas e mecánicas intrínsecas no interior da matriz termoplástica. Entre os diversos tipos de aditivos, as nanofibras de carbono, CNFs, demostran un potencial elevado debido ás súas características eléctricas e mecánicas, similares aos nanotubos de carbono, CNTs, pero cun custo asociado máis reducido. Estas características, relacionadas coa relativa facilidade de incorporación e dispersión en polímeros, aumentaron o interese nas CNFs como novos materiais capaces de achegaren solucións nalgunhas aplicacións innovadoras para os materiais compósitos.

As CNFs poden ser preparadas con diámetros de dimensións nanométricas e dan lugar a materiais cunha razón lonxitude/diámetro bastante elevada. Neste traballo foron utilizadas nanofibras Pyrograf [Applied Sciences Inc. (ASI), Ohio, EUA], procesadas por evaporación química de fase vapor, CVD, que revelan unha morfoloxía similar a unha serie de vasos amoreados.

Asociadas á súa elevada área superficial específica, as CNFs tenden a formar agregados que poderán reducir as propiedades dos nanocompósitos onde estas son inseridas, especialmente de non se producir a súa dispersión de maneira correcta e uniforme. O éxito para a aplicación das CNFs está estreitamente vinculado ao coñecemento do seu grao de dispersión nas propiedades finais dos nanocompósitos. Con base nesta premisa, realizouse un estudo intensivo en compósitos de CNTs e CNFs de base polimérica, motivado pola importancia da influencia dalgúns factores chave: morfoloxía, dispersión e distribución das nanofibras na matriz polimérica, interacción polímero-nanofibra e relación coas propiedades do posprocesamento.

Co fin de definir de forma clara e sistemática a relación entre o procesamento, a morfoloxía e as propiedades finais, é importante identificar inicialmente as vantaxes e desvantaxes da contribución de cada compoñente (CNFs, matriz polimérica e método de procesamento) nas propiedades eléctricas, térmicas e mecánicas.

Este estudo aséntase na introdución de diferentes tipos de nanofibras de carbono nunha matriz de polipropileno, PP, procesados nunha extrusora de duplo fuso. Esta técnica emprégase amplamente na industria de transformación de plásticos, o que permitirá un "scale-up" e a consecuente produción en masa que promoverá unha boa relación calidade/prezo destes materiais compósitos.

O principal obxectivo deste traballo ten que ver coa investigación e o control do efecto das diferentes estruturas intrínsecas das CNFs nas propiedades morfolóxicas, térmicas, mecánicas, eléctricas, reolóxicas e electromecánicas dos nanocompósitos de CNF/PP.

Inicialmente, catro tipos de CNFs (Pyrograf®-III VGCNF) foron sistematicamente incorporados na mesma matriz de polipropileno a través da extrusión de duplo fuso e mesturados so un efecto de corte relativamente elevado. Axiña ficou caracterizada a relación entre a morfoloxía e as propiedades térmicas, mecánicas e eléctricas. A morfoloxía foi analizada por microscopia electrónica de varrido, SEM, e a través dunha análise de escala de cincentos, GSA, con base en microscopia óptica de transmisión, LOM. As propiedades térmicas foron caracterizadas a través de ensaios de termogravimetría, TGA, e calorimetría diferencial de varrido, DSC. Como resultado desta caracterización, a evolución da morfoloxía e a distribución das CNFs na matriz polimérica foi correlacionada. Posteriormente, as propiedades reolóxicas e eléctricas dos nanocompósitos illantes e condutores foron estudadas e correlacionadas coa finalidade de avaliar a análise reolóxica como ferramenta útil que permita diferenciar comportamentos condutores dos non-condutores neste tipo de sistemas. Finalmente, a última parte deste estudo dedicouse á caracterización das propiedades electromecánicas destes compósitos para aplicacións como materiais transdutores.

Este estudo establece os contidos e as estruturas máis axeitadas das CNFs para as propiedades físicas desexadas dos nanocompósitos de polipropileno baseados nas nanofibras de carbono. En particular, os nanocompósitos procesados con CNFs con elevados contidos de grafito na parede exterior e con tratamentos térmicos a 1500 ºC posúen resposta eléctrica e exhiben uns baixos límites de percolación e uns requisitos próximos dos escudos de protección electromagnéticos e de radiofrecuencia, EMI/RFI. Por outra parte, os nanocompósitos procesados con CNFs, en que a camada exterior foi removida por efecto pirolítico, revelaron posuír un bo desempeño mecánico; porén, estes mostraron ser illantes eléctricos para a mesma cantidade de carga no interior da matriz de PP.

As análises termogravimétricas amosan un aumento da estabilidade térmica dos nanocompósitos poliméricos co aumento da concentración de CNF na matriz de PP. Os ensaios por DSC amosaron un incremento da estabilidade térmica dos nanocompósitos poliméricos co aumento da concentración de CNF na matriz de PP. O DSC sinalou un aumento do grao de cristalinidade coa inclusión de nanofibras de carbono, independente do tipo e concentración das CNF. O grao de dispersión avaliado mediante o uso de LOM e GSA amosou unha correlación entre a concentración de carga e a variancia, un parámetro que permite cuantificar a dispersión: canto máis elevada sexa a variancia, mellor será a dispersión dos aglomerados de CNF na matriz polimérica.

Detectouse unha diferenza nas propiedades viscoelásticas entre os nanocompósitos condutores e illantes. As propiedades reolóxicas permitiron establecer unha relación viscosidade–propiedades eléctricas dos compósitos.

Por outra banda, os nanocompósitos condutores de CNF/PP amosaron unha resposta piezorresistiva máis elevada e unha meirande variación da resistividade eléctrica na presenza dunha acción mecánica externa, para concentracións preto do límite de percolación eléctrico.

Finalmente, foi caracterizada a dependencia do factor de Gauge, GF, parámetro asociado á resposta piezorresistiva, en función da deformación mecánica e da velocidade de deformación. Neste sentido, ficou demostrado que os nanocompósitos condutores obtidos no ámbito deste estudo poderán ser utilizados como sensores.

Resumen

Los polímeros termoplásticos se conocen, en general, por su amplio uso en extrusión y moldeo, con una gran variedad de aplicaciones tales como envasado, textiles y componentes para la industria automovilística.

Un intento de ampliar su rango de aplicación consiste en incorporar partículas nanométricas con propiedades eléctricas y mecánicas intrínsecas, en el interior de la matriz termoplástica. Entre los diversos tipos de cargas, las nanofibras de carbono, CNFs, demuestran un elevado potencial debido a sus propiedades eléctricas y mecánicas similares a los nanotubos de carbono, CNTs, pero a un menor coste. Estas propiedades, junto con la facilidad que presentan para ser incorporadas y dispersas en los polímeros, han aumentado el interés de las CNFs como nuevos materiales capaces de ofrecer soluciones a algunas aplicaciones innovadoras en el ámbito de los materiales compuestos.

Las CNFs se pueden producir con diámetros con dimensiones nanométricas, dando lugar a materiales con una razón de longitud/diámetro bastante elevada. En este trabajo se han empleado nanofibras Pyrograf®-III [Applied Sciences Inc. (ASI), Ohio, EUA], procesadas por deposición química de vapor, CVD, y que muestran una morfología parecida a la de vasos apilados.

Debido a su elevada área superficial específica, las CNFs tienden a formar agregados que pueden reducir las propiedades de los nanocompuestos en los que se encuentran, especialmente si la dispersión de las mismas no se produce de forma correcta y uniforme. El éxito para la aplicación de las CNFs depende de modo muy directo del conocimiento de los niveles de dispersión de las mismas en las propiedades finales de los nanocompuestos. Teniendo en cuenta este hecho, se ha producido un estudio intensivo de compuestos de base polimérica con CNTs y CNFs, motivado por la importancia de la influencia de algunos factores clave: morfología, dispersión y distribución de las nanofibras en la matriz polimérica, interacción polímero con nanofibra y relación con las propiedades del post-procesado.

Con el objetivo de definir de modo claro y sistemático la relación entre procesado, morfología y propiedades finales, es importante identificar primero las ventajas y desventajas

de la contribución de cada componente: CNFs, matriz polimérica y el método de procesado, en las propiedades eléctricas, térmicas y mecánicas.

Este estudio muestra la introducción de diferentes tipos de nanofibras de carbono en una matriz de polipropileno, PP, procesadas en una extrusora doble husillo. Esta técnica es muy empleada en la industria de transformación de plásticos, lo que permitirá una producción a gran escala, proporcionando así una buena relación entre calidad / precio para este tipo de materiales compuestos.

El principal objetivo de este trabajo se centra en la investigación y control del efecto de las diferentes estructuras intrínsecas de las CNFs en las propiedades morfológicas, térmicas, mecánicas, eléctricas, reológicas y electromecánicas de los nanocompuestos de CNFs / PP.

Inicialmente, cuatro tipos de CNFs (Pyrograf®-III VGCNFs) fueron sistemáticamente incorporados en la misma matriz de polipropileno a través de extrusión doble husillo y mezclados a tasas de corte relativamente elevadas. A continuación, se caracterizó la relación entre morfología, y las propiedades térmicas, mecánicas y eléctricas fue caracterizada. La morfología fue analizada por microscopía electrónica de barrido, SEM, y a través de un análisis de la escala de grises, GSA, con base en microscopía óptica de transmisión, LOM. Las propiedades térmicas fueron caracterizadas a través de ensayos termogravimétricos, TGA y de calorimetría diferencial de barrido, DSC. Como resultado de esta caracterización, se correlacionó la evolución de la morfología y la distribución de las CNFs en la matriz polimérica. Posteriormente, se estudiaron y correlacionaron las propiedades reológicas y eléctricas de los nanocompuestos aislantes y conductores con el objetivo de evaluar el análisis reológico como herramienta útil que permita diferenciar comportamientos conductores de aislantes en este tipo de sistemas. Por último, la parte final de este estudio está dedicada a la caracterización de las propiedades electromecánicas de estos compuestos para aplicaciones como materiales transductores.

Este estudio establece los contenidos y las estructuras más adecuadas de las CNFs para las propiedades físicas deseadas en nanocompuestos de polipropileno basados en nanofibras de carbono. En particular, los nanocompuestos procesados con CNFs con elevados contenidos de grafito en la pared externa y con tratamientos térmicos de 1500 ºC demuestran tener

respuesta eléctrica, mostrando bajos límites de percolación y requisitos próximos a los requeridos por los escudos de protección electromagnética y de radio-frecuencia (EMI / RFI). Por otro lado, los nanocompuestos procesados con las CNFs en las que la pared exterior fue retirada por efecto pirolítico, mostraron poseer un buen comportamiento mecánico, aunque al mismo tiempo demostraron ser aislantes eléctricos, para la misma cantidad de carga en el interior de la matriz de PP.

Los análisis termogravimétricos muestran un aumento de la estabilidad térmica de los nanocompuestos poliméricos con el aumento de la concentración de CNFs en la matriz de PP. El análisis por DSC ha mostrado un aumento del grado de cristalinidad con la introducción de las nanofibras de carbono, independientemente del tipo y concentración de CNFs. El grado de dispersión evaluado mediante el uso de LOM y GSA demostró la existencia de una correlación entre la concentración de la carga y la varianza, un parámetro que permite cuantificar la dispersión: cuanto más elevada es la varianza, mejor resultará la dispersión de los aglomerados de CNFs en la matriz polimérica.

Se ha detectado una diferencia considerable en las propiedades viscoelásticas entre los nanocompuestos conductores y aislantes. Así mismo las propiedades reológicas permitieron establecer una relación entre la viscosidad y las propiedades eléctricas de los compuestos.

Por otro lado, los nanocompuestos conductores de CNFs / PP han mostrado una respuesta piezoresistiva más elevada y por tanto una mayor variación de la resistividad eléctrica en presencia de una acción mecánica externa, a concentraciones próximas al del límite de percolación eléctrica.

Por último, se caracterizó la dependencia del factor de Gauge, GF, parámetro asociado con la respuesta piezoresistiva, en función de la deformación mecánica y de la velocidad de deformación, fue caracterizada. De este modo, queda demostrado que los nanocompuestos conductores obtenidos en el ámbito de este estudio, pueden ser utilizados como futuros sensores.

Abstract

Thermoplastic polymers are known, in general, for their broad use in the melt extrusion and moulding plastic industry with a large variety of applications such as packaging, textiles and automotive components.

One attempt to increase their application range is to incorporate into them, nanoscale fillers with intrinsically high electrical and mechanical performance. Among nanoscale modifiers, carbon nanofibers, CNFs are very suitable due to show similar mechanical and electrochemical properties compared to the carbon nanotubes, CNTs, but at a lower cost. These facts, together to the relatively easier incorporation and dispersion into polymers also raised the interest in CNFs as adequate new materials to provide solutions to some challenges in composite applications.

CNFs can be prepared with diameters in the nanometer scale, resulting in high aspect ratios, AR. Pyrograf®-III nanofibers [Applied Sciences Inc. (ASI), Ohio, USA], used in this study in particular, are a sort of vapor-grown carbon nanofibers, VGCNFs, fabricated by chemical vapor deposition, CVD, with stacked-cup morphology.

Associated with their large surface area, CNFs tend to come in aggregated structures which may negatively affect the composites properties if not dispersed correctly. Success strongly depends on knowing the influence of degree of dispersion of CNFs in the final properties. In this regard, an intensive research in CNTs and CNFs based polymer composites has been motivated by the importance of several key-factors: morphology, dispersion and distribution of nanofillers in the host polymer, polymer-nanofiller interactions and finding out processing-structure-final properties relationships.

In order to define clear and systematic relationships between processing, final structure and final properties, is important to identify first the advantages and disadvantages that each kind of CNFs, polymer and processing method may contribute to the final electrical, thermal and mechanical performance.

This study introduces different carbon nanofiber-based polypropylene, PP, nanocomposites processed by twin-screw extrusion, a common-use industrial technique which allows a large-scale production and provides a good relation between quality and cost of the composite materials.

The main focus is to investigate and tailor, if possible, the effect of the content and the different intrinsic CNFs´ structures on morphology and thermal, mechanical, electrical, rheological and electro-mechanical performance of the final nanocomposites.

First, four different Pyrograf®-III VGCNFs were systematically incorporated in the same polypropylene matrix by twin-screw extrusion under relatively high shear mixing conditions. Then, the relations between morphology, thermal and mechanical and electrical analysis were studied. Morphology was analyzed by scanning electron microscopy, SEM, and by statistical greyscale analysis, GSA, based on transmitted light optical microscopy, LOM. Thermal properties were characterized by thermogravimetric analysis, TGA, and differential scanning calorimetry, DSC. As a result of this first approach, the morphology together with distribution in the polymer was evaluated. After, rheological and electrical properties in electrical and non-electrical conducting composites were evaluated and correlated with the aim of examining if rheological analysis, besides being a method to assess processing performance, allows distinguishing electrical conducting from electrical isolating response in this kind of systems. The last part of this study was dedicated to investigate the electromechanical performance of these composites as piezoresistive transductors.

This study establishes that the desired physical properties of carbon nanofiber based-polypropylene nanocomposites fabricated by shear extrusion can be tailored when the adequate CNFs structure and content are chosen. In particular, nanocomposites fabricated with CNFs with highly graphitic outer wall layer and with heat treatments of 1500 ºC revealed to have electrical response, exhibiting low thresholds and values close to meet the electromagnetic / radio-frequency interference (EMI / RFI) shielding requirements. On the other hand, nanocomposites fabricated with CNFs with pyrolitical stripped outer layer showed good mechanical performance, but they revealed non-electrical conducting response at the same contents of CNFs.

Thermogravimetric analysis showed shift to higher temperatures of the main thermal degradation of the polymer with the addition of CNFs. DSC indicated a strong enhancement of the degree of crystallinity with the inclusion of the filler, independently on the filler content and type. The degree of dispersion evaluated using LOM and GSA shows a correlation between the filler concentration and the variance, a parameter which measures quantitatively the dispersion: the lower the variance, the better the cluster´s dispersion, for all composites.

Besides, it was also observed a large difference in viscoelastic properties between electrical conducting and isolating composites. In this regard, rheological analysis demonstrated to establish direct viscoelastic – electrical properties relationships.

On the other hand, the electrical conducting CNFs / PP composites showed to have better piezoresistive performance or variation of the electrical resistivity in the presence of external deformations at concentrations close to the electrical thresholds.

Finally, the dependence of Gauge Factor, GF, parameter associated with piezoresistive response, as a function of the deformation and velocity of deformation was calculated. In this way, it was demonstrated that the electrical conducting composites obtained in this study can also be used as self-sensing materials.

Resumo

Os polímeros termoplásticos são conhecidos, em geral, pela sua ampla empregabilidade em extrusão e moldação, com uma grande variedade de aplicações tais como embalagem, têxteis e componentes para a indústria automóvel.

Uma tentativa de aumentar a sua aplicabilidade envolve a incorporação de partículas nanométricas com propriedades eléctricas e mecânicas intrínsecas, no interior da matriz termoplástica. Entre os diversos tipos de aditivos, as nanofibras de carbono, CNFs, demonstram um potencial elevado devido às suas características eléctricas e mecânicas, similares aos nanotubos de carbono, CNTs, mas com um custo associado mais reduzido. Estas características, associadas à relativa facilidade de incorporação e dispersão em polímeros, aumentaram o interesse nas CNFs como novos materiais capazes de promover soluções em algumas aplicações inovadoras para os materiais compósitos.

As CNFs podem ser preparadas com diâmetros com dimensões nanométricas, resultando em materiais com uma razão comprimento/diâmetro bastante elevada. Neste trabalho foram utilizadas nanofibras Pyrograf®-III [Applied Sciences Inc. (ASI), Ohio, EUA], processadas por evaporação química de fase vapor, CVD, revelando uma morfologia similar a um serie de copos empilhados.

Associados à sua elevada área superficial especifica, as CNFs tendem a formar agregados que poderão reduzir as propriedades dos nanocompósitos onde estas são inseridas, especialmente se a dispersão das mesmas não ocorrer correcta e uniformemente. O sucesso para a aplicação das CNFs está fortemente dependente do conhecimento do grau de dispersão das mesmas nas propriedades finais dos nanocompósitos. Tendo por base esta premissa, um estudo intensivo em compósitos de CNTs e CNFs de base polimérica tem sido realizado, motivado pela importância da influência de alguns factores chave: morfologia, dispersão e distribuição das nanofibras na matriz polimérica, interacção polímero-nanofibra e relação com as propriedades pós-processamento.

Com o intuito de definir de forma clara e sistemática a relação entre o processamento, morfologia e propriedades finais, é importante identificar inicialmente as vantagens e as desvantagens da contribuição de cada componente: CNFs, matriz polimérica e o método de processamento, nas propriedades eléctricas, térmicas e mecânicas.

Este estudo reporta a introdução de diferentes tipos de nanofibras de carbono numa matriz de polipropileno (PP), processados numa extrusora de duplo fuso. Esta técnica é amplamente utilizada na indústria de transformação de plásticos, o que permitirá um "scale-up" e consequente produção em massa, promovendo uma boa relação entre a qualidade/preço destes materiais compósitos.

O principal objectivo deste trabalho prende-se com a investigação e controlo do efeito das diferentes estruturas intrínsecas dos CNFs nas propriedades morfológicas, térmicas, mecânicas, eléctricas, reológicas e electromecânicas dos nanocompósitos de CNFs/PP.

Inicialmente, quatro tipos de CNFs (Pyrograf®-III VGCNFs) foram sistematicamente incorporados na mesma matriz de polipropileno através da extrusão de duplo fuso e misturados sob um efeito de corte relativamente elevado. Em seguida, a relação entre a morfologia, e as propriedades térmicas, mecânicas e eléctricas foi caracterizada. A morfologia foi analisada por microscopia electrónica de varrimento, SEM e através de uma análise de escala de cinzentos, GSA, com recurso à microscopia óptica de transmissão, LOM. As propriedades térmicas foram caracterizadas através de ensaios de termogravimetria, TGA, e calorimetria diferencial de varrimento, DSC. Como resultado desta caracterização, a evolução da morfologia e a distribuição das CNFs na matriz polimérica foram correlacionadas. Posteriormente, as propriedades reológicas e eléctricas dos nanocompósitos isoladores e condutores foram estudadas e correlacionadas com o intuito de avaliar a analise reológica como ferramenta útil que permita diferenciar comportamentos condutores de isoladores neste tipo de sistemas. Finalmente, a última parte deste estudo foi dedicada à caracterização das propriedades electromecânicas destes compósitos para aplicações como materiais transdutores.

Este estudo estabelece os conteúdos e as estruturas mais adequadas das CNFs para as propriedades físicas desejadas dos nanocompósitos de polipropileno baseados nas nanofibras de carbono. Em particular, os nanocompósitos processados com CNFs com elevados conteúdos de grafite na parede exterior e com tratamentos térmicos a 1500 ºC possuem resposta eléctrica, exibindo baixos limites de percolação e requisitos próximos dos escudos de protecção electromagnéticos e de rádio-frequência (EMI / RFI). Por outro lado, os nanocompósitos processados com CNFs em que a camada exterior foi removida por efeito pirolítico, revelaram possuir bom desempenho mecânico, contudo estes mostraram ser isoladores eléctricos, para a mesma quantidade de carga no interior da matriz de PP.

As análises de termogravimetria mostraram um incremento da estabilidade térmica dos nanocompósitos poliméricos com o aumento da concentração de CNFs na matriz de PP. O DSC indicou um aumento do grau de cristalinidade com a inclusão de nanofibras de carbono, independente do tipo e concentração das CNFs. O grau de dispersão avaliado mediante o uso de LOM e GSA mostrou uma correlação entre a concentração de carga e a variância, um parâmetro que permite quantificar a dispersão: quanto mais elevada seja a variância, melhor será a dispersão dos aglomerados de CNFs na matriz polimérica.

Uma diferencia nas propriedades viscoelásticas entre os nanocompósitos condutores e isoladores foi detectada. As propriedades reológicas permitiram estabelecer uma relação viscosidade – propriedades eléctricas dos compósitos.

Por outro lado, os nanocompósitos condutores de CNFs/PP mostraram uma resposta piezoresistive mais elevada e uma maior variação da resistividade eléctrica na presença de uma acção mecânica externa, para concentrações perto do limite de percolação eléctrico.

Finalmente, a dependência do factor de Gauge, GF, parâmetro associado à resposta piezoresistiva, em função da deformação mecânica e da velocidade de deformação, foi caracterizada. Neste sentido, foi demonstrado que os nanocompósitos condutores obtidos no âmbito deste estudo, poderão ser perfeitamente utilizados como futuros sensores.

Chapter 1 - Introduction

1.1 Carbon-based polymer nanocomposites

1.1.1 Interest

Polymers are versatile materials with unique properties such as low density, proper strength, flexibility, ease of processing, etc. However, by the fact that their intrinsic properties are insufficient to address a wide range of applications, processing of polymers with all kind of additives and/or fillers, has been one of the most common methods to improve their intrinsic properties. In this way, many studies have dealt with the incorporation of different fillers in polymers: silicates such as mica, talcum, clays, precipitated silica or glass, metal oxides (titanium, aluminium or magnesium) or others such as calcium carbonate and carbon black, to mention just a few.

Polymer nanocomposites, PNCs, can be defined as a class of composites constituted by several components in which some of them have at least one dimension (length, width, thickness) in the nanometric range [1].

In PNCs, above certain concentrations, distance among nanoparticles may be of the order of radius of gyration, Rg, from polymer itself or in other words, in the range of size of polymeric chains, in such a way that properties such as curing reaction, (thermoset polymers), crystallinity and polymeric chains´ mobility might be completely affected [2]. This is just an example to assess that, in principle; these materials have different properties and need different processing conditions when compared to the traditional composites.

There are several ways to classify nanocomposites, one of them is by mean of the nanoparticle shapes employed: spherical (carbon black, silicates), laminates (clays) or fibrous.

Among the various types of PNCs, one of the systems that aroused most interest is the consisting of polymers and carbon fibrous nanostructures: carbon nanofibers and carbon nanotubes, CNFs and CNTs, respectively.

These two types of carbon structures possess remarkable intrinsic properties such as high strength, high thermal and electrical conductivity and low chemical reactivity [3-5], which once they are appropriately incorporated to the polymer may produce composites suitable for

applications as diverse as lightweight structures, electromagnetic interference shielding, EMI, sporting goods, automotive components, electrostatic paint, electronic components for heating dissipation and multifunctional materials for high structural performance, just to mention a few [6].

1.1.2 Properties

The incorporation of CNFs and CNTs in polymer matrixes results therefore in new multifunctional composite materials with significant improvement of mechanical properties and new thermal and electric properties. Some of the main responsible factors for the final resulting composites behaviors are the processing methods, the intrinsic nature of CNFs and CNTs and their consequent Aspect Ratio, AR, (or length / diameter ratio), the particular kind of polymer, the weight or volume fraction of CNTs / CNFs and fibers´ dispersion in the polymer [7,8]. In general, the choice of a certain type of processing method may be beneficial for a particular property but it may not be the most appropriate for another one. For instance, some process methods such as surface functionalization or modification by chemical means in CNTs / CNFs to improve compatibility with matrix, generally increase mechanical properties but it may be worse the electrical properties [9].

Mechanical Properties

The use of low contents of CNFs or CNTs as structural reinforcement with the aim of gain significant increases in tensile modulus and tensile strength has focused the major part of research. Though a brief state-of-art is presented later, overall it is possible to assert that all the expected results that intrinsic properties of CNFs / CNTs point out has not yielded yet.

Due to the fact that mechanical transferring loads across the CNF / CNT – matrix interface play a key role in the mechanical properties of nanocomposites, it is fundamental that a proper interaction polymer with CNF or CNT exists [10]. Several studies suggest that interfacial interactions with nanotubes result in an interfacial region of polymer with morphology and properties different to the bulk [11]. The nature of this interface and its role in the final mechanical properties is a topic of discussion up to now.

Although the length scales of reinforcements in polymer nanocomposites are smaller than those of traditional composites, there are some known mechanisms of energy dissipation in these last ones which can be taken into account as starting research points for the first ones: fiber fracture, fiber pullout, debonding / crack bridging and matrix cracking [12].

In general, it can be said that good mechanical performance depends mainly on two variables. First, there should be a high degree of load transfer between the matrix and the nanotubes or nanofibers in order to avoid local stress concentrations. Second, the nanotubes / nanofibers should be well dispersed; otherwise CNFs / CNTs will fail by separation of the bundle rather than by failure of the nanofiber / nanotube itself [13, 14]. In this regard, intensive research has focused on improving interfacial bonding by means of surface treatment or functionalization without creating defects in CNTs / CNFs which can compromise their intrinsic properties [15].

Electrical properties

Besides their unique mechanical properties, CNFs and CNTs exhibit also high electrical conductivity, σ. Values in the range of metals between 10^7 to 10^8 S/m have been estimated, for CNTs [16, 17], whereas for CNFs, several studies have reported values of 10^5 S/m [5].

The variation in electrical properties in PNCs is usually understood under the framework of statistical percolation theory [18-20]. The application of the percolation theory to study the conductive behavior of PNCs is based on some important assumptions and concepts. One of these concepts is the percolation threshold, Φ_c, defined as the critical concentration at which an infinite cluster emerges in an infinite lattice. When $\Phi > \Phi_c$ a cluster spreads throughout the system, whereas for $\Phi < \Phi_c$ the system is made of many isolated and disconnected clusters. The maximum size of these clusters is denominated as the correlation length of the system. The way that this length tends to infinite as a function of Φ in the vicinity of percolation thresholds obeys a typical power-law $|\Phi - \Phi_C|^{-\nu}$ in which ν is the critical exponent, assumed as universal because of only depends on system´s dimensions.

For the particular case of PNCs reinforced with CNFs / CNTs, the percolation threshold is calculated representing electrical conductivity as function of volume fraction or weight content, and depends on several factors such as AR, dispersion / distribution, intrinsic

electrical conductivity of CNFs / CNTs and principal properties of polymer such as crystallinity, surface tension and molecular weight [21, 22].

Furthermore, composites with different conductivity levels can be produced and tailored with controlling the volume fraction or weight content of CNFs / CNTs [23, 24].

Thermal properties

As important as electrical and mechanical properties, thermal properties must be taken into consideration in order to choose the best processing conditions and application area. PNCs reinforced with nanofibers or nanotubes can be used as dissipative devices due to the negative value of thermal expansion coefficient, TEC. High values of thermal conductivity of 1950 W/mK have been reported for CNFs [25]. Properties such as AR, orientation and dispersion, and thermal resistance between polymer interface and CNFs will influence the final performance [26-28].

Overall, thermal conductivity increases with increasing content of nanofibers, though without experimenting percolation thresholds as it happens with electrical behaviors [29, 30].

1.1.3 Applications

An important application of these materials lies in the effective use of their electrical conductivities for protection against electromagnetic interference, EMI, and as electrostatic dissipative materials, ESD, [23, 31]. Their final application will be determined as a function of their electrical conducting levels. For instance, for EMI applications, the composites must attach surface resistivity levels of ~ 10 Ω/sq, whereas for ESD applications, the surface resistivities must be in the range from 10^6 to 10^9 Ω/sq.

Furthermore, PNCs reinforced with CNTs or CNFs may be used in the automotive area for specifically applications such as painted electrostatic pieces, innovative braking systems, engine components, etc.

In addition, these composites are promising materials for using as batteries, available both as electrodes and as catalyst support [4]. For this kind of applications, these composites offer clear advantages over different materials, such as metal oxides and sulphites, in terms of cost, thermal and chemical stability, ease of processing and lower environmental impact.

Polymer based on CNTs or CNFs may be also candidates in other applications such as drug-carrier delivers by incorporating biological structures such as proteins and ADN in the core hollow of CNTs and CNFs [32].

Finally, these materials are also expected to replace traditional composites based on carbon black or conventional carbon fibers by exploiting their lower bulk densities.

1.1.4 Processing

Three methods are commonly used to incorporate nanotubes or nanofibers into a polymer: solution mixing, in situ polymerization, and mixing in molten polymers. Melt mixing is the industrially preferred method in many cases because of its environmentally benign character, its versatility, and its compatibility with current polymer processing techniques [33, 34].

Melt mixing processing

From an industrial point of view, melt mixing represents a good option due to its low-cost and large-scale implementation. In general, melt processing involves the melting of polymer pellets to form a viscous liquid. Any additives, such as nanotubes and nanofibers can be mixed into the melt by shear mixing in single screw extruder, SSE, or, twin screw extruder, TSE, and also by internal mixing. Bulk samples can then be fabricated by techniques such as compression molding, injection molding or extrusion [14, 34, 35].

In particular, twin screw extruders can have conical or parallel design. The two screws can be counter-rotating or co-rotating, intermeshing or non-intermeshing. Also, the screws´ configurations can be varied using different conveying and mixing elements. For instance, the co-rotating twin-screw extrusion is commonly used in compounding materials for which thorough mixing is important. Co-rotating twin-screw extruders may have modular configurations which make this kind of processing technique suitable for CNTs and CNFs melt compounding.

In internal mixing, which commonly uses equipment made by HAAKE (Thermo-scientific, Germany) and Brabender (C. W. Brabender instruments, EEUU), the mixing is produced in a seal chamber with two rotors of different geometry inside [36]. A particular version is the chaotic mixing, which applies low shear stress by means of two cylindrical rotors [37].

Solution Mixing processing

Solution mixing is other common method for preparing polymer nanocomposites. In this technique, CNTs or CNFs are mixing in a suitable solvent before evaporating the solvent to form a composite film. The process has three broad steps: dispersion of CNTs or CNFs in a solvent or in a polymer solution, mixing of CNTs or CNFs with the host polymer in solution and controlled evaporation of solvent resulting in the final film [38].

Some of the disadvantages of this technique are: pristine CNTs and/or CNFs cannot be well-dispersed in most of the solvents, the solvents are not compatibles with most of the polymers and the step towards large-scale production is more complicated. Nevertheless, the lowest electrical thresholds have been obtained by using this method [39].

In situ polymerization processing

This technique is particularly important for the preparation of insoluble and thermally unstable polymers, which cannot be processed by solution or melt processing. More particularly, polymerization allows grafting of polymer macromolecules onto the walls of carbon nanotubes, maintaining AR and getting good dispersion levels and bounding (covalent or not) between CNFs and host polymer [38].

1.2 Carbon nanofibers and carbon nanotubes

Even though CNTs and CNFs have important likenesses, they have also different characteristics. Before 1985 carbon was known in only two allotropic forms: diamond and graphite. Diamond is a tri-dimensional material with isotropic properties, whereas graphite is a bi-dimensional material. More recently, zero dimensional carbon structures such as fullerenes and one dimensional carbon structures such as CNTs and CNFs were developed [40].

CNTs can be described as long cylinders of covalently bonded carbon atoms. There are two main types of CNTs: single wall carbon nanotube, SWCNT, which can be considered as a single graphene (a monolayer of sp^2-bonded carbon atoms) sheet rolled into a seamless cylinder, and multi wall carbon nanotube, MWCNT, consist of nested graphene cylinders coaxially arranged around a central hollow core. SWCNTs have diameters in the range of nanometers, whereas MWCNTs have diameters in the range of tens of nanometers [41, 42].

Carbon nanofibers, CNFs, which comprise graphitic networks in concentric cylinders, are mainly differentiated from nanotubes by the orientation of the graphene planes, whereas for nanotubes these layers are parallel to the axis, nanofibers can show a wide range of angles of the graphitic layers with respect to the fibre axis. They are also intrinsically less perfect due to the amorphous carbon terminations on their surface [43, 44]. Their total diameter is normally in the range of hundreds of nanometer, for this reason they can be named as submicron fibers in literature.

In order to see their differences and similarities the synthesis, morphology and main properties of them are discussed in the lower sections.

1.2.1 Synthesis

Even though a wide variety of methods exist in order to produce CNTs and CNFs [45-47], chemical vapor deposition, CVD, is one of the most common technologies due to its simplicity, high output, low-cost and ease of large scale implementation. In this method, vapor grown carbon fibers, VGCFs, are manufactured by using small metal particles, almost always containing iron, nickel, or cobalt which are exposed to CO or hydrocarbon gases at temperatures between 500 and 1200 ºC. When the catalyst particles are properly dispersed and activated with sulfur, carbon filaments are abundantly produced in a reactor with a diameter similar to the metal particle [45-51].

Other techniques for producing CNTs and CNFs have been developed, for instance, nanotubes were observed in 1991 in the carbon soot of graphite electrodes during an Arc discharge. In this process, the carbon contained in the negative electrode sublimates because of the high-discharge temperatures. In the laser ablation process, a pulsed laser vaporizes a graphite target in a high-temperature reactor while an inert gas is bled into the chamber. When the vaporized carbon condenses, the nanotubes develop on the cooler surfaces of the reactor [52-54].

More in particular, the CNFs used in this work, Pyrograf III ^{TM} by Applied Sciences, Inc, [55] have been produced by CVD and implemented through a process which uses natural gas as the primary feedstock, while the catalytic iron particles are produced by the decomposition of Fe $(CO)_5$. When the catalyst particles are properly dispersed and activated with sulfur, carbon fibers are produced in a reactor maintained near 1100 ºC [56, 57].

1.2.2 Morphology

As it has been noted, single wall carbon nanotubes, SWCNTs, may be considered as bi-dimensional single graphene walls rolled into seamless cylinders. They can be metallic or semiconducting, depending on the diameter and the various ways of rolling graphene into tubes described by their tube chirality (or helicity or wrapping), which describes the carbon´s orientation in the wall [58]. MWCNTs, on their hand, contain a variety of chyralities, so their physical properties are more complicated to predict.

The main difference between CNTs and CNFs is the orientation of graphene´s walls relative to their axis [59]. Depending on this particular orientation, the internal structures vary, forming different structures such as bamboo-like, truncated cones or cup-stacked, to name a few [60]. These structures have a chemically active surface area which is important for their functionalization [61].

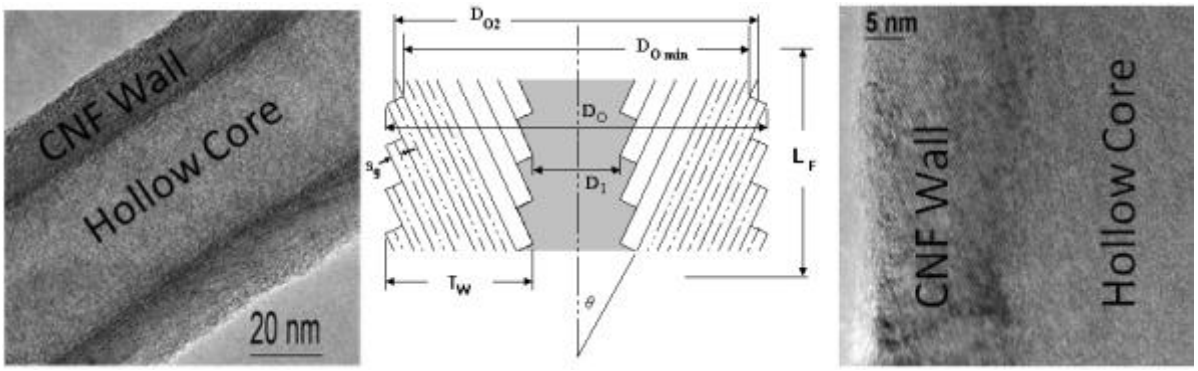

Figure 1. 1 – High resolution transmission electron microscopy, HRTEM, Micrograph of nanofiber PR-25. Center and right images show in further detail internal and external frontiers in a typical cup-stacked carbon nanofiber [62, 63].

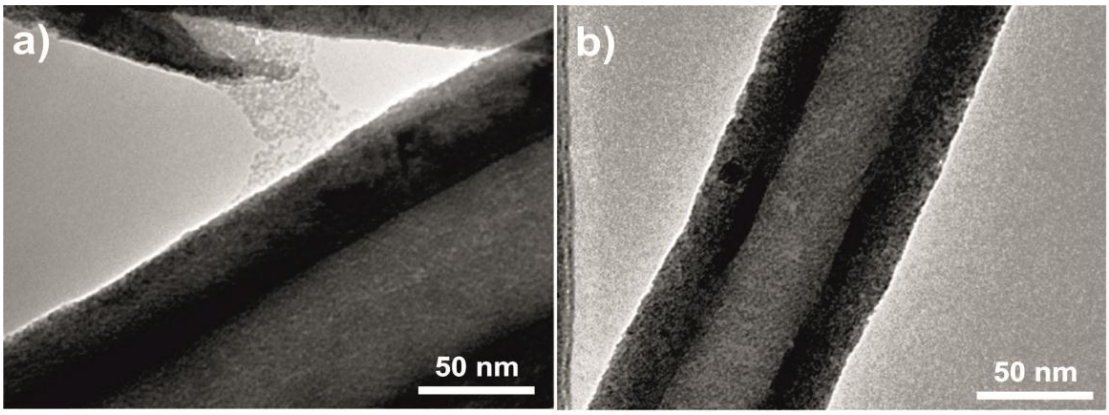

Figure 1. 2 – Transmission electron microscopy,TEM, micrograph of PR-19-LHT-XT (left) and PR-25-PS-XT (right).

Overall, fibers used in this study have diameters from 80 to 120 nm, with lengths between 125 to 200 μm. More in particular, three different grades PR-19, PR-24 and PR-25 (Figure 1.1 and 1.2) with different intrinsic nature in diameters and outer wall properties were used. Further details about the carbon nanofibers used, are described in the particular chapters of this thesis.

1.2.3 Properties

As it has already been indicated before, polymer composites based on carbon nanostructures show a variety of significantly relevant properties: high tensile strength, high thermal and electrical conductivity and good chemical stability, to name a few [43]. Recently, some studies have reported nanoparticles and inorganic nanofilaments incorporated into their hollows cores [64, 65]. The CNTs or CNFs´ surfaces can be functionalized to improve dispersion in polymers and solvents, or, for instance for creating links with organic molecules to act as transportation containers that could deliver active drug ingredients [66]. CNFs with larger diameters than CNTs are easier for dispersion [67], furthermore CNFs with cup-stacked structure have high chemical reactivity ideal for functionalization [68]. In the following sections these three main properties are discussed with further detail.

Mechanical Properties

The structural properties in CNTs with strong covalent bonds C-C show high Young´s modulus and tensile strength. CNTs have also good elastic performance because of 2D graphene walls allowing high distortions. Experimental and theoretical studies show, in

MWCNTs, Young´s modulus values of approximately 1 TPa and tensile strengths of 10-200 GPa [69], which means several hundred times higher and six times lighter than steel. From an elastic point of view, CNTs show deformations up to 15 % from their original size before fracture, showing high flexibility and reversible bending without rupture up to 110º [70].

More in particular, values of 2.9 to 180 GPa in modulus and 2.35 to 245 GPa in tensile strength for different types of Pyrograf III CNFs have been reported in recent studies [71].

Electrical Properties

From an electrical point of view, CNTs can be metallic or semiconductor, depending on their chirality. Some studies estimates the theoretical conductance, G, (resistance´s reverse) of SWCNTs with a value of $2G_0$, independently from their diameter and length, where $G_0 = (2e^2/h) = (12.9\ k\Omega)^{-1}$ with e, electron charge, and h, Planck constant, [72]. The temperature and magnetic fields also influence the nanotubes electrical resistance. Values of electrical resistivity of 10^{-4} Ω cm at temperatures of 300 K have been reported [73]. Additionally, CNTs can transport high electrical current densities, I, in the range of 10^9 A/cm^2 [74].

In the case of CNFs, the outer layers of amorphous carbon and outer impurities affect their electrical properties. According to this and with the aim of improve their crystallinity and counteract these impurities a thermal treatment and functionalization is recommended for the required application [75, 76].

Different studies have showed electrical conducting values in the range from 10^{-3} to10^{-4} Ω cm for CNFs [4].

Other properties

CNFs have thermal conductivity values of 1950 W/ (m K) [25]. In the MWCNTs´ case, experimental values of approximately 3000 W/ (m K) have been published [77].

Other kind of studies assesses the transport properties as a function of CNTs´ spin, effect known as magnetoresistance, MR**,** [78].

Studies developed by atomic force microscopy, AFM**,** in metallic carbon nanotubes, show that their conductance diminishes several orders of magnitude under deformation, phenomenon known as piezoresistance [79]. In semiconductor carbon nanotubes, the

deformation changes the quantum states in conduction band which causes changes in electrical conductivity. Furthermore, in this kind of CNTs, electrons can pass beyond the band gap by means of other different sources of energy such as thermal, electrical and magnetic fields [80, 81].

The subtle electronic properties of CNTs suggest that they have the ability to promote electron transfer when used as the electrode material in electrochemical reactions. These properties provide a new manner of electrode surface modification in the design of new electrochemical sensors and novel electrocatalytic materials. It has been reported that CNT-modified electrodes have been successfully applied to identify many biological and organic molecules [82, 83].

1.3 Carbon nanofiber reinforced polymer composites

In this section, a general and brief state of the art of polymer thermoplastics reinforced exclusively with carbon nanofibers is summarized. The section summarizes some specific works related with dispersion and diverse composite properties and it is finished with some challenges for the future which still need to be overcome.

Dispersion

As it was already mentioned, most part of the research made through the last years was focused on investigating methods of processing with the aim of achieve good levels of dispersion without altering the CNFs´ structure. In this regard, processing methods such as extrusion and injection molding have been, since the beginning, subject of intense research due to wide use in traditional plastic industry.

A hopeful and ambitious study of dispersion in nylon was carried out by van Hattum et al, who used extensive calculations coupled with a Multi Objective Evolutionary Algorithm to optimize the performance of a single screw extruder. They achieved optimal composite properties by adjusting the extruder parameters to minimize the weighted average total strain suffered by a fiber during compounding, a clear indication that preserving fiber length was crucial [84].

Zeng et al. extruded and then melt spun samples of polymethyl methacrylate reinforced with 5 wt % and 10 wt % CNFs. They were able to achieve an 80 % improvement in modulus with 5 wt % loading of CNFs, although tensile strength did not improve. With a 10 wt % loading

of CNFs, the samples processed by extrusion showed a substantial decrease in modulus, while the samples processed by melt spun showed only a slight decrease, probably due to the melt spinning step improved dispersion [85].

In a previous study, low loadings of CNFs in polypropylene, PP, were processed by twin screw extrusion with the aim of study morphology and mechanical properties in final composites. The final results showed that the modulus increased by 50 % whereas the compressive strength increased by 100 % [86].

Dispersion of CNFs and MWCNTs in different polymers was determined quantitatively using optical microscopy first and after a dispersion´s value was calculated in the range from 1 to 10, based upon the frequency of occurrence of agglomerates in the matrix. Among theirs conclusions is established that while achieving a homogeneous composite with uniformly dispersed nanotubes should enhance the mechanical properties, its effect on the electrical conductivity is less clear. Indeed, if the objective is to produce polymer composites that exhibit electrical conductivity at very low concentration then uniform dispersion of the conducting fillers may be disadvantageous [14].

Anderson et al., on their hand, have attacked the study of dispersion by combining several light and X-ray techniques to generate a collective scattering curve that yields structural information about the rod-like fibers, inter-fiber spacing, and morphology of the individual fibers [87].

Mechanical Properties

Mechanical reinforcement in carbon based polymer composites is still today a serious challenge and overall it is possible to assert that it has not yielded yet all the expected results that intrinsic properties of CNFs / CNTs point out.

In the study by Tibbetts and McHugh, the mechanical properties of CNFs/nylon and CNFs/PP made with ball-milled are discussed. CNFs reinforced in nylon slightly improved the tensile strength and double the modulus, while CNFs in PP doubled the tensile strength and quadrupled the modulus compared to unreinforced material [88]. One interesting point is that fibers with graphitic structure show worse results.

In other study, the strength of partially aligned discontinuous fiber in PP composites is described. Here the composite strength increased with increase in fiber volume fraction and

the degree of fiber alignment. An x-ray-diffraction technique is used to obtain information about fiber alignment and then normal distribution is calculated. Furthermore, they showed that composite strength is sensitive to fiber length when the average fiber length is less than a certain critical fiber length [89]. Other research with 1 wt % loading of CNFs dispersed in polyester/glass fiber composites demonstrates to improve delamination resistance about 100 % [90].

One of the first studies focused on damping shows that this property is strongly dependent of surface treatment of fibers [91, 92]. In other study, damping is improved with temperature due to the increase in thermal conductivity caused by CNFs in the polymer [85].

Thermal properties

The excellent thermal conductivity of individual carbon nanofibers lead to expectations that it will enhance the thermal conductivity of carbon nanofiber based polymer composites. In contrast to the abrupt enhancement in electrical conductivity with very low loading of nanofibers, the thermal conductivities of the composites have shown only modest improvements [29, 30]. Further, by using thermogravimetric analysis, TGA, several groups have reported improved thermal stability in carbon nanofiber / polymer composites.

CNFs in adhesives have demonstrated adequate thermal conducting values for aerospace applications [93]. The observed improvement in thermal stability hints that nanofibers could be efficient as fire-retardant additives in polymer matrices, in this regard, there are studies comparing similar reduced flammability values in CNFs with nanoclays in polyurethane [94]. Also a direct relationship between flame retardant property and carbon nanofiber networks in polymer has been found. Further, viscoelastic properties have been directly related with flame retardant behavior [95]. The network created with nanofibers in polymer showed also better performance at high temperatures when compared to nanoclay fillers [96].

Electrical Properties

The potential of nanofibers as conducting fillers in multifunctional polymer composites has already successfully realized and several orders of magnitude enhancement in electrical conductivity have been achieved with a very small loading of nanofibers, while maintaining other performance aspects such as optical clarity, mechanical properties, low melt flow viscosities, etc. Two main objectives in this kind of composites are to attach the percolation

thresholds with low volume fractions of CNFs and to increase σ as much as possible with the aim of obtain adequate values for electrostatic dissipation (10^{8}-10^{12} ohm cm), electrostatic painting (10^{2}-10^{8} ohm cm) and electromagnetic interference shielding (10^{-2}-10^{2} ohm cm) applications (Figure 1.3).

The study of dispersion and distribution of nanofibers and their influence in percolation thresholds has been intensively investigated. One recent review regarding with this point assess four possible cases of dispersion/distribution: bad dispersion and distribution, good distribution and bad dispersion, bad distribution and good dispersion, and good distribution and dispersion [98]. In this study is pointed out that if the goal is to obtain electrical conductivity a bad distribution and good dispersion is necessary (Figure 1.4c). In any case, the final role of dispersion and distribution of nanofibers in final electrical performance is still today under discussion.

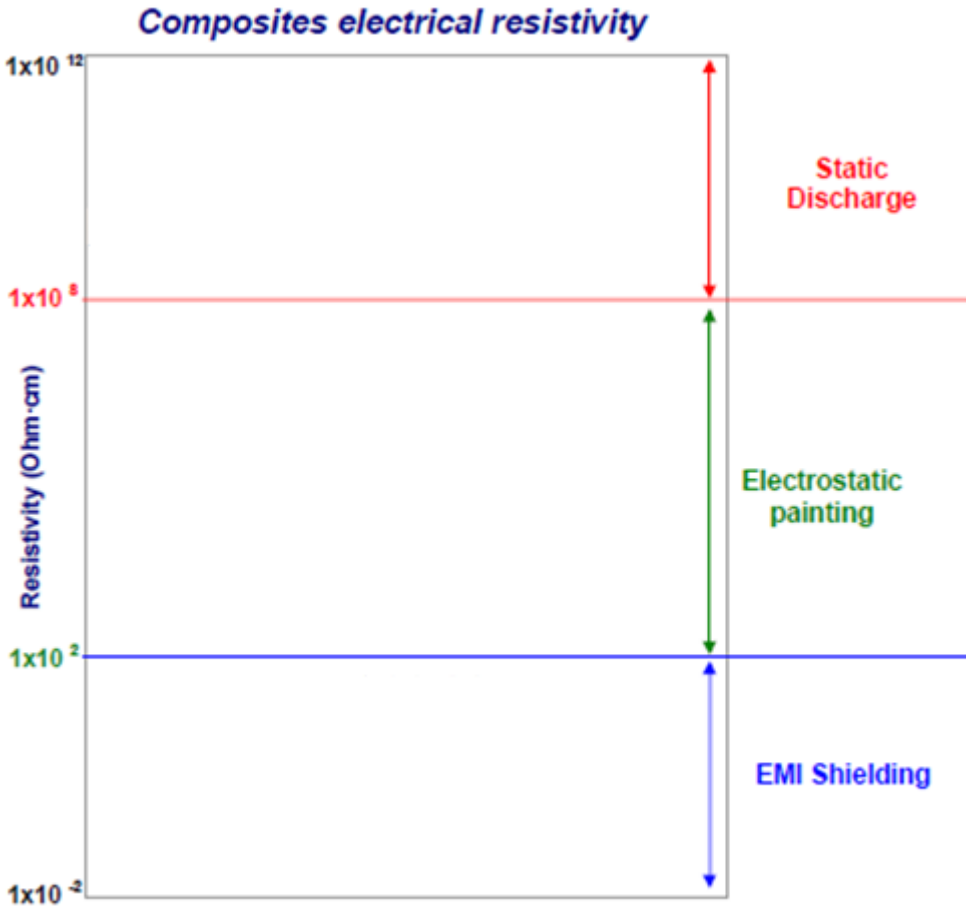

Figure 1. 3 - Possible applications of CNFs/polymer composites as function of electrical resistivity level [97].

On the other hand, the role of CNFs´ outer layers plays an important role in final electrical behavior. Overall, amorphous outer layers show lower conductivity than highly ordered outer layers [44, 99]. Besides dispersion / distribution and nanofiber conductivity, percolation thresholds and electrical conductivity in CNF based polymer nanocomposites depends on aspect ratio, polymer matrix crystallinity, molecular weight, and polymer matrix surface tension [24, 100-103]. The lower the surface tension, the best dispersion; on the contrary the higher the surface tension, the easier producing agglomerates and poor dispersion in the composites [98]. In terms of crystallinity, some studies show how nanofibers tend to agglomerate in the amorphous regions during crystallization [24, 102]. Molecular weight may play another important role; the longer length of polymer chains may hinder the creation of a conducting network [24, 104].

Without any doubt, the processing method is another important aspect to take in consideration. Well dispersed composites produced by melt mixing, for instance, resulted in unsatisfactory properties due to the decrease in the nanofibers aspect ratio caused by high-shear mixing conditions [33, 34]. In other study, the influence of melting temperature, rotation velocity and time residence in percolation thresholds is evaluated [105]. Other study uses the grafting technique in order to improve dispersion of CNFs in the polymer [106].

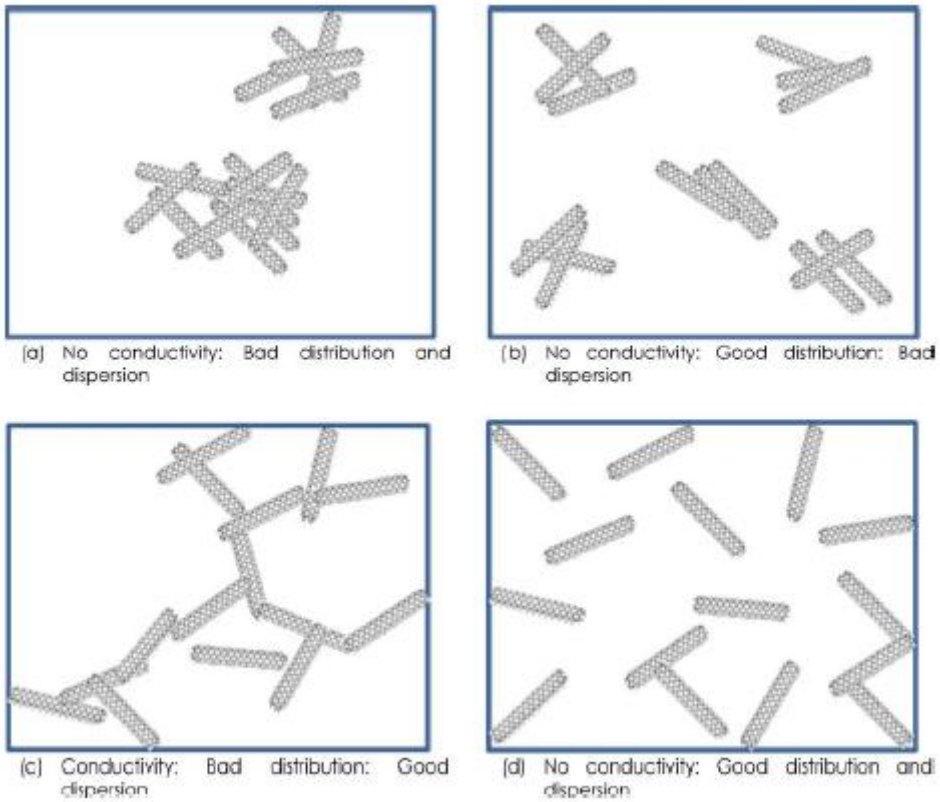

Figure 1. 4 - Different possible morphologies of 1D filler in polymer composites [98].

Future scope

CNFs and CNTs are promising nano-sized carbon materials. EMI, ESD protection and heat dissipation are some of the major applications of CNFs or CNTs / polymer composites at present. The better mechanical properties, lower density and smaller diameter are the major advantages of CNTs compared to CNFs, however CNFs have lower cost. Preliminary research in PNCs has indicated that there is potential in CNTs and CNFs for reinforcement, as well, but experimental results show that the strength of carbon nanostructured based polymer composites is lower than that predicted by theory. One of the main problems is in creating a good interface between nanofibers / nanotubes and the polymer matrix to achieve satisfactory load transfer in final composites. Besides, the CNTs or CNFs´ clusters must be disentangled in order to facilitate their dispersion in the polymer matrix during processing. Therefore, in spite of the mechanical improvements reported up until today, there is still a need for optimizing and tailoring the actual processing methods.

On the other hand, there is insufficient information about their structure-property relationships. This can be done by characterizing the interface and the effect of the CNTs/CNFs on the surrounding matrix at the nano length scale by different methods. For instance, optical and electron microscopy are often used to give a qualitative morphological analysis about the degree of dispersion but they are not sufficient for a complete analysis.

In conclusion, there is still a technological frontier to overcome between the intrinsic properties of carbon nanostructures and final PNCs´ properties. In order to achieve the potential of these materials further work is necessary to obtain fully multifunctional performance yielding improvements in mechanical, electrical, thermal, magnetic and optical properties. The existing technologies must be also improved to control and to tailor the dispersion and of CNTs/CNFs in the polymer. Therefore, although these materials appear attractive for many applications, there is still a question of whether the final PNCs will able to achieve these promising high-performances.

1.4 Objectives

In order to suit the desired applications of CNFs based polymer composites, it is important to provide insight by means of establishing processing-structure-property relationships. Since a majority of research and results have been conducted on several processes, polymers and carbon nanostructures, this research is focused on melt compounding systematically, by means of a laboratory-scale mini twin screw extruder, different CNFs´ types with the same polypropylene at the same processing conditions, with the aim of characterizing the particular final structure and explain the fundamental mechanisms governing the final properties.

With the above main objective in view, the composites were morphologic, thermic, rheological, electric, mechanic and electro-mechanically characterized after processing. The first chapter (chapter 2) was focused on an overall research of the relations between morphological analysis and the main principal physical properties. According to these first results, the final effective properties and potential applications were correlated with the appropriate CNFs´ intrinsic structure. After this first approach several more particular chapters were dedicated to the investigation and relation of rheological with electrical percolation in electrically conducting and non-conducting composites (chapter 3); the investigation of electrical percolation, electrical conductivity and piezoresistivity as function of CNFs´ content (chapter 4); and finally, as a consequence of this particular electro-

mechanical behavior, a more particular analysis of these composites as possible mechanical piezoresistive transducers was analyzed (chapter 5). A further description of the previously mentioned objectives is addressed in each one of the corresponding chapters.

***

The results of the current study have been published in the following international journals and congresses:

"***Carbon nanofibre/polyproylene composites by tailored-shear extrusion***", Van Hattum, F.W.J, Leer, C, VIEITO, A, Lake, P. International SAMPE Symposium and Exhibition (Proceedings). Volume 52, 2008, 10p

"***The piezoresistive effect in polypropylene-carbon nanofiber composites obtained by shear extrusion"*** A. J. PALEO, F. W. J. van Hattum, J. Pereira, J. G. Rocha, J. Silva, V. Sencadas, S. Lanceros-Méndez. Smart Materials and Structures 2010;19 (6) art. no. 065013

"*Piezoresistive polypropylene-carbon nanofiber composites as mechanical transducers*" A. J. PALEO, F. W. J. van Hattum, J. G. Rocha and S. Lanceros-Méndez. Microsystem Technologies 2012; 18(5), 592-597

The results of the current study have been submitted in the following international journals:

"***Carbon nanofiber type and content dependence of the physical properties of carbon nanofiber reinforced polypropylene composites***" PALEO A. J, Sencadas V, van Hattum F. W. J, Lanceros-Méndez S, Ares-Pernas, A, Macromolecular Materials and Engineering (September 2012).

"***Rheological and electrical analysis in carbon nanofibre reinforced polypropylene composites***" A. J. PALEO, J. Silva, F. W. J. van Hattum, S. Lanceros-Méndez, A. Ares-Pernas, Journal of Polymer Science Part B: Polymer Physics (August 2012).

References

1. Ajayan PM, Redlich P, Ruhle M. Structure of carbon nanotube-based nanocomposites. J Microsc-Oxf. 1997;185:275-282.

2. Galeski A. Strength and toughness of crystalline polymer systems. Prog Polym Sci. 2003;28(12):1643-1699.

3. Ishikawa H, Fudetani S, Hirohashi M. Mechanical properties of thin films measured by nanoindenters. Appl Surf Sci. 2001;178(1-4):56-62.

4. Endo M, Kim YA, Hayashi T, Nishimura K, Matusita T, Miyashita K, et al. Vapor-grown carbon fibers (VGCFs) - Basic properties and their battery applications. Carbon. 2001;39(9):1287-1297.

5. Zhang L, Austin D, Merkulov VI, Meleshko AV, Klein KL, Guillorn MA, et al. Four-probe charge transport measurements on individual vertically aligned carbon nanofibers. Appl Phys Lett. 2004;84(20):3972-3974.

6. Daenen M, de Fouw RD, Hammers B, Janssen PGA, Schouteden K, Veld MAJ, The Wondrous World of Carbon Nanotubes: A Review of Current Nanotube Technologies . Eindhoven University of Technology, Eindhoven N.

7. Breuer O, Sundararaj U. Big returns from small fibers: A review of polymer/carbon nanotube composites. Polymer Composites. 2004;25(6):630-645.

8. Moniruzzaman M, Winey KI. Polymer nanocomposites containing carbon nanotubes. Macromolecules. 2006;39(16):5194-5205.

9. Frankland SJV, Caglar A, Brenner DW, Griebel M. Molecular simulation of the influence of chemical cross-links on the shear strength of carbon nanotube-polymer interfaces. Journal of Physical Chemistry B. 2002;106(12):3046-3048.

10. Schadler LS, Giannaris SC, Ajayan PM. Load transfer in carbon nanotube epoxy composites. Appl Phys Lett. 1998;73(26):3842-3844.

11. Barber AH, Cohen SR, Wagner HD. Measurement of carbon nanotube-polymer interfacial strength. Appl Phys Lett. 2003;82(23):4140-4142.

12. Chung DDL. Comparison of submicron-diameter carbon filaments and conventional carbon fibers as fillers in composite materials. Carbon. 2001;39(8):1119-1125.

13. Xie JI, Zhang NY, Guers M, Varadan VK. Ultraviolet-curable polymers with chemically bonded carbon nanotubes for microelectromechanical system applications. Smart Materials & Structures. 2002;11(4):575-580.

14. Andrews R, Jacques D, Minot M, Rantell T. Fabrication of carbon multiwall nanotube/polymer composites by shear mixing. Macromol Mater Eng. 2002;287(6):395-403.

15. Hill DE, Lin Y, Rao AM, Allard LF, Sun YP. Functionalization of carbon nanotubes with polystyrene. Macromolecules. 2002;35(25):9466-9471.

16. Ebbesen TW, Lezec HJ, Hiura H, Bennett JW, Ghaemi HF, Thio T. Electrical conductivity of individual carbon nanotubes. Nature. 1996;382(6586):54-56.

17. Dai HJ, Wong EW, Lieber CM. Probing electrical transport in nanomaterials: Conductivity of individual carbon nanotubes. Science. 1996;272(5261):523-526.

18. Shante VKS, Kirkpatr.S. Introduction to percolation theory. Adv Phys. 1971;20(85):325-357.

19. Stroud D, Bergman DJ. Frequency-dependence of the polarization catastrophe at a metal-insulator-transition and related problems. Phys Rev B. 1982;25(3):2061-2064.

20. Nan CW. Physics of inhomogeneous inorganic materials. Prog Mater Sci. 1993;37(1):1-116.

21. Prasse T, Cavaille JY, Bauhofer W. Electric anisotropy of carbon nanofibre/epoxy resin composites due to electric field induced alignment. Composites Science and Technology. 2003;63(13):1835-1841.

22. Hammel E, Tang X, Trampert M, Schmitt T, Mauthner K, Eder A, et al. Carbon nanofibers for composite applications. Carbon. 2004;42(5-6):1153-1158.

23. Das NC, Yamazaki S, Hikosaka M, Chaki TK, Khastgir D, Chakraborty A. Electrical conductivity and electromagnetic interference shielding effectiveness of polyaniline-ethylene vinyl acetate composites. Polymer International. 2005;54(2):256-259.

24. Huang JC. Carbon black filled conducting polymers and polymer blends. Advances in Polymer Technology. 2002;21(4):299-313.

25. Lozano K, Barrera EV. Nanofiber-reinforced thermoplastic composites. I. Thermoanalytical and mechanical analyses. Journal of Applied Polymer Science. 2001;79(1):125-133.

26. Huxtable ST, Cahill DG, Shenogin S, Xue LP, Ozisik R, Barone P, et al. Interfacial heat flow in carbon nanotube suspensions. Nature Materials. 2003;2(11):731-734.

27. Agari Y, Ueda A, Nagai S. Thermal-conductivities of composites in several types of dispersio-systems . Journal of Applied Polymer Science. 1991;42(6):1665-1669.

28. Agari Y, Ueda A, Nagai S. Thermal-conductivity of a polymer composite. Journal of Applied Polymer Science. 1993;49(9):1625-1634.

29. Biercuk MJ, Llaguno MC, Radosavljevic M, Hyun JK, Johnson AT, Fischer JE. Carbon nanotube composites for thermal management. Appl Phys Lett. 2002;80(15):2767-2769.

30. Hone J, Llaguno MC, Biercuk MJ, Johnson AT, Batlogg B, Benes Z, et al. Thermal properties of carbon nanotubes and nanotube-based materials. Applied Physics a-Materials Science & Processing. 2002;74(3):339-343.

31. Huang JC. EMI shielding plastics – a review. Advances in Polymer Technology. 1995;14(2):137-150.

32. Shim BS, Starkovich J, Kotov N. Multilayer composites from vapor-grown carbon nano-fibers. Composites Science and Technology. 2006;66(9):1174-1181.

33. Tibbetts GG, Lake ML, Strong KL, Rice BP. A review of the fabrication and properties of vapor-grown carbon nanofiber/polymer composites. Composites Science and Technology. 2007;67(7-8):1709-1718.

34. Lozano K, Bonilla-Rios J, Barrera EV. A study on nanofiber-reinforced thermoplastic composites (II): Investigation of the mixing rheology and conduction properties. Journal of Applied Polymer Science. 2001;80(8):1162-1172.

35. Ma HM, Zeng JJ, Realff ML, Kumar S, Schiraldi DA. Processing, structure, and properties of fibers from polyester/carbon nanofiber composites. Composites Science and Technology. 2003;63(11):1617-1628.

36. Yang LY, Bigio D, Smith TG. Melt blending of linear low-density polyethylene and polystyrene in a haake internal mixer. 2. Morphology-processing relationships. Journal of Applied Polymer Science. 1995;58(1):129-141.

37. Jimenez GA, Jana SC. Electrically conductive polymer nanocomposites of polymethylmethacrylate and carbon nanofibers prepared by chaotic mixing. Compos Pt A-Appl Sci Manuf. 2007;38(3):983-993.

38. Coleman JN, Khan U, Blau WJ, Gun'ko YK. Small but strong: A review of the mechanical properties of carbon nanotube-polymer composites. Carbon. 2006;44(9):1624-1652.

39. Sandler JKW, Kirk JE, Kinloch IA, Shaffer MSP, Windle AH. Ultra-low electrical percolation threshold in carbon-nanotube-epoxy composites. Polymer. 2003;44(19):5893-5899.

40. Ebbesen TW. Carbon nanotubes : preparation and properties. CRC Press. 1996.

41. Dekker C. Carbon nanotubes as molecular quantum wires. Physics Today. 1999;52(5):22-28.

42. Kwon YK, Tomanek D. Electronic and structural properties of multiwall carbon nanotubes. Physical Review B. 1998;58(24):16001-16004.

43. Kang IP, Heung YY, Kim JH, Lee JW, Gollapudi R, Subramaniam S, et al. Introduction to carbon nanotube and nanofiber smart materials. Composites Part B-Engineering. 2006;37(6):382-394.

44. Gordeyev SA, Macedo FJ, Ferreira JA, van Hattum FWJ, Bernardo CA. Transport properties of polymer-vapour grown carbon fibre composites. Physica B. 2000;279(1-3):33-36.

45. Terranova ML, Sessa V, Rossi M. The world of carbon nanotubes: an overview of CVD growth methodologies. Chem. Vapour Depos. 2006;(12):315-325.

46. Harris PJF. Carbon nanotubes and related structures. New materials for the twenty-fisrt century. Cambridge University Press. 1999.

47. Jong KPD, Geus JW. Carbon nanofibers: Catalytic Synthesis and Applications. Catal. Rev. 2000;42(4):481-510.

48. Endo M. Grow carbon-fibers in the vapor-phase. Chemtech. 1988;18(9):568-576

49. Rodriguez NM. A review of catalytically grown carbon nanofibers. Journal of Materials Research. 1993;8(12):3233-3250.

50. Jiang N, Koie R, Inaoka T, Shintani Y, Nishimura K, Hiraki A. Carbon nanofibers synthesized by decomposition of alcohol at atmospheric pressure. Appl Phys Lett. 2002;81(3):526-528.

51. Rakov EG, Blinov SN, Ivanov IG, Rakova EV, Digurov NG. Continuous process for obtaining carbon nanofibers. Russian Journal of Applied Chemistry. 2004;77(2):187-191.

52. Minus ML, Kumar S. The processing, properties, and structure of carbon fibers. Jom. 2005;57(2):52-58.

53. Guo T, Nikolaev P, Rinzler AG, Tomanek D, Colbert DT, Smalley RE. Self-assembly of tubular fullerenes. Journal of Physical Chemistry. 1995;99(27):10694-10697.

54. Ebbesen TW, Ajayan PM. Large-scale synthesis of carbon nanotubes. Nature. 1992;358(6383):220-222.

55. Applied Sciences, Inc. (2001) Cedarville. http://www.apsci.com

56. Tibbetts GG, Bernardo CA, Gorkiewicz DW, Alig RL. Role of sulfur in the production of carbon-fibers in the vapor phase. Carbon. 1994;32(4):569-576.

57. Tibbetts GG, Devour MG, Rodda EJ. An adsorption-diffusion isotherm and its application to the growth of carbon filaments on iron catalyst particles. Carbon. 1987;25(3):367-375.

58. Harris PJF . Carbon nanotubes and related structures. University C, Press. 2001

59. Uchida T, Anderson DP, Minus ML, Kumar S. Morphology and modulus of vapor grown carbon nano fibers. Journal of Materials Science. 2006;41(18):5851-5856.

60. Klein KL, Melechko AV, McKnight TE, Retterer ST, Rack PD, Fowlkes JD, et al. Surface characterization and functionalization of carbon nanofibers. Journal of Applied Physics. 2008;103(6).

61. Prolongo SG, Buron M, Gude MR, Chaos-Moran R, Campo M, Urena A. Effects of dispersion techniques of carbon nanofibers on the thermo-physical properties of epoxy nanocomposites. Composites Science and Technology. 2008;68(13):2722-2730.

62. Oak Ridge National Laboratory's High Temperature Materials Laboratory, U. S. Department of Energy, Office of Energy Efficiency and Renewable Energy.

63. Afzal M. Heuristic Model for Conical Carbon Nanofiber. M.S. Thesis, University of Toledo, Toledo, OH, 2004.

64. Nhut JM, Nguyen P, Pham-Huu C, Keller N, Ledoux MJ. Carbon nanotubes as nanosized reactor for the selective oxidation of H2S into elemental sulfur. Catalysis Today. 2004;91-2:91-97.

65 Pan X, Fan Z, Chen W, Ding Y, Luo H, Bao X. Enhanced ethanol production inside carbon-nanotube reactors containing catalytic particles. Nature Materials. 2007;6(7):507-511.

66. Prato M, Kostarelos K, Bianco A. Functionalized carbon nanotubes in drug design and discovery. Accounts of Chemical Research. 2008;41(1):60-68.

67. Nyden MR, Stoliarov SI. Calculations of the energy of mixing carbon nanotubes with polymers. Polymer. 2008;49(2):635-641.

68. Landis EC, Klein KL, Liao A, Pop E, Hensley DK, Melechko AV, et al. Covalent Functionalization and Electron-Transfer Properties of Vertically Aligned Carbon Nanofibers: The Importance of Edge-Plane Sites. Chemistry of Materials. 2010;22(7):2357-2366.

69. Li F, Cheng HM, Bai S, Su G, Dresselhaus MS. Tensile strength of single-walled carbon nanotubes directly measured from their macroscopic ropes. Appl Phys Lett. 2000;77(20):3161-3163.

70. Iijima S, Brabec C, Maiti A, Bernholc J. Structural flexibility of carbon nanotubes. Journal of Chemical Physics. 1996;104(5):2089-2092.

71. Ozkan T, Naraghi M, Chasiotis I. Mechanical properties of vapor grown carbon nanofibers. Carbon. 2010;48(1):239-244.

72. Frank S, Poncharal P, Wang ZL, de Heer WA. Carbon nanotube quantum resistors. Science. 1998;280(5370):1744-174.

73. Thess A, Lee R, Nikolaev P, Dai HJ, Petit P, Robert J, et al. Crystalline ropes of metallic carbon nanotubes. Science. 1996;273(5274):483-487.

74. Wei BQ, Vajtai R, Ajayan PM. Reliability and current carrying capacity of carbon nanotubes. Appl Phys Lett. 2001;79(8):1172-1174.

75. Howe JY, Tibbetts GG, Kwag C, Lake ML. Heat treating carbon nanoribers for optimal composite performance. Journal of Materials Research. 2006;21(10):2646-2652.

76. Lafdi K, Fox W, Matzek M, Yildiz E. Effect of carbon nanofiber heat treatment on physical properties of polymeric nanocomposites - Part I. Journal of Nanomaterials. 2007;1-6.

77. Yang DJ, Zhang Q, Chen G, Yoon SF, Ahn J, Wang SG, et al. Thermal conductivity of multiwalled carbon nanotubes. Physical Review B. 2002;66(16):165440-165446.

78. Mehrez H, Taylor J, Guo H, Wang J, Roland C. Carbon nanotube based magnetic tunnel junctions. Physical Review Letters. 2000;84(12):2682-2685.

79. Tombler TW, Zhou CW, Alexseyev L, Kong J, Dai HJ, Lei L, et al. Reversible electromechanical characteristics of carbon nanotubes under local-probe manipulation. Nature. 2000;405(6788):769-772.

80. Zhang Y, Han M. Band gap of carbon nanotubes under combined uniaxial-torsional strain. Physica E-Low-Dimensional Systems & Nanostructures. 2011;43(10):1774-1778.

81. Shimizu T, Haruyama J, Marcano DC, Kosinkin DV, Tour JM, Hirose K, et al. Large intrinsic energy bandgaps in annealed nanotube-derived graphene nanoribbons. Nature Nanotechnology. 2011;6(1):45-50.

82. Otani M, Okada S, Okamoto Y. Intrinsic dipole moment on the capped carbon nanotubes. Physical Review B. 2009;80(15):153413-153416.

83. Tahhan M, Truong VT, Spinks GM, Wallace GG. Carbon nanotube and polyaniline composite actuators. Smart Materials & Structures. 2003;12(4):626-632.

84. Van Hattum FWJ, Gaspar-Cunha A, Lake ML, Bernardo CA. Processing and properties of carbon nanofiber/thermoplastic composites. 2004. p. 2427-2433.

85. Zeng JJ, Saltysiak B, Johnson WS, Schiraldi DA, Kumar S. Processing and properties of poly(methyl methacrylate)/carbon nano fiber composites. Composites Part B-Engineering. 2004;35(2):173-178.

86. Kumar S, Doshi H, Srinivasarao M, Park JO, Schiraldi DA. Fibers from polypropylene/nano carbon fiber composites. Polymer. 2002;43(5):1701-1703.

87. Anderson DP, Brown JM, Schaefer DW, Justice RS. Hierarchical morphology of nanoconstituents in water-based suspensions and epoxy resins by scattering techniques. vol. 502005. p. 2267-2278.

88. Tibbetts GG, McHugh JJ. Mechanical properties of vapor-grown carbon fiber composites with thermoplastic matrices. Journal of Materials Research. 1999;14(7):2871-2880.

89. Kuriger RJ, Alam MK, Anderson DP. Strength prediction of partially aligned discontinuous fiber-reinforced composites. Journal of Materials Research. 2001;16(1):226-232.

90. Sadeghian R, Gangireddy S, Minaie B, Hsiao KT. Manufacturing carbon nanofibers toughened polyester/glass fiber composites using vacuum assisted resin transfer molding for enhancing the mode-I delamination resistance. Composites Part A: Applied Science and Manufacturing. 2006;37(10):1787-1795.

91. Finegan IC, Tibbetts GG, Gibson RF. Modeling and characterization of damping in carbon nanofiber/polypropylene composites. Composites Science and Technology. 2003;63(11):1629-1635.

92. Ting JM, Lake ML. Vapor-grown carbon-fiber-reinforced carbon composites. Carbon. 1995;33(5):663-667.

93. Gibson T, Rice B, Ragland W, Silverman EM, Peng HH, Strong KL, et al. Formulation and evaluation of carbon nanofiber-based conductive adhesives. vol. 502005. p. 1713-1726.

94. Zammarano M, Kraemer RH, Harris R, Jr., Ohlemiller TJ, Shields JR, Rahatekar SS, et al. Flammability reduction of flexible polyurethane foams via carbon nanofiber network formation. Polymers for Advanced Technologies. 2008;19(6):588-595.

95. Kashiwagi T, Du FM, Winey KI, Groth KM, Shields JR, Harris RH, et al. Flammability properties of PMMA-single walled carbon nanotube nanocomposites. Abstracts of Papers of the American Chemical Society. 2004;228:U423-U423.

96. Kashiwagi T, Mu MF, Winey K, Cipriano B, Raghavan SR, Pack S, et al. Relation between the viscoelastic and flammability properties of polymer nanocomposites. Polymer. 2008;49(20):4358-4368.

97. Foro sobre Nuevos Materiales y Nanotecnología. Grupo Antolín. 2008 http://www.grupoantolin.com/

98. Al-Saleh MH, Sundararaj U. A review of vapor grown carbon nanofiber/polymer conductive composites. Carbon. 2009;47(1):2-22.

99. Finegan IC, Tibbetts GG. Electrical conductivity of vapor-grown carbon fiber/thermoplastic composites. Journal of Materials Research. 2001;16(6):1668-1674.

100. Lee BO, Woo WJ, Kim MS. EMI shielding effectiveness of carbon nanofiber filled poly(vinyl alcohol) coating materials. Macromol Mater Eng. 2001;286(2):114-118.

101. Wu JH, Chung DDL. Increasing the electromagnetic interference shielding effectiveness of carbon fiber polymer-matrix composite by using activated carbon fibers. Carbon. 2002;40(3):445-447.

102. Kandasubramanian B, Gilbert M. An electroconductive filler for shielding plastics. Macromolecular Symposia. 2005;221:185-195.

103. Miyasaka K, Watanabe K, Jojima E, Aida H, Sumita M, Ishikawa K. Electrical-conductivity of carbon polymer composites as a function of carbon content. Journal of Materials Science. 1982;17(6):1610-1616.

104. Grady BP, Arthur DJ, Ferguson J. Single-Walled Carbon Nanotube/Ultrahigh-Molecular-Weight Polyethylene Composites With Percolation at Low Nanotube Contents. Polymer Engineering and Science. 2009;49(12):2440-2446.

105. Krause B, Poetschke P, Haeussler L. Influence of small scale melt mixing conditions on electrical resistivity of carbon nanotube-polyamide composites. Composites Science and Technology. 2009;69(10):1505-1515.

106. Jin ZX, Pramoda KP, Goh SH, Xu GQ. Poly(vinylidene fluoride)-assisted melt-blending of multi-walled carbon nanotube/poly(methyl methacrylate) composites. Materials Research Bulletin. 2002;37(2):271-278.

Chapter 2 - Carbon nanofiber type and content dependence of the physical properties of carbon nanofiber reinforced polypropylene composites

Abstract

The variation of the physical properties of four different carbon nanofibers, CNFs, based-polymer nanocomposites processed by twin-screw extrusion, TSE, was investigated. Nanocomposites fabricated with CNFs with highly graphitic outer wall layer revealed electrical isolation-to-conducting behaviour as function of CNFs´ content. Nanocomposites fabricated with CNFs with an outer layer consisting on a disordered pyrolitically stripped layer, in contrast, revealed better mechanical performance and enhanced thermal stability. Further, incorporation of CNFs to the polymer matrix increases the thermal stability and the degree of crystallinity of the polymer, independently on the filler content and type. In addition, dispersion of the carbon nanofibers´ clusters in polypropylene composites was analysed by transmitted light optical microscopy, LOM, and greyscale analysis, GSA. The results show a correlation between the filler concentration and the variance, a parameter which measures quantitatively the dispersion, for all composites. This method indicated a value of 1.4 vol % above which large clusters of CNFs cannot be dispersed effectively and as a consequence only slight changes in mechanical performance are observed. The cluster´s dispersion and distribution quantified by GSA can be used as an indicator for electrical conductivity levels. Finally, this study establishes that the physical properties of carbon nanofiber based-polymer nanocomposites can be tailored as function of both adequate CNFs´ structure and content.

2.1 Introduction

Several nanostructures composed of graphitic layers, including nanographene platelets, NGPs, carbon nanofibers and nanotubes, CNTs are currently the focus of intense experimental and theoretical investigation. CNTs can be classified into single-walled nanotubes , SWNTs, and multi-walled nanotubes, MWNTs. SWNTs consist on a single and tubular graphene layer with diameters of 1–2 nm and lengths from many microns to centimetres in special cases [1, 2]. In contrast, MWNTs are comprised of a number of graphene layers coaxially rolled together with diameters ranging from 2 to 100 nm and lengths of tens of microns [3]. CNFs, also known as Cup-Stacked Carbon Nanotubes, CSCNT, have a unique morphology in which graphene planes with exposed edges are placed on the outer surface of the fiber [4]. Their outer diameter is slightly larger than for CNTs, ranging from 50 to 200 nm; the inner diameter ranges from 30 to 90 nm and the lengths are in the range from 50 to 100 μm [5, 6].

The main difference among CNFs and CNTs is the orientation of the graphene planes, which in the case of CNFs are canted at a certain angle from the fiber axis. This characteristic promotes a higher chemical reactivity across the sidewalls in CNFs, a key factor for chemical functionalization and electrochemical applications. Furthermore, they show excellent mechanical properties, with values of tensile strength of a few GPa, tensile modulus of some hundreds GPa [7], electrical conductivity of ~ 10^{-3} Ω cm [8] and thermal conductivity with values of 1950 W/ (m K) [9]. These characteristics, together with the lower production cost than CNTs, have lead CNFs to be under intense investigation.

One important application of CNFs is in the field of composite materials. By incorporating relatively small loadings of CNFs in the polymer matrix, electrically conductive composites can be produced with increased mechanical performance.

Few studies exist that report the effects of CNFs on the crystalline morphology and thermal degradation of polymers. It has been reported that the nucleation rate of PP increases with 5 wt % of CNFs [9] and a two-layer structure for the interface existing between PP and CNFs was proposed based on thermogravimetric analysis [10], influencing thermal degradation of the polymer.

Associated to their large surface area and growth method, CNFs tend to aggregate which may negatively affect the composites properties. Dispersion is one of the hardest technological challenges for the successful use of CNFs in composite applications. Success strongly

depends on controlling the degree of dispersion of CNFs in the host matrix and investigating its influence in the macroscopic properties of the final composite. In this regard, a quantitative assessment of dispersion and distribution represent, therefore, a crucial prerequisite to accurately determine the best route to high-performance multifunctional CNFs or CNTs based nanocomposites [11-15].

Several studies focused on the quantitative analysis of dispersion can be found in the literature. Recently, Schulte et al. correlated electrical conductivity of MWNT/carbon black CB epoxy nanocomposites with morphology, through transmission electron microscopy, TEM, and transmission light micrographs, TLM [16]. Lillehei et al. through radial power spectral density, RPSD, fractal dimension, and Minkowski functional analysis methods based on optical, OM, and electron microscopy, EM, characterised morphology in several laser ablated–SWCNTs based polymer composites. In their study values of bundle diameters and spacing, segment lengths and degree of randomness were reported [11]. In their comparative study of dispersion in MWCNTs and CNFs polyester resin composites, Vera-Agullo et al. evaluated the dispersion in microscale using the method suggested by Andrews et al. [12] and the dispersion at the nanoscale through TEM. The study analysed processing-morphology relationships, concluding that the best dispersion is attained with the more energetic mixing conditions [17]. The analysis done by Gershon et al. on high impact polystyrene (HIPS)/CNFs composites fabricated by TSE is based in a rule-of-mixtures, ROM formulation which allows determining a dispersion limit of 3 vol % above which CNFs do not further dispersed in the host matrix [13]. Finally, Brooker et al. quantified the dispersion of CNTs with thermoplastic in epoxy systems using greyscale and quadrat methods to analyse macro and nanoscale respectively. The ratios variance/mean are calculated and compared for both methods [18]. In summary, although several routes to correlate structure with final properties have been proposed, a method which establishes clearly dispersion-structure-properties relationships is still under investigation.

In this work, four different carbon nanofibers were systematically incorporated in the same polypropylene matrix by twin-screw extrusion under the same processing conditions. The main focus is to systematically investigate the effect of the content and the different CNFs´ structures on final microstructure and thermal, mechanical and electrical performance of the composite.

A quantitative method based on transmitted light optical microscopy by means of greyscale analysis, as previously described in [19], is used to determine the dispersion and correlate with the nanocomposite´s properties.

2.2 Experimental

2.2.1 Materials

A Polypropylene powder was purchased from Borealis EE002AE, with a specific gravity of 0.905 g/cm3, melt mass-flow rate, MFR, of 11 g/10 m. Carbon nanofibers PR19 LHT XT, PR24 LHT XT , PR25 PS XT and PR 25 AG, commercially known as Pyrograf III TM were provided by Applied Sciences, Inc. (ASI, Cedarville, OH, USA) [20]. An overview of the main properties of the CNFs and formulations are summarized in Table 2.1 and Table 2.2, respectively. A TEM image of two kinds of CNFs is shown in Figure 2.1, the main characteristics being in accordance to the description presented in Table 2.1.

CNF type	CNF grade	Properties
PR 19	LHT XT	Graphitic tubular core surrounded by two layers: internal "stacked-cup" layer followed by catalytic outer layer. Total diameter: 110 nm; outer two-layers diameter: 35 nm Debulked form to lower the bulk density of fibre (XT) Heat-treated to temperatures of 1500 º C (LHT)
PR 24	LHT XT	Graphitic tubular core surrounded by two layers: internal "stacked-cup" layer followed by catalytic outer layer. Total diameter: 80 nm; outer two-layers diameter: 25 nm Debulked form to lower the bulk density of fibre (XT) Heat-treated to temperatures of 1500 ºC (LHT)
PR 25	PS XT	Graphitic tubular core surrounded by two layers: internal "stacked-cup" layer followed by pyrolitically outer stripped layer. Total diameter: 115 nm; outer two-layers diameter: 30 nm Debulked form to lower the bulk density of fibre (XT) Heat-treated to temperatures of 600 ºC
PR 25	AG	Graphitic tubular core surrounded by two layers: internal "stacked-cup" layer followed by pyrolytic outer hydrocarbon layer. Total diameter: 130 nm

Table 2. 1 - CNFs types and properties.

Composite Nr	CNF type	CNF grade	Polypropylene	CNFs Loadings
1	PR19	LHT XT	Borealis EE002AE	0.2, 0.5, 0.9, 1.4, 1.9, 2.4 % vol
2	PR24	LHT XT		
3	PR25	PS XT		
4		AG		0.2, 0.5, 0.9, 1.4 % vol

Table 2. 2 - CNFs types and formulations.

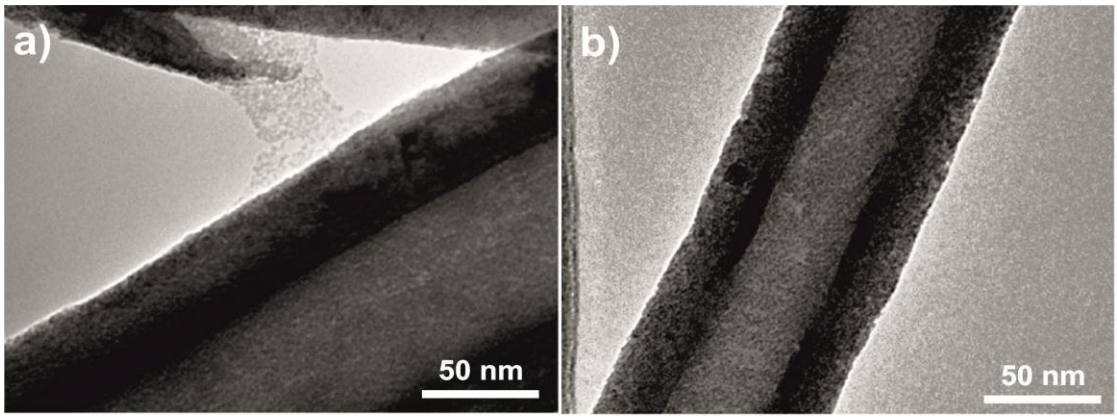

Figure 2. 1 - TEM micrograph of PR-19-LHT-XT (left) and PR-25-PS-XT (right).

2.2.2 Processing of the nanocomposites

The series of PP / CNFs nanocomposites were fabricated under the same processing conditions on a modular lab-scale intermeshing mini-co-rotating twin-screw extruder with a screw diameter of 13 mm, barrel length of 31 cm and an approximate L / D ratio of 26, coupled to a cylindrical rod dye of approximate 2.85 mm of diameter.

The modular screw geometry was comprised of one special transport module with a small pitch of 6.5 mm located in the solid conveying zone together to a series of 8 kneading block disks with a staggering reverse angle of -30^{o} ("left-handed"), located just before the melt conveying zone, and two final transport modules with a pitch of 13 mm in the melt conveying zone. Thus, the screw configuration used represents relatively high shear mixing conditions and long residence times during processing. The extrusion process was performed at a constant feed rate of 150 g/h of PP by means of a volumetric dosing unit Moretto DVM 18 L,

while CNFs were gradually fed downstream in the melting zone of the extruder in order to obtain the controlled fiber loadings in the nanocomposites. The screw rotational speed was kept constant at 50 rpm and all compounded blends were carried out at a fixed barrel temperature of 190 ºC.

Finally, the extruded and pelletized PP / CNFs nanocomposites were compression moulded into rectangular plates. Further details about melt-compounding conditions, machining and final dimensions of the samples used for the mechanical and electrical characterization have been previously published [21].

2.2.3 Sample characterization

Specimens were broken under cryogenic conditions and then examined using a JEOL JSM-6400 scanning electron microscope, SEM, at an accelerating voltage of 20 kV in order to study morphology and CNF dispersion of the composites. The samples were previously sputter-coated with a thin layer of gold.

Differential scanning calorimetry analyses were performed using a DSC-7 (Perkin Elmer Cetus Instruments, Norwalk CT) between room temperature and 190ºC in heating and cooling runs at a scan rate of 10 ºC/min under nitrogen atmosphere in order to evaluate the influence of CNFs on crystallization behavior of PP.

The study of the thermal stability of nanocomposites and their degradation kinetics was carried out in a TGA-7 thermo balance (Perkin-Elmer). Nickel and Perkalloy were used for the temperature calibration. The samples with weights between 5 and 10 mg were tested from 50ºC to 650ºC in a nitrogen atmosphere at heating rate of 10ºC/min.

Electrical characterization was obtained from the average of the bulk resistance measured in ten rectangular replicates per sample with an automated Keithley 487 picoammeter/voltage source. The dimensions of the samples were 49 mm x 10 mm x 1 mm. All the experiences were performed at room temperature in direct current, DC, by using the two-probe method. The extremities of the samples were painted with conductive silver paste and volume conductivity in S cm^{-1} was calculated [21].

The tensile modulus was measured in ten replicates per sample with dimensions 15 mm (length) x 4 mm (width) x 2 mm (thickness) in parallel section, using an AG-IS Shimadzu testing machine with a load cell of 500 N at a speed of 2 mm min^{-1}.

2.2.4 Greyscale Analysis

Dispersion was studied by a greyscale analysis based on transmitted light optical microscopy, according to the methodology explained in [19]. An Olympus BH2 transmittance light microscope was used. The total scanned area was about 2.3 mm^2 (equivalent to 100 adjacent micrographs of 170 x 135 μm), which is considered large enough to be representative of the sample. Because LOM has a scale limitation of approximately 1 μm, carbon nanofibers agglomerates above 1000 nm would be visible and individual carbon nanofibers will scatter light.

PP / CNFs composite samples were cut into rectangles of approx. 4 x 2 mm and 10 μm in thickness using a sliding Leitz 1300 microtome equipped with a glass slicing knife. The samples were then placed between a microscope glass slide and a cover glass. In order to prevent curling up or corrugating, Canada balsam (Alfa Aesar, CAS# 8007-47-4) was used. All samples were left to cure under pressure prior to analysis.

A number of 100 adjacent optical micrographs were taken using at least two samples for each composite. The size of each captured image was 1280 x 1024 pixels corresponding to an analysed area of approx. 170 x 135 μm per picture.

After capturing the images, the micrographs were post-processed using image analysis software developed in-house which assigned a greyscale to each pixel (0 for a black pixel and 255 for a white pixel on an 8-bit resolution case), acquiring the histograms for all 100 adjacent images and their individual variance which is directly related to the shape of the histograms, was calculated. Subsequently, the overall histogram was then created from which the final variance was obtained.

2.3 Results and Discussion

2.3.1 Dispersion and morphology of the nanocomposites

The SEM images of 0.9 vol % CNFs filled nanocomposites demonstrate that the four composites reveal different structures. In PR 25 PS XT and PR 25 AG composites (Figures 2.2c and 2.2d), the CNFs are well dispersed, distributed, and seem to be wrapped with the PP, indicating a good adhesion between the PP matrix and the CNFs. In PR 19 LHT XT and PR

24 LHT XT composites, in contrast, the CNFs are also well dispersed and distributed, but less wrapped with the PP, indicative of worse adhesion, (Figures 2.2a and 2.2b).

In addition, the SEM images of 0.2, 0.9 and 1.4 vol % for the PR 19 LHT XT (Figure 2.3) show closer distances between CNFs with increasing filler concentrations. In these composites in particular the electrical percolation threshold is bounded between 0.5 and 0.9 vol % as it will be discussed in the electrical properties section.

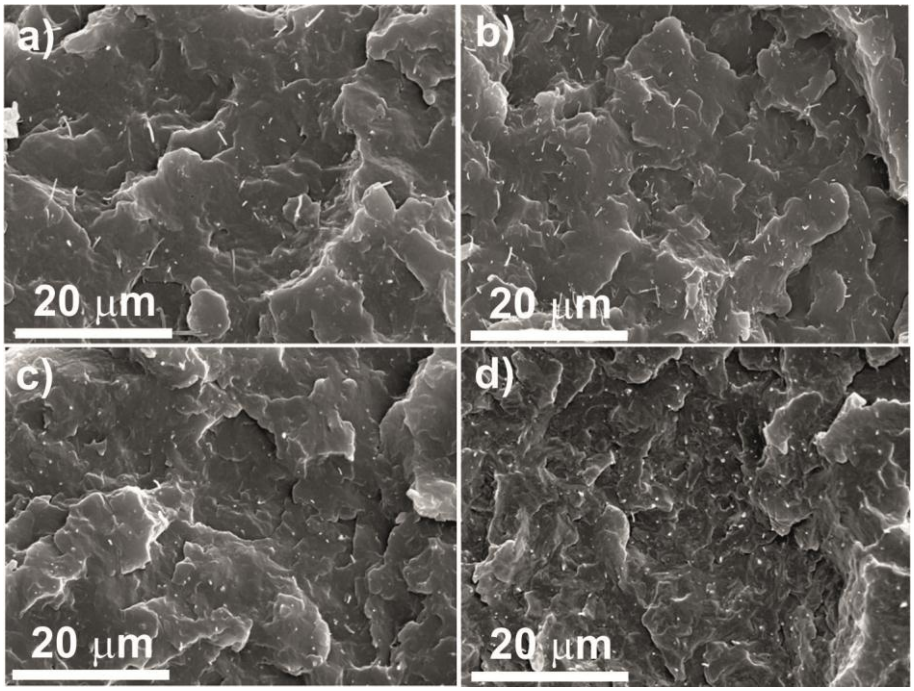

Figure 2. 2 - SEM micrographs of 0.9 vol % PP / CNFs composites: **a** PP / PR 19 LHT XT composites, **b** PP / PR 24 LHT XT composites, **c** PP / PR 25 PS XT composites and **d** PP / PR 25 AG composites.

Due to the similar microstructure founded between PP / PR 25 PS XT and PP / PR 25 AG composites, and between PP / PR 19 LHT XT and PP / PR 24 LHT XT composites, only the PP / PR 19 LHT XT and PP / PR 25 PS XT composites were thermally characterized for all CNFs´ contents, whereas the four composites were systematically mechanical and electrical characterized.

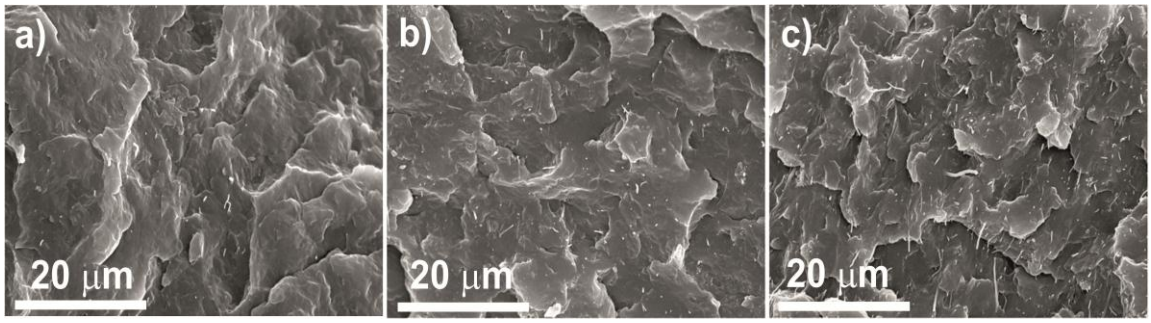

Figure 2. 3 -. SEM micrographs of PP / PR 19 LHT XT composites: **a** 0.2 vol %, **b** 0.9 vol % and **c** 1.4 vol % composites.

Figure 2.4 represents a layout of 100 contiguous 8-bit greyscale micrographs for the sample PP / 24 LHT XT (composite 2) with a loading of 0.5 vol %. This composition, representative for the rest of the samples, is presented with the aim of describing the way in which the GSA was performed. Overall, some agglomerates randomly distributed with different geometries and sizes, ranging from a few to a hundred micrometers, are noted. The two micrographs to the right in Figure 2.4b show two large agglomerates of different shape, in contrast to the two micrographs to the left which show smaller clusters or groups of carbon fibers apparently well distributed. Figure 2.4c shows the greyscale histograms constructed from the 4 micrographs of Figure 2.4b. The 2.4 histograms demonstrate how the method allows to differentiate the images with small agglomerates (histograms to the left with only one peak) from those images with large aggregates (histograms to the right with two peaks and, as a consequence, a larger value of variance). Figure 2.5 shows a series of three representative micrographs with different loadings of 0.9, 1.4 and 1.9 vol %, from left to right, for the same PP / 24 LHT XT composite. In general terms, the images give information about an increase in the number of agglomerates randomly distributed as a function of loading. Furthermore, a change in the degree of grey is observed, showing darker levels of grey for the case of 1.9 vol % loading, which is directly related to the lower transparency of the higher loaded samples. The 1.9 vol % micrograph shows a larger number of agglomerates as compared to the other ones. The histograms calculated from these three images (Figure 2.5b) reflect a change from a sample with isolated agglomerates and a dominant presence of a lighter type of grey (0.9 vol %) to an increasing number of large clusters, a darker type of grey-values (indicative of a larger volume concentration of CNFs) and finally a bi-modal-like curve which indicates the largest agglomerates (1.9 vol %). The values of variance as a function of concentrations are shown for all composites in Figure 2.6. From the data it is observed that the composites with

PR24LHTXT fibers show the best dispersion for all fiber loadings. Furthermore, all samples show a similar trend: an increase in the value of variance with increasing CNF loading, indicating increased difficulty in dispersing the CNFs at higher concentrations. All samples show a maximum variance for the concentration of 1.4 vol %, above this concentration the value of the variance decreasing consistently for all samples. This can be explained by an upper limiting characteristic of the analytical method: above a critical concentration, the variance results in narrower dispersion peaks due to the presence of large clusters uniformly appearing over the complete scanned area, thus resulting in consistently darker areas.

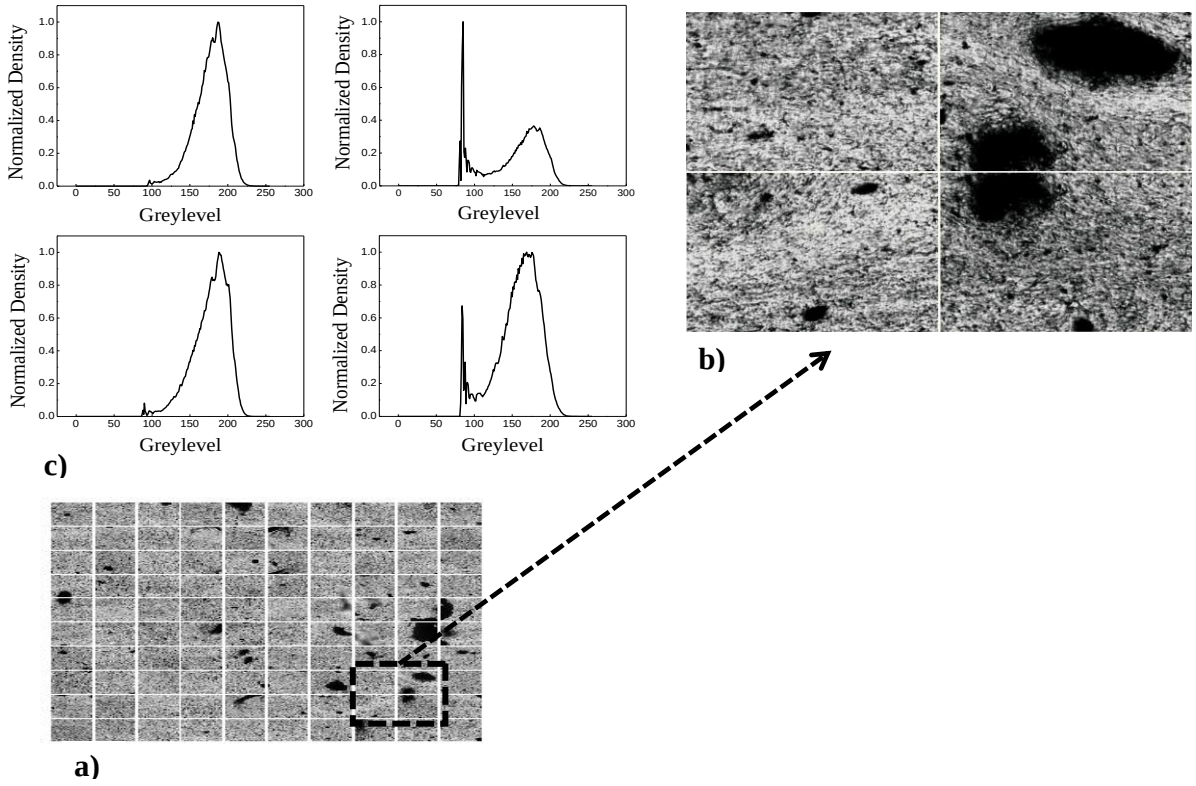

Figure 2. 4 - PP / 24 PR LHT XT CNFs composites at 0.5 vol %: **a** Composition of 100 adjacent micrographs representative of approx. 2.3 mm^2, **b** four adjacent images of 175 x 135 µm, **c** histograms (density vs. greylevel) corresponding to the four adjacent micrographs presented in Figure 2.4b.

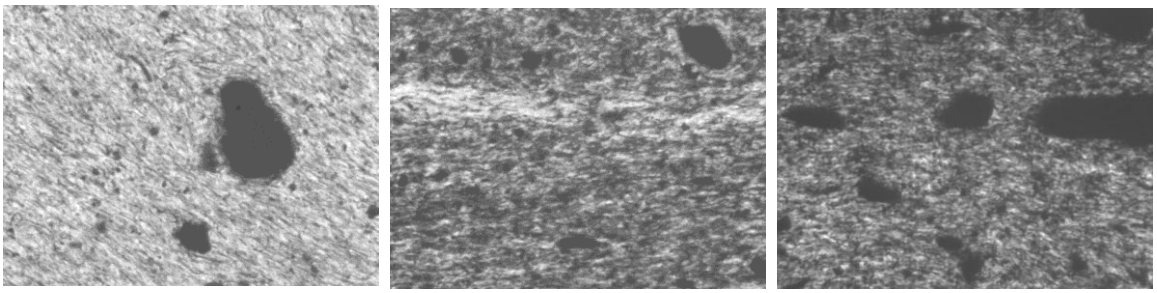

a)

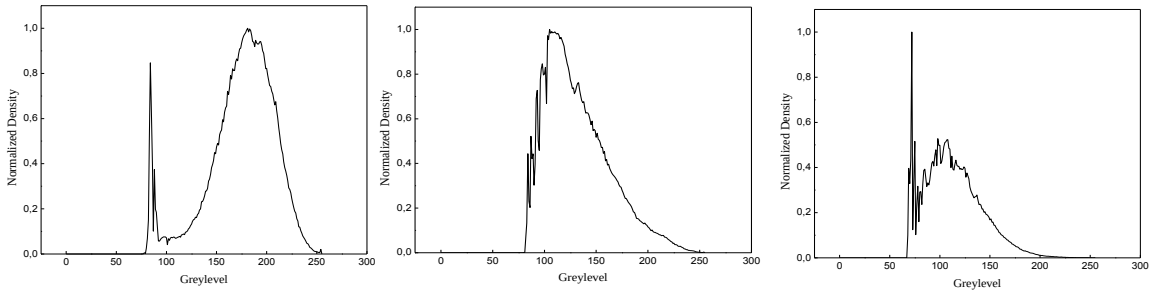

b) **0.9 vol %** **1.4 vol %** **1.9 vol %**

Figure 2. 5 - Representative micrographs (170 x 135 μm) for the PP / PR 24 LHT XT composites with loadings of 0.9, 1.4 and 1.9 vol % (from left to right) and the corresponding histograms **b** calculated from the micrographs.

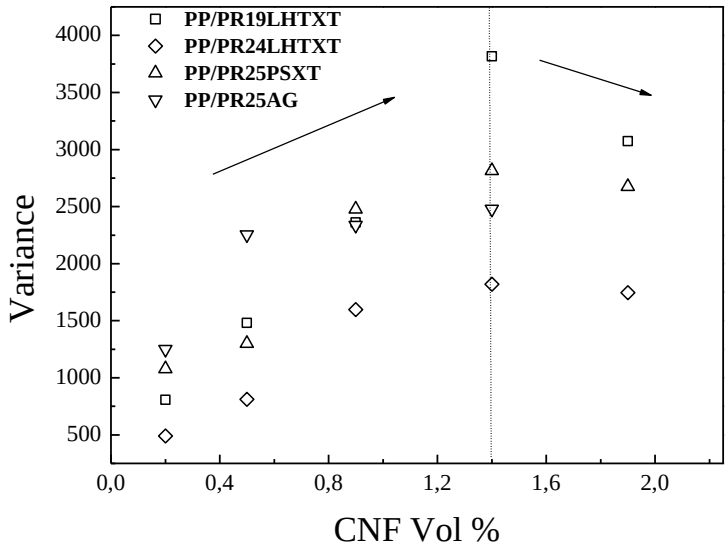

Figure 2. 6 - Variance as a function of CNF loading for the different composites.

2.3.2 Thermal Behaviour

DSC analyses were performed in order to obtain information about the influence of different carbon nanofibers on the melting and crystallization behaviour of polypropylene. DSC thermographs for PP / PR 25 PS XT nanocomposites as a function of CNF content are shown in Figure 2.7a, whereas thermographs for all nanocomposites at 0. 9 vol % of CNFs are showed in Figure 2.7b. Table 2.3 shows the compilation of the main parameter obtained from the DSC scans for PP and the composites with different CNF corresponding to second heating scan.

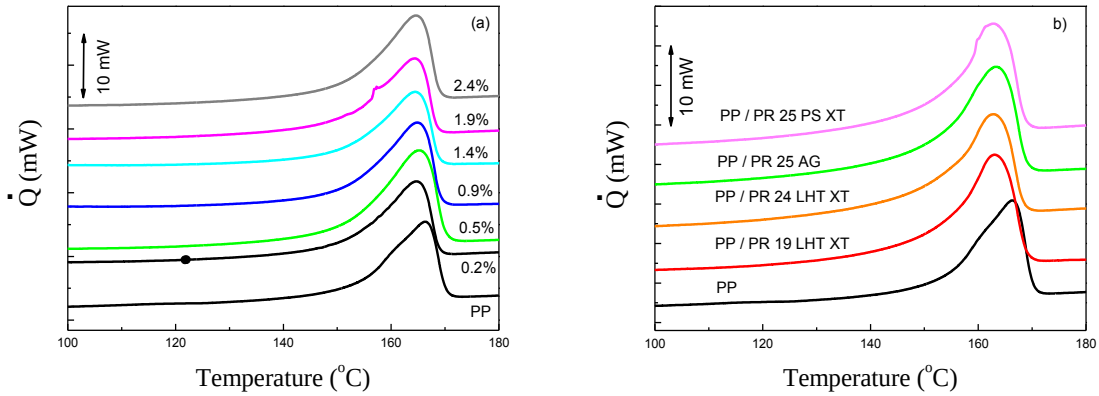

Figure 2. 7 - DSC thermographs for PP / CNFs nanocomposites: **a** PP / PR 25 PS XT nanocomposites for all loadings, **b** the different nanocomposites with a 0.9 vol % content of CNF.

All composites and concentrations show a single melting (Figure 2.7) and crystallization (cooling scans, not shown) peak corresponding to the melting of the crystalline phase of the PP. The crystallization temperature, *Tc*, (Table 2.3) decreases slightly with respect to pure PP independently of the type of CNF. On the other hand, the melting temperature, T_m, of the PP was 165,3 ºC, whereas the T_m of the composites was somewhat lower independently of CNFs´ type (Table 2.3). The decrease of T_c is to be ascribed to a reduction in crystallite size in the presence of CNFs: the CNF causing a more heterogeneous crystallization, reducing size and perfection of the polymer crystals [22].

The degree of crystallinity , ΔX_c , was calculated using equation 2.1:

$$\Delta Xc = \frac{\Delta H_m}{\Delta H_0} \times 100\ \% \quad (2.1)$$

where ΔH_m is the sample melting enthalpy and ΔH_0, is the melting enthalpy of the 100% crystalline PP, which was reported to be 207 J.g-1 [23].

The incorporation of CNF into the polymer matrix is accompanied by an increase of crystallinity from 38 % for the PP up to around 46 % for the nanocomposites (Table 2.3), related to the promotion of a more heterogeneous crystallization of the polymer by the fillers [24]. This effect was observed even for the lower CNF concentrations. The variations due to the filler concentration (not shown) or filler type (Table 2.3) in composites are not significant in all composites.

Sample	Tm (^{0}C)	Tc (^{0}C)	ΔHm (J/g)	ΔX / %
PP	165.3	127.3	77	38
PP/PR19LHTXT	162.4	123.5	89.6	44.2
PP/PR24LHTXT	162.4	123	92.85	45.8
PP/PR25PSXT	162.4	124.3	94.07	46.4
PP/PR25AG	162.9	123.8	92.83	45.8

Table 2. 3 - DSC data of neat PP and PP / CNF nanocomposites at 0.9 vol %**.**

2.3.3 Thermal stability of composites

Thermogravimetric analysis, TGA, was used to evaluate the thermal degradation of PP and nanocomposites and the filler matrix interaction [24].

Figure 2.8 shows the TGA data obtained for PP and for the PP / PR 19 LHT XT and PP / PR 25 PS XT composites with different filler contents. All samples show a major weight loss process between 300 and 450 ºC due to degradation of polymeric matrix.

From the TGA experiments the initial temperature, $T_{initial}$, defined as the temperature at which the material begins to lose its mass, and the onset temperature, T_{onset}, calculated by extending the pre-degradation portion of the curve to the point of the interception with a line drawn as a tangent to the steepest portion of the mass curve occurring during degradation [25-27] were

identified. These two temperatures, $T_{initial}$ and T_{onset}, together with the maximum of derivative thermogravimetric analysis, DTGA, defined as the temperature of maximum loss weight rate, are including in Table 2.4 for the different composites.

The degradation temperature increases with increasing fiber loading, being nevertheless differences for the different fillers. The enhanced thermal stability of PP / PR 25 PS XT nanocomposites (Figure 2.8b) compared with PP / PR 19 LHT XT nanocomposites (Figure 2.8a), is ascribed to a better interaction between the polymer matrix and the filler that was observed in SEM. In this regard, it has been proposed that the CNFs surface absorbs the free radical produced by the decomposition of PP, which retards the nanocomposites´ thermal degradation [28]. Moreover, for the PR 25 PS XT nanocomposites, it was noticed that a small amount of 0.2 vol % of CNFs affects the PP degradation process significantly, whereas for filler loadings higher than 1.4 vol %, the thermal behavior improvement remains practically unaltered.

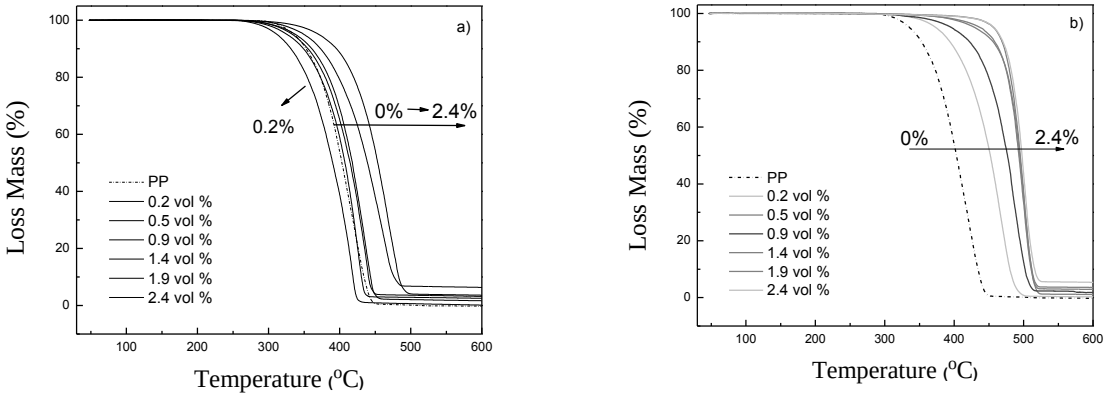

Figure 2. 8 - TGA results for **a** PP / PR 19 LHT XT composites with different fillers contents and **b** PP / PR 25 PS XT composites obtained at 20 ºC/min.

Sample	T_{onset} (ºC)	T_{max} (ºC)	Ea (kJ/mol)	ln A	R
PP	367	424	118,1	15,35	0,999
PP /PR19LHTXT					
0.2 vol %	363	417	93,91	11,18	0,999
0.5 vol %	373	422	91,51	10,15	0,997
0.9 vol %	386	433	96,04	10,69	0,998
1.4 vol %	386	439	95,01	10,66	0,999
1.9 vol %	416	467	103,12	11,01	0,999
2.4 vol %	410	455	95,21	10,17	0,997
PP /PR24LHTXT					
0.9 vol %	412	449	114,97	13,47	0,996
PP /PR25PSXT					
0.2 vol %	421	467	112,80	12,83	0,999
0.5 vol %	462	496	91,92	9,36	0,998
0.9 vol %	463	481	109,79	11,44	0,992
1.4 vol %	474	498	166,01	20,03	0,991
1.9 vol %	482	501	305,53	42,85	0,998
2.4 vol %	484	505	273,51	37,49	0,996
PP /PR25AG					
0.9 vol %	365	420	90,07	10,30	0,992

Table 2. 4 - TGA data of neat PP and PP / CNF nanocomposites.

2.3.4 Kinetic analysis of thermal decomposition

To complete the thermal degradation study, the thermal degradation kinetics was obtained for all composites. Kinetic parameters such as, activation energy, Ea, and pre-exponential factor, *A*, for the thermal decomposition of PP and nanocomposites have been determined using Coats-Redfern, CR, method [29]. Other authors used successfully this method for the thermal degradation study of other polymer systems [30-32].

This method makes use of an asymptotic expression to determine both Ea and A, following the equation:

$$ln\frac{g(\alpha)}{T^2} = ln\ \frac{AR}{qE}\left(1-\frac{2RT}{E}\right) - \frac{E_a}{RT} \quad (2.2)$$

where

$$g(\alpha) = \left\{\frac{1-(1-\alpha)^{1-n}}{(1-n)}\right\} for\ (n\ \neq 1) \quad (2.3)$$

and

$$g(\alpha) = -\ln(1-\alpha)\ for\ (n=1) \quad (2.4)$$

According to the above equation, a plot of ln $\left[\frac{g(\alpha)}{T^2}\right]$ vs. 1/T should result in a straight line with a slope equal to −Ea / R, for the correctly chosen value of n. The order (n) of decomposition reaction was determined from the best linear fit of the kinetic curve (shown in Figure 2.9) which gives the maximum correlation coefficient. The curves are fitted by the method of lest squares, in the range of conversion $0.05 < \alpha < 0.30$. For all the fittings, R is higher of 0,997. From the slope of the curve and from the intercept, the values of Ea and A were calculated respectively. Finally, the Arrhenius equation (equation 2.5) was used to calculate the rate constants for the thermal decomposition of PP and nanocomposites. The results are included in Table 2.4.

$$k = A\exp\left(-\frac{E_a}{RT}\right) (2.5)$$

The activation energy of degradation of PP was found to be about 118,1 kJ/mol, similar to the value obtained for other authors [32-37]. In the case of PR 19 LHT XT, the activation energy maintains practically constant around 100 kJ.mol-1 with increasing filler content (Table 2.4 and Figure 2.10). On the other hand, for the PR 25 PS XT nanofibers, a continuous increase is observed with increasing CNT content (Table 2.4 and Figure 2.10) which is ascribed to the stronger interaction between the PR 25 PS XT nanofibers when compared to the PR 19 LHT XT ones. All the values of R are higher than 0,990.

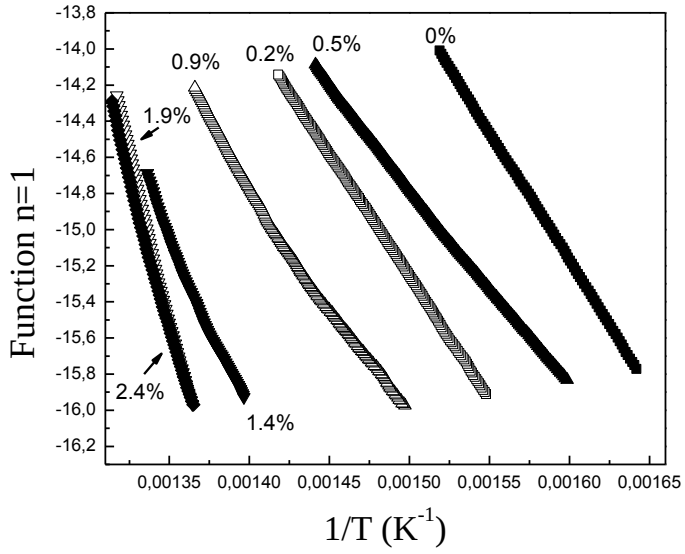

Figure 2. 9 - Coats and Redfern plots of the PP / PR 25 PS XT composites at different volume fractions.

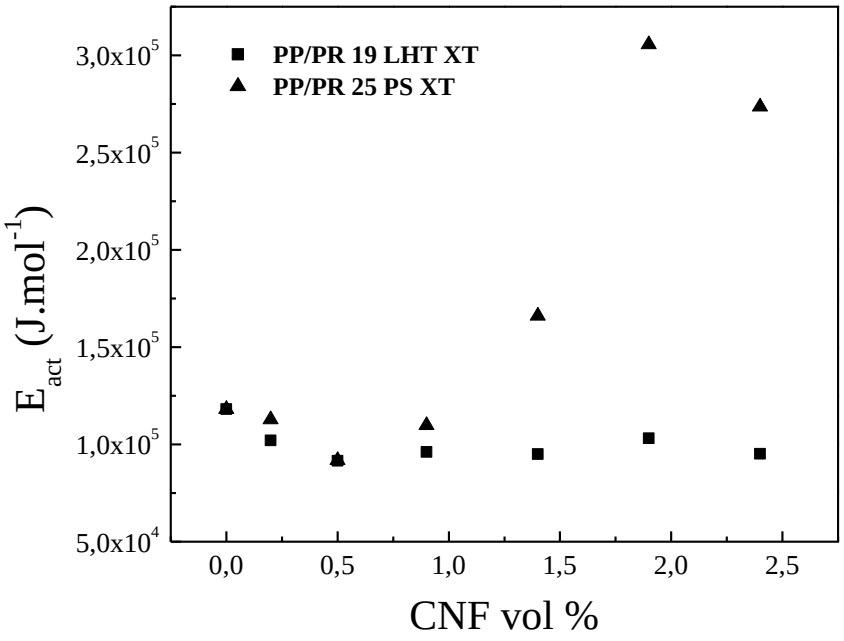

Figure 2. 10 - Activation energy for PP / PR 19 LHT and PP / PR 25 PS XT composites as a function of volume fraction.

It is worthwhile to note that the reactions involved during the polymer degradation follow complex mechanisms and each one has its own activation energy. Accordingly, it is difficult to draw conclusions because of from the C-R method only global activation energy can be calculated. However, this method is good enough to compare the behaviour of different composites.

2.3.5 Mechanical Properties

The elastic modulus of the neat PP and CNFs nanocomposites obtained though strain-stress measurements is shown in Figure 2.11. Overall a gradual and similar improvement in modulus with loading is noted independently of the type of CNFs. In particular, the PP / PR 19 LHT XT and PP / PR 25 PS XT nanocomposites show better performance with an improvement of 29 and 32 % in Young´s modulus for CNF loadings of 0.9 and 2.4 vol %, respectively. The combination of larger diameter together with heat treatment to temperatures of 1500 º C, demonstrates to have good effect in mechanical performance for the first case, whereas for the second case, the disordered pyrolitically stripped layer seems to promote better adhesion between matrix and this particular kind of fiber, as it is revealed by SEM (Figure 2.2c).

The comparison of the variance parameter obtained in the GSA analysis and the Young modulus show a correlation, both increasing as a function of fiber fraction is observed in both curves (Figure 2.6 and Figure 2.11) up to a value which occurs at 1.4 vol % CNF loading (for the variance´s case), and between 0.9 and 1.4 vol %, depending on the type of CNF (for the elastic modulus´ case).

These facts are consistent with the study by Gershon et al. with PR-19 CNFs in HIPS composites processed by TSE [13]. In their analysis, it was determined that at lower loadings of CNF, 70-75% of the CNFs are successfully dispersed by the TSE process. More specifically, a dispersion limit of approximately 3 vol % was calculated. Above this limit the relative volume fraction of the dispersed CNF decreases. In our study, the analysis of variance suggests a dispersion limit of 1.4 vol %. For higher loadings, clustering dominates against CNFs dispersion, which would explain the stabilization of the Young´s modulus for concentrations above 1.4 vol % for all composites.

Nevertheless, the variance should be complemented with other type of morphological analysis if the goal is to find direct relationships between dispersion and final mechanical

properties: the PR 24 LHT XT composites, which show the lowest variance and therefore the better dispersion according to the analysis by GSA, do not exhibit however the best Young´s modulus. This fact is related to the intrinsic physical chemical properties of fiber´s surface which also plays an important role in composite´s mechanical properties for a given degree of dispersion.

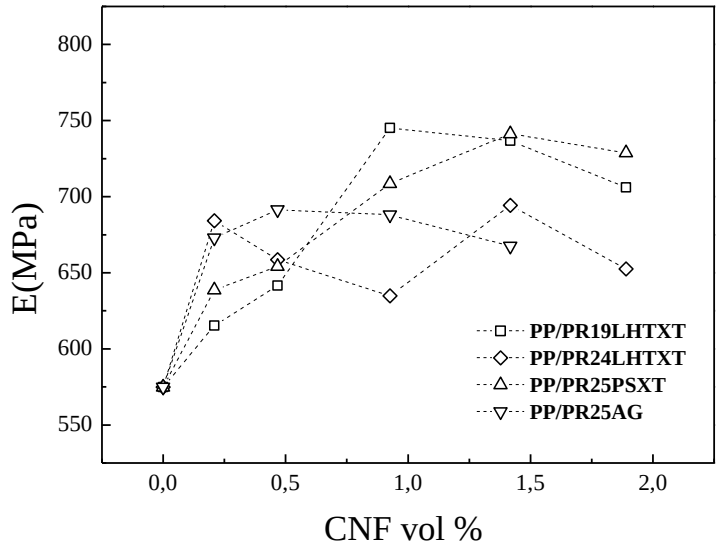

Figure 2. 11 - Tensile modulus average of PP and PP / CNFs composites [21].

2.3.6 Electrical Properties

The electrical volume conductivities of the PP / CNF composites are represented in Figure 2.12 as a function of CNF concentration. The conductivity of the neat PP is close to 10^{-10} S cm^{-1}. In general, except for PP / PR 25 PS XT composites which show to be independent of filler loading, the volume conductivity increases as a function of CNF volume fraction. PP / PR 25 AG composites, on their hand, show a slight increase of the electrical conductivity at 1.4 vol % fiber loading. These two last non-electrically conductive composites probably reach electrical thresholds at higher loading concentrations. PP / PR 19 LHT XT and PP / PR 24 LHT XT nanocomposites, in contrast, show sharp enhancements of the electrical conductivity: for the first case the samples at 0.9 vol % reach electrical conductivity values above 10^{-3} S cm^{-1}, whereas for the PR 24 LHT XT fibers, the most pronounced increase is produced at 0.5 vol %, with values of 10^{-4} S cm^{-1}. In addition, the PR 24 LHT XT fibers with shorter diameters showed to get electrical thresholds with lower content of CNFs and the

maximum values of conductivity. The heat treatment at temperatures of 1500 ºC of PR 24 and PR 19 fibres (LHT grade) with a more ordered structure on the fiber´s surface and better intrinsic conductivity, together with the higher bulk density which allows better distribution and dispersion in the PP, unlike PR 25 fibers, demonstrate superior electrical conducting results for this particular polymer and processing method.

Although the variation of the electrical properties with concentration for polymer/CNF composites is usually understood in the framework of percolation theory, recent studies point out the interparticle and mean tunnelling distance as the main mechanisms for the electrical behaviour [38-41]. Further, models involving the formation of capacitor networks seem to be more suitable to explain low percolation thresholds [42]. A further discussion about conductivity in these two types of electrical conducting PP / CNFs nanocomposites has been recently published [21].

In general, with the processing by TSE it is possible to tailor electrical conductivity. The conductive samples in the neighbourhood of the electrical thresholds are well within the range of electrostatic dissipative materials (10^{-12}-10^{-6} S cm^{-1}), (ESD). At the same time, for the highest loadings, the composites demonstrate to offer protection from electromagnetic interference (10^{-6}-10^{-1} S cm^{-1}), (EMI).

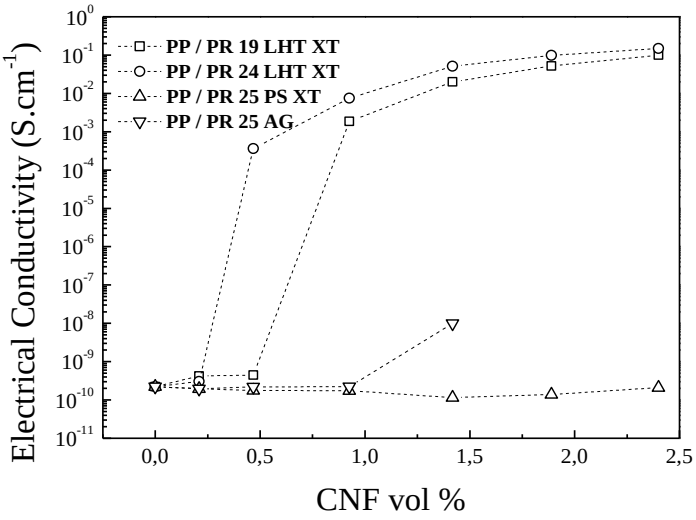

Figure 2. 12 - Electrical conductivity values versus volume fraction loadings of CNFs for the various composites [21].

Finally, it is possible to observe that for the fibers better structurally tailored for conductivity (LHT grade fibers), the lower variance for PR 24 LHT XT as compared to the PR 19 LHT XT composites obtained from the GSA analysis, correlates well with the higher conductivity values and the lower threshold level. If cluster distribution seems to be more important than nanofibers´ dispersion for obtaining low percolation thresholds and high conductivity values, then this method which quantifies clusters dispersion at resolutions of approximately 1 μm (1000 nm) may be a possible indicator to correlate with conductivity [41].

2.4 Conclusions

A quantitative method based on transmitted light optical microscopy by means of greyscale analysis, GSA, is used to determine the dispersion of PP / CNFs composites fabricated by twin screw extrusion, TSE. In addition, the electrical conductivity, morphology, thermal and mechanical properties were characterized and correlated with GSA. Different CNF have been used to prepare PP / CNFs composites and evaluate the variation of the main physical parameters as a function of fiber type and content.

Nanocomposites fabricated with CNFs with highly graphitic outer wall layers (PR 19 LHT XT and PR 24 LHT XT) revealed to have good electrical performance with a significant increase in volume conductivity for 0.5 vol %, in nanocomposites with CNFs which have the shortest diameter (PR 24 LHT XT). Nanocomposites fabricated also with highly graphitic outer wall layers and larger diameters (PR 19 LHT XT), showed to have good mechanical and electrical performance, the combination of fiber structure, aspect ratio together with heat treatment to temperatures of 1500 º C, demonstrated to have good effect in both final properties. Nanocomposites fabricated with disordered pyrolitically stripped layer type of CNFs (PR 25 PS XT), revealed to have good mechanical performance with an increase of 32 % in Young´s modulus for 2.4 vol % and enhanced thermal stability, which may be the result from the better adhesion between PP and this particular nanofiber´s type. In contrast, composites with PR / 25 PS XT and PR 25 AG fibers showed no relevant increase of the electrical conductivity for all filler loadings. Overall, thermogravimetric analysis (TGA) showed shift to higher temperatures of the main thermal degradation of the polymer with the addition of CNFs. Differential scanning calorimetry (DSC) indicated an enhancement of the

degree of crystallinity with the inclusion of the filler, being practically independent on the fiber content and type.

The results from analysis by GSA indicated a good correlation between variance and filler concentration. Furthermore, the analysis by GSA suggests that a dispersion limit, (related to the dispersions´ capacity in processing by TSE), was attained at 1.4 vol %. Above this limit a majority of fiber clustering, possibly correlated with only slight changes in Young´s modulus, was observed. On the other hand, the cluster´s dispersion and distribution quantified by GSA can be used as an indicator for electrical conductivity levels for the fibers structurally tailored for conductivity.

Finally, the present study shows that the final properties of the composites strongly depend on fiber structure and content.

Acknowledgements

Financial support for this work has been provided by Consellería de Educación e Ordenación Universitaria, Xunta de Galicia through grant CN2011/008. The support of Applied Sciences Inc. for generously supplying the CNFs used. We would also like to thank Carla Leer and Patrick Lake for their assistance in the production of the CNF composites. A. J. Paleo wants to thank to IP-SME Pegasus through grant NMP2-CT-2006-026673.

References

1. Bethune, D.S., Kiang, C.H., Devries, M.S., Gorman, G., Savoy, R., Vazquez, J., et al.: Cobalt-catalyzed growth of carbon nanotubes with single-atomic-layerwalls. Nature. **363**(6430), 605-607 (1993).

2. Iijima, S., Ichihashi, T.: Single-shell carbon nanotubes of 1-nm diameter. Nature. **364**(6439), 737-737 (1993).

3. Iijima, S.: Helical microtubules of graphitic carbon. Nature. **354**(6348), 56-58 (1991).

4. Kang, I.P., Heung, Y.Y., Kim, J.H., Lee, J.W., Gollapudi, R., Subramaniam, S., et al.: Introduction to carbon nanotube and nanofiber smart materials. Compos. Part B: Eng. **37**(6), 382-394 (2006).

5. Burton, D.J., Glasgow, D.G., Lake, M.L., Kwag, C., Finegan, J.C.: Influence of carbon nanofiber surface characteristics on composite properties. In: Repecka L, Saremi FF (eds) Soc Advancement Material & Process Engineering. Covina (2001).

6. Gordeyev, S.A., Macedo, F.J., Ferreira, J.A., van Hattum, F.W.J., Bernardo, C.A.: Transport properties of polymer-vapour grown carbon fibre composites. Physica B. **279**(1-3), 33-36 (2002).

7. Tibbetts, G.G., McHugh, J.J.: Mechanical properties of vapor-grown carbon fiber composites with thermoplastic matrices. J. Mater. Res. **14**(7), 2871-2880 (1999).

8. Forro, L., Schonenberger, C.: Physics of Multiwall-Carbon nanotubes. Phys. World. **13** (6), 37-41 (2000).

9. Lozano, K., Barrera, E.V.: Nanofiber-reinforced thermoplastic composites. I. Thermoanalytical and mechanical analyses. J. Appl. Polym. Sci. **79**(1), 125-133 (2001).

10. Chipara M, Lozano K, Hernandez A, Chipara M. TGA analysis of polypropylene-carbon nanofibers composites. Polymer Degradation and Stability. **93**(4):871-876. (2008).

11. Lillehei, P.T., Kim, J-W., Gibbons, L.J., Park, C.: A quantitative assessment of carbon nanotube dispersion in polymer matrices. Nanotechnology **20**(32), 325708-325714 (2009).

12. Andrews, R., Jacques, D., Minot, M., Rantell, T.: Fabrication of carbon multiwall nanotube/polymer composites by shear mixing. Macromol. Mater. Eng. **287**(6), 395-403 (2002).

13. Gershon, A.L., Cole, D.P., Kota, A.K., Bruck, H.A.: Nanomechanical characterization of dispersion and its effects in nano-enhanced polymers and polymer composites. J. Mater. Sci. **45**(23) 6353-6364 (2010).

14. Lozano, K., Bonilla-Rios, J., Barrera, E.V.: A study on nanofiber-reinforced thermoplastic composites (II): Investigation of the mixing rheology and conduction properties. J. Appl. Polym. Sci. **80**(8), 1162-1172 (2001).

15. Kashiwagi, T., Fagan, J., Douglas, J.F., Yamamoto, K., Heckert, A.N., Leigh, S.D., et al.: Relationship between dispersion metric and properties of PMMA/SWNT nanocomposites. Polymer **48**(16), 4855-4866 (2007).

16. Sumfleth, J., Adroher, X.C., Schulte, K.: Synergistic effects in network formation and electrical properties of hybrid epoxy nanocomposites containing multi-wall carbon nanotubes and carbon black. J Mater. Sci., **44**(12), 3241-3247 (2009).

17. Vera-Agullo, J., Gloria-Pereira, A., Varela-Rizo, H., Gonzalez, J.L., Martin-Gullon, I.: Comparative study of the dispersion and functional properties of multiwall carbon nanotubes and helical-ribbon carbon nanofibers in polyester nanocomposites. Compos. Sci. Technol. **69**(10), 1521-1532 (2009).

18. Brooker, R.D., Guild, F.J., Taylor, A.C.: Quantifying the dispersion of carbon nanotubes in thermoplastic-toughened epoxy polymers. J. Mater. Sci. **46**(9), 3108-3118 (2011).

19. van Hattum, F.W.J., Leer, C., Carneiro, O.S., Maruyama, B.: Quantitative Assessment of Mixing Quality in Nanoreinforced Polymers Using a Multi-Scale Image Analysis Method in 38th SAMPE Fall Technical Conference (2006).

20. Applied Sciences, Inc. Cedarville. http://www.apsci.com (2001).

21. Paleo, A.J., van Hattum, F.W.J., Pereira, J., Rocha, J.G., Silva, J., Sencadas, V., et al.: The piezoresistive effect in polypropylene-carbon nanofibre composites obtained by shear extrusion. Smart. Mater. Struct. **19**(6), 065013-065019 (2010).

22. Sui G, Zhong W-H, Fuqua MA, Ulven CA. Crystalline structure and properties of carbon nanofiber composites prepared by melt extrusion. Macromolecular Chemistry and Physics. **208**(17):1928-1936 (2007).

23. Yuan Q, Misra RDK. Impact fracture behavior of clay-reinforced polypropylene nanocomposites. Polymer. **47**(12):4421-4433 (2006).

24. Lee S, Hahn JR, Ku B-C, Kim J. Effect of Carbon Nanofiber Structure on Crystallization Kinetics of Polypropylene/Carbon Nanofiber Composites. Bulletin of the Korean Chemical Society. **32**(7):2369-2376 (2011).

25. Turi E. Thermal Characterization of Polymeric Materials. New York 1997.

26. Kim JY, Kim DK, Kim SH. Thermal decomposition behavior of poly(ethylene 2,6-naphthalate)/silica nanocomposites. Polymer Composites. **30**(12):1779-1787 (2009).

27. Li X-G, Huang M-R. Thermal degradation of Kevlar fiber by high-resolution thermogravimetry. Journal of Applied Polymer Science. **71**(4):565-571 (1999).

28. Chen X, Wei S, Yadav A, Patil R, Zhu J, Ximenes R, et al. Poly(propylene)/Carbon Nanofiber Nanocomposites: Ex Situ Solvent-Assisted Preparation and Analysis of Electrical and Electronic Properties. Macromol Mater Eng. **296**(5):434-443 (2011).

29. Coats A.W., Redfern J.P., Kinetic parameters from thermogravimetric data**,** Nature (1964), 201, 68-9.

30. Abad M.J., Barral L., Cano J., López J., Nogueira P., Ramirez C., Torres A., Thermal decomposition behaviour and the mechanical properties of an epoxy/cycloaliphatic amine resin with ABS, European Polymer Journal, 37, 1613-1623, (2001).

31. Jose S., Thomas P.S., Thomas S., Karger-Kocsis J., Thermal and crystallisation behaviours of blends of polyamide 12 with styrene-ethylene/butylene-styrene rubbers, Polymer 47, 6328-6336, (2006).

32. Gonzalez J., Albano C., Scianana R., Ichazo M., Rosales C., Martinez J., Candal M., Dynamic termal decomposition of blends of polyamide 6 with funcitionalized and non-functionalized PP, Polym. Deg. Stab. 68, 9-19 (2000).

33. Jun, HC., Lee, HP., Yi, SC., Yoo, KO., Oh SC., A kinetic analysis of the thermal-oxidative decomposition of polypropylene, Journal of Fire Sciences, 18(4), 245-264 (2000).

34. Saikrasun S., Saengsuwan S., Thermal decomposition kinetics of in situ reinforcing composite based on polypropylene and liquid crystalline polymer, Journal of materials Processing Technology, 209 (7), 3490-3500 (2009).

35. Pehlivan H., Balkose, D., Ulku, S., Tihminlioglu, F., Effect of zeolite filler on the thermal degradation kinetics of polypropylene, Journal of Applied Polymer Science, 101(1), 143-148 (2006).

36. Rakkhimkulov, AD., Lomakin, SM., Dubnikova, IL., Shchegolikhin, AN., Davidov, EY., Kozlowski, R., The effect of multi-walled carbon nanotubes addition on the thermo-oxidative decomposition and flammability of PP/MWCNT nanocomposites, Journal Mater Sci, 45(3), 633-640 (2010).

37. Dogan, F., Sirin, K., Kaya, I., Balcan, M., The influence of $CaCO_3$ filler component on termal decomposition process of PP/LDPE/DAP ternary blend, Polym Adv Technologies, 21(7), 512-519 (2010).

38. Stauffer, D., Aharony, A.: Introduction to Percolation Theory. Taylor and Francis, London (1994).

39. Stroud, D., Bergman, D.J.: Frequency-dependence of the polarization catastrophe at a metal-insulator-transition and related problems. Phys. Rev. B **25**(3), 2061-2064 (1982).

40. Nan, C.W.: Physics of inhomogeneous inorganic materials. Prog. Mater. Sci. **37**(1), 1-116 (1993).

41. Cardoso, P., Silva, J., Paleo, A.J., van Hattum, F.W.J., Simoes, R., Lanceros-Mendez, S.: The dominant role of tunneling in the conductivity of carbon nanofiber-epoxy composites. Phys. Status Solidi A-Appl.Mat. **207**(2), 407-410 (2010).

42. Simoes R, Silva J, Vaia R, Sencadas V, Costa P, Gomes J, et al. Low percolation transitions in carbon nanotube networks dispersed in a polymer matrix: dielectric properties, simulations and experiments. Nanotechnology. **20**(3):8. (2009).

Chapter 3 - Rheological and electrical analysis in carbon nanofibre reinforced polypropylene composites

Abstract.

Two different types of carbon nanofibers, CNFs, were incorporated in the same polypropylene, PP, matrix by twin-screw extrusion under the same processing conditions. The electrical characterization of both CNFs / PP composites as a function of volume fraction show different electrical performance: conducting and non-conducting. The principal objective of this work is to study the rheological behaviour of both composites with the aim of relating it to the electrical behaviour. The experimental results indicate that the rheological behaviours are also different, suggesting that rheology differentiates the microstructural variations responsible for the electrical conducting performance. Furthermore, the main rheological parameters were correlated to the electrical conductivity. The results show that inverse of loss tangent, G′/ G′′, and, in less extent, the storage modulus, G′, are the most sensitive parameters when compared to the onset of electrical percolation. Finally, in spite of the intrinsic measuring differences between electrical and rheological analysis, the two calculated percolation thresholds are very similar: ~ 0.5 for the rheological threshold and ~ 0.4 for the electrical threshold.

3.1 Introduction

Several nanostructures composed of graphitic layers, including nanographene platelets, NGPs, carbon nanofibers, CNFs and nanotubes, CNTs are currently the focus of intense investigation. CNFs in particular have a unique morphology in which exposed graphene edge planes are placed on the outer surface of the fiber [1]. Their outer diameter, which ranges from 50 to 200 nm, is slightly larger than CNTs. The inner diameters and lengths range from 30 to 90 nm and from 50 to 100 μm, respectively [2, 3]. Furthermore, their excellent electrical, thermal and mechanical characteristics as well as their simple incorporation and dispersion into polymers at a lower cost in comparison to carbon nanotubes, have converted CNFs into an object of study in several fields of materials science [4, 5].

An important area of application of carbon nanofibers is in the field of composite materials. By incorporating relatively small loadings of CNFs in a polymer matrix, electrically conductive composites can be produced, while at the same time increasing its mechanical properties. Some of the final uses of these CNFs based polymer composites are electrostatic dissipative, ESD, electromagnetic interference, EMI, and radio frequency interference, RFI materials [6, 7].

Up to now, the majority of research in CNTs and CNFs based polymer composites has been motivated by the importance of several key-factors for the development of conducting and structural multifunctional materials: composites morphology, analysis of dispersion and distribution of nanofillers in the polymer, polymer-nanofiller interactions and the lowest loading required for conductive network formation [4], [8], [9], [10] and [11].

Additionally, it has been commonly established that rheological analysis, besides being a method to study viscoelastic properties to assess processing behavior, provides insights on the interaction between carbon nanostructures and polymer in the melt state [12] and [13]. Kharchenko et. al characterized the transport property transitions in multiwall nanotubes dispersed in polypropylene. In their study the electrical threshold (0.0025 volume fraction) precedes the rheological threshold (0.01 volume fraction), based on the rheological analysis of the inverse of loss tangent , G´/G´´ [14]. By plotting G´ as a function of nanotube loading in single-walled carbon nanotube / poly(methyl methacrylate), PMMA, nanocomposites, Du et. al reported a rheological threshold of 0.12 wt %, whereas a value of 0.39 wt % was obtained for the electrical threshold. In this study, the onset of viscoelastic behavior was

explained as the loading from which the distance between nanotube´s clusters is shorter than the size of the polymer chain causing restriction of polymer motion [12]. More recently, in their attempt to compare quantitatively electrical with rheological values in polystyrene, PS, containing MWCNTs, Kota et. al conclude that the storage modulus, G´, and G´/G´´, rheological parameters related to the elastic load transfer, are more sensitive to the onset of electrical percolation than η* and G´´, rheological parameters related to dissipation mechanisms [15].

Though several attempts to correlate conductivity with rheological properties have been discussed in CNT based polymer nanocomposites, there are only few studies focused on the investigation of percolation thresholds through electrical and rheological analysis of CNF based polymer nanocomposites [16]. Furthermore, to our knowledge, there is no investigation evaluating rheological and electrical properties in electrical and non-electrical conducting composites with the aim of discussing if rheological analysis allows distinguishing electrical conducting from electrical isolating response in this kind of systems. Besides, in order to compare electrical with rheological thresholds, the most sensitive rheological parameter is calculated. The work has been performed with two different CNFs incorporated in the same polypropylene matrix through twin-screw extrusion under the same processing conditions.

3.2 Experimental

3.2.1 Materials

A PP powder, Borealis EE002AE, was used as polymer matrix. The two types of stacked-cup CNFs used in this study (PR 24 LHT XT and PR 25 PS XT), commercially known as Pyrograf III^{TM}, were supplied by Applied Sciences, Inc. (ASI, Cedarville, OH, USA). Electrically conducting fibers, PR 24 LHT XT, in the form of a loose powder with a bulk density of ~ 2-4 lb/ft^3 and a highly graphitic outer wall layer, have an average diameter of 80 nm. They have been heat-treated at temperatures of 1500 ºC. Electrically conducting fibers, PR 25 PS XT, with a bulk density of ~ 0.5-3.5 lb/ft^3 and an outer layer consisting on a disordered pyrolytically stripped layer with a large number of graphitic edge sites available along the length, have an average diameter of 120 nm [17] and [18]. They have been heat-treated at temperatures of 600 ºC. Both types of CNFs had a debulking treatment in order to lower their respective bulk densities.

3.2.2 Melt-compounding

PP/CNF nanocomposites were fabricated, under the same processing conditions, on a modular lab-scale intermeshing mini-co-rotating twin-screw extruder, with a screw diameter of 13 mm, barrel length of 31 cm and an approximate L / D ratio of 26, coupled to a cylindrical rod dye of approximate 2.85 mm of diameter. The extruded PP/CNF nanocomposites were then pelletized and pressed into compression-moulded with the appropriate geometries for electrical and rheological tests. A detailed description of the melt-compounding conditions and machining of samples has been previously published [19].

The nomenclature used to designate the composites is summarized in Table 3.1.

Composite Nr	CNF type	CNF grade	Polypropylene	CNFs Loadings
1	PR24	LHT XT	Borealis EE002AE	0.2, 0.5, 0.9, 1.4, 1.9, 2.4 % vol
2	PR25	PS XT		

Table 3. 1 - Composites nomenclature.

3.2.3 Characterization

Morphological characterization and CNF dispersion of the composites were examined using a JEOL JSM-6400 scanning electron microscope (SEM) at an accelerating voltage of 20 kV. The samples were broken under cryogenic conditions and then sputter-coated with a thin layer of gold before testing.

Electrical characterization was performed by measuring the bulk resistance of ten rectangular replicates per sample with an automated Keithley 487 picoammeter/voltage source and then the total average was calculated. The samples´ dimensions were 49 mm x 10 mm x 1 mm. All the experiences were performed at room temperature in direct current, DC, by using the two-probe method. The samples´ extremities were painted with conductive silver paste. The volume conductivity in S m^{-1} was calculated taken into account the geometrical characteristics of the samples [19].

Viscoelastic characterization was performed using a controlled strain rheometer (ARES, TA Instruments) with parallel-plate geometry (25 mm diameter, 2 mm gap) at 190 ºC. Complex viscosity, η*, storage modulus, G', loss modulus, G'' and inverse of loss tangent, G´ / G´´ were measured as a function of frequency, ω. The rheological tests were performed in the

linear viscoelastic region, LVE, where the modulus is independent of strain. The linear viscoelastic region was determined by a strain sweep before testing the viscoelasticity of the composites under a frequency test. At the end, frequency sweep measurements were set up in the frequency range from 1 x 10^{-1} to 10^{2} rad/s.

3.3 Results and Discussion

3.3.1 Morphological analysis

The SEM observations of the 1.9 vol % CNFs filled nanocomposites demonstrate that the two composites reveal different structures. PR 24 LHT XT composites, electrically conducting for 1.9 vol % loading, show that CNFs are well dispersed, distributed and close enough to each other, (Figure 3.1a). PR 25 PS XT composites, in opposite, though show also well distributed and dispersed morphology, exhibit a larger distance between fibers for the same loading of 1.9 vol %. This fact suggests the need of a larger content of CNFs to provide electrical conductive composites (Figure 3.1b).

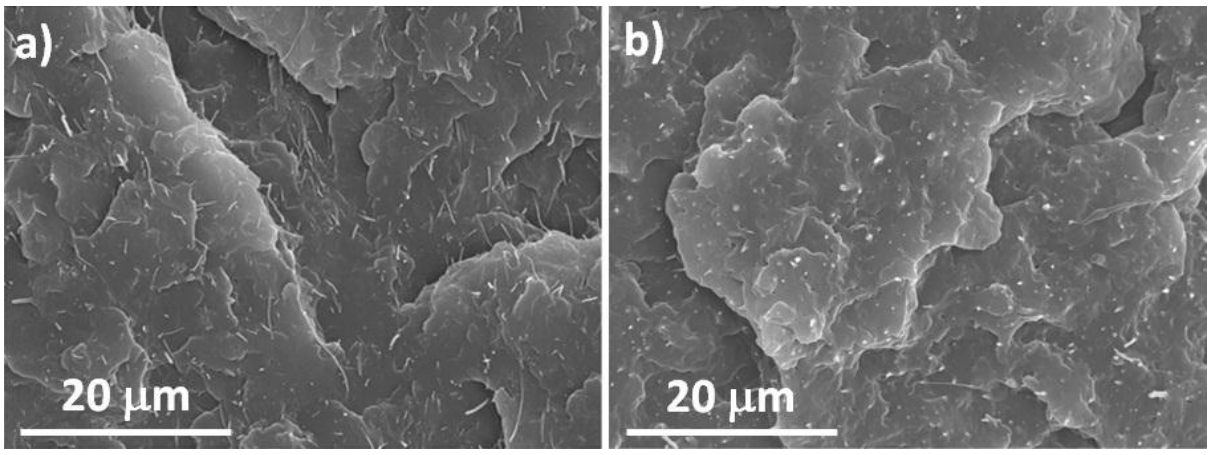

Figure 3. 1 - SEM micrographs of 1.9 vol % PP / CNFs composites: **a** PP / PR 24 LHT XT composites, **b** PP / PR 25 PS XT composites.

3.3.2 Electrical properties in CNFs / PP nanocomposites

The electrical volume conductivity of the neat PP and CNF/PP composites as a function of CNF concentration is represented in Figure 3.2. Each data point on the plot represents the average of 10 samples. Pure PP has an electrical conductivity of 2.22 x 10^{-8} S m^{-1}. PR 24 LHT XT composites increased by 9 orders of magnitude, approaching a value of 14.9 S m^{-1} for 2.4 vol % loading, whereas PR 25 PS XT composites showed no relevant increase of the electrical conductivity for all filler loadings. The heat treatment at temperatures of 1500 ºC of

PR 24 fibres (LHT grade) with a more ordered structure on the fiber´s surface and better intrinsic conductivity, together with the higher bulk density which allows better distribution and dispersion in the PP, unlike PR 25 fibers, demonstrate superior electrical conducting results for this particular polymer and processing method [20].

The variation of the transport properties with dispersion state of carbon-based nanocomposites is usually understood in the framework of the percolation theory [21], [22] and [23]. According to this, the behavior of the conductivity can be described by the following power law relation:

$$\sigma \, \alpha \, (\phi - \phi_c)^{\,t} \quad (3.1)$$

where σ is the electrical conductivity, t is a critical exponent, Φ_c the critical volume fraction and Φ the filler volume fraction. Experimental percolation threshold for PR 24 LHT XT composites is bounded between ~0.2 and ~ 0.5 vol %, as shown in Figure 3.2. More precisely, by means of equation 1, a value of 0.42 vol % ± 0,07 is obtained. The critical exponent value ~1,75 is in agreement with the theoretical 3D values. The critical exponent points out that the conductivity is related to the formation of a 3D network that spans the system, whereas the experimental values of percolation threshold represent a deviation from theoretical prediction associated to the existence of small agglomerates, as previously discussed [19].

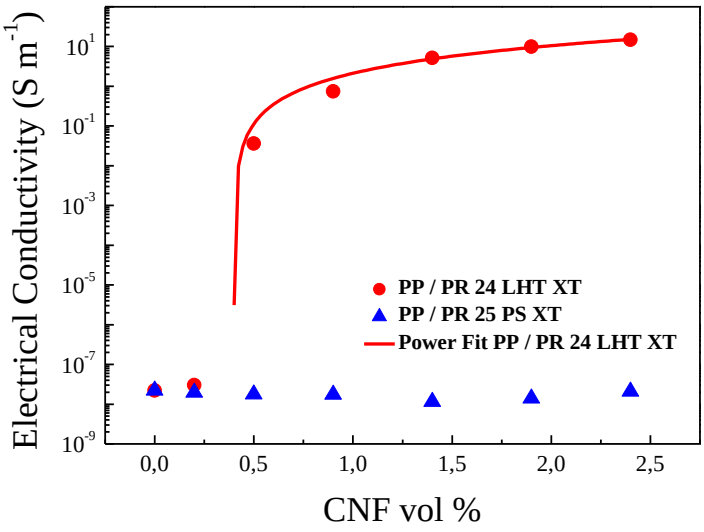

Figure 3. 2 - Electrical conductivity values versus volume fraction loadings of CNFs and corresponding fit using equation 1. R2 is 0.99 for the PP / PR 24 LHT XT composites fitting.

3.3.3 Rheological properties in CNFs / PP nanocomposites

The frequency dependence of the shear storage modulus G´, the loss modulus G´´, inverse of the loss tangent G´/ G´´, and complex viscosity η*, for the two composites with different loadings of CNF, at the temperature used during the extrusion, i. e., 190 ºC, are shown in Figures 3.3, 3.4, 3.5 and 3.6 , respectively. Several common features can be observed. First, a reduction for the two lowest loadings 0.2 and 0.5 vol % compared with the neat PP is observed in all rheological properties which results from that at lower contents of CNFs, the low agglomeration of CNFs allow higher slipperiness in the interlayer PP/CNFs.

The filled composites and the neat PP exhibit similar results due to shear-thinning effect in the high frequency region [24]. Overall, it is accepted that, at low frequencies, viscoelastic behavior shows information about the formation of fibers´ networks at a certain levels of reinforcement [12], while at high frequencies the rheological analysis reflects motions of short molecular chains independently of filler [25].

Particularly in Figure 3.3, the storage modulus, G´, which provides a measure of “stiffness” [26], [12] and [14], is compared for all composites as a function of frequency. For PP / PR 24 LHT XT composites (Figure 3a), for a frequency of 0.1 rad/s, G´ exhibits an abrupt change in

modulus between 0.5 and 0.9 vol % with values of 21 and 860 Pa, respectively, with a maximum of 15411 Pa for 2.4 vol %. A total increase of three orders of magnitude therefore. This point indicates the creation of a continuous filler´s network which restrains the long-range motions of the polymer chains [25]. In addition, at loadings higher than 0.5 vol %, the G´ is clearly less dependent on frequency than for lower volume fractions. This particular response is associated with the transition from liquid-like to solid-like viscoelastic behavior [12].

It has been discussed in previous studies that dispersion plays a key role in the viscoelastic properties of CNT/polymer nanocomposites. In this study, PP / PR 24 LHT XT composites demonstrate to have a low-frequency slope of G´ at the highest loadings of CNFs, which has been associated to good dispersion [12].

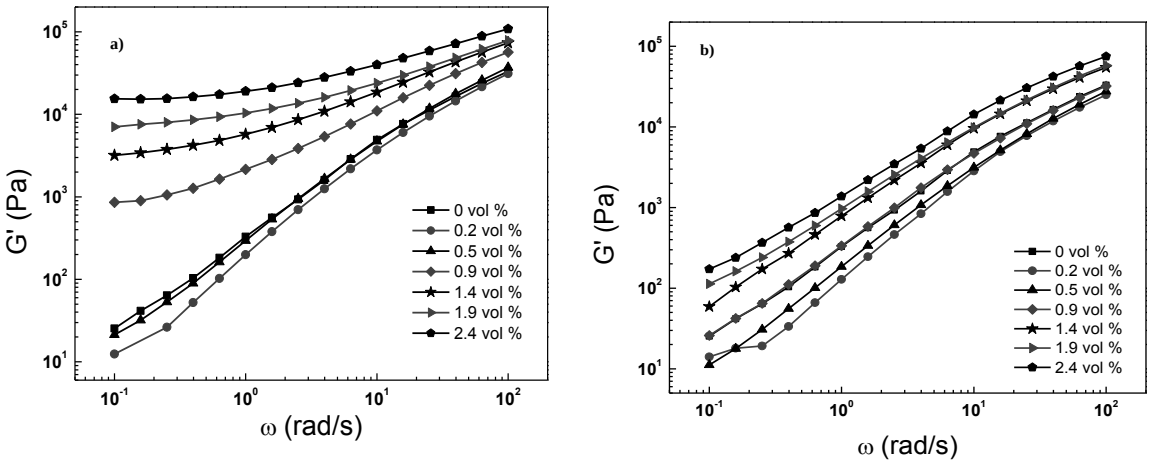

Figure 3. 3 - Storage modulus of **a** PP / PR24LHTXT composites, and **b** PP / PR25PSXT composites as a function of frequency at 190 º C.

PP / PR 25 PS XT composites, on other hand, do not reveal significant changes in behavior compared to pure PP (Figure 3.3b). Further, a modest increase of modulus with a maximum of 173 Pa for 2.4 vol % loading is observed for 0.1 rad/s. According to the above discussion, this behavior together with the frequency dependence of G´ for all volume fractions may indicate that PP / PR 25 LHT XT composites have not formed yet an interconnected structure even at the maximum loading of 2.4 vol %.

The loss modulus, G´´, which provides a measure of viscous resistance to deformation, as a function of frequency, is shown in Figure 3.4. Consistently with storage modulus, at low

frequencies G´´ increases with increasing CNF content for all composites, with exception of the two lowest loading contents of CNF 0.2 and 0.5 vol %. On the other hand, the increase in G´´ is lower than the storage modulus G´ at a fixed CNF content. This lower behavior was already reported [26] and [27]. Again, the increase is more pronounced for PP / PR 24 LHT XT composites, which above a content of 0.9 vol % show a clear change in behavior compared to pure PP. This last circumstance is not observed for PP / PR 25 PS XT composites, which suggests that there is no evidence of interconnected nanofiber´s networks.

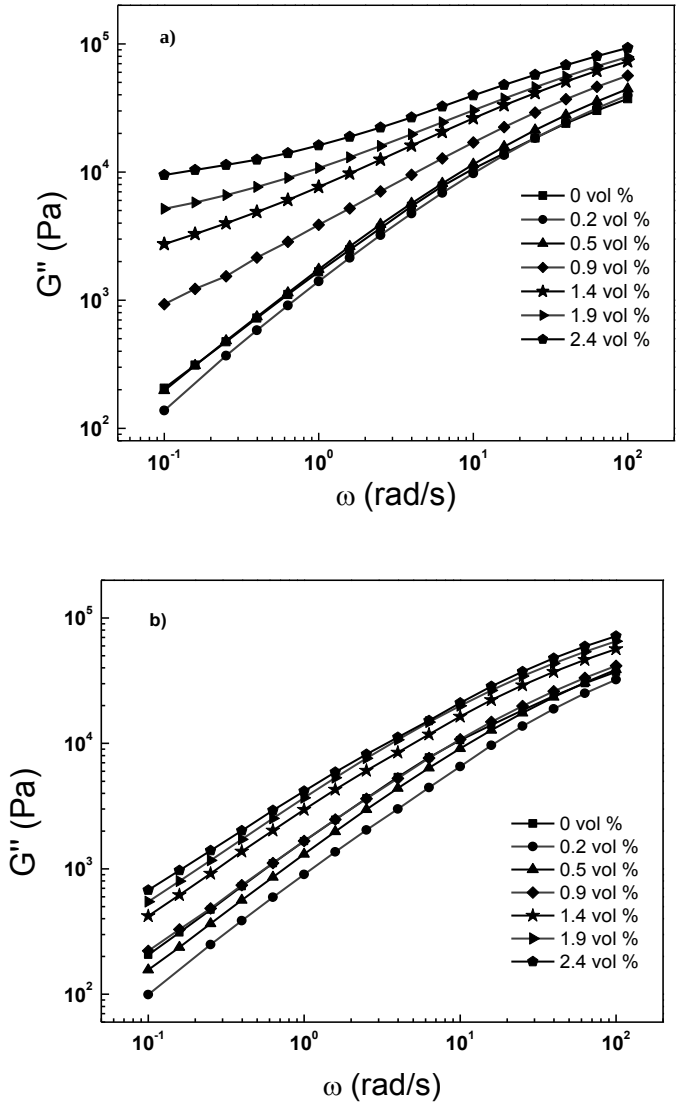

Figure 3. 4 - Loss moduli of **a** PP / PR24LHTXT composites and **b** PP / PR25PSXT composites as a function of frequency at 190 º C.

Supplementary information about interaction between CNFs and the polymer can also be estimated through the inverse loss tangent, G´´/G´ (Figure 3.5), which relates elastic, G´ with

dissipative, G´´ characteristics of the composites [14]. The curves follow the same trend of G´ and G´´. Nevertheless, it is important to highlight the sharp variation between 0.5 and 0.9 vol %, as it happens with G´ for the same content of CNF, in PP / PR 24 LHT XT composites.

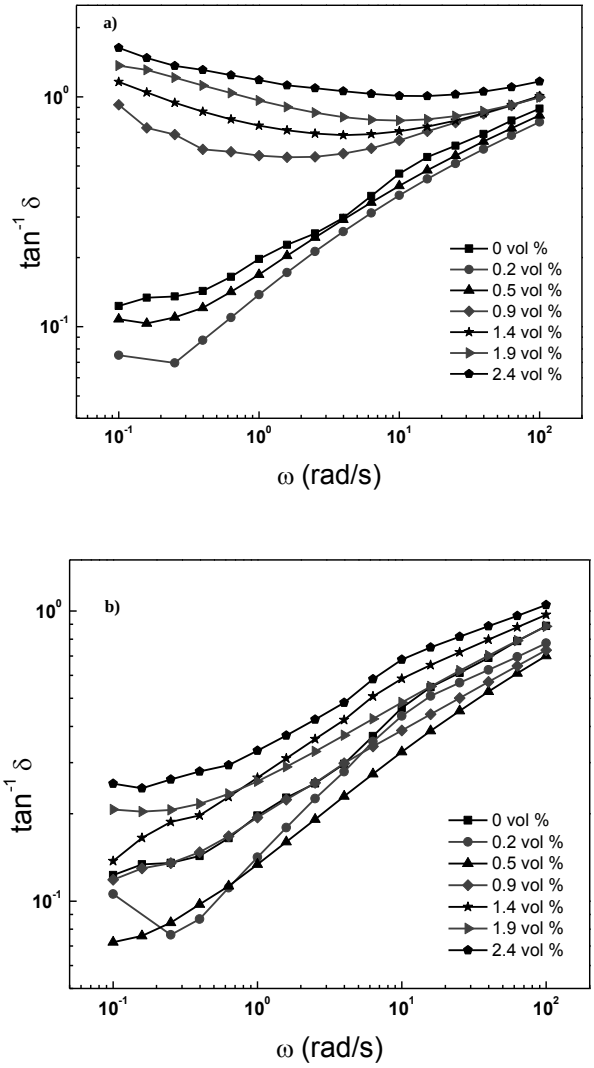

Figure 3. 5 - Inverse loss tangent of **a** PP / PR24LHTXT composites, and **b** PP / PR25PSXT composites as a function of frequency at 190 º C.

The frequency dependence of the complex viscosity, η*, for the PP / CNFs nanocomposites is shown in Figure 3.6. The pure PP shows a Newtonian plateau at low frequencies, whereas for PP / PR 24 LHT XT composites, from 0.5 vol % the plateau decreases and yield stress appears, consistently with behaviors observed for G´ and G´´. PP / PR 25 LHT XT

composites, although show a clear variation in value of η* between 0.9 and 1.4 vol %, do not change apparently the shape of the curve.

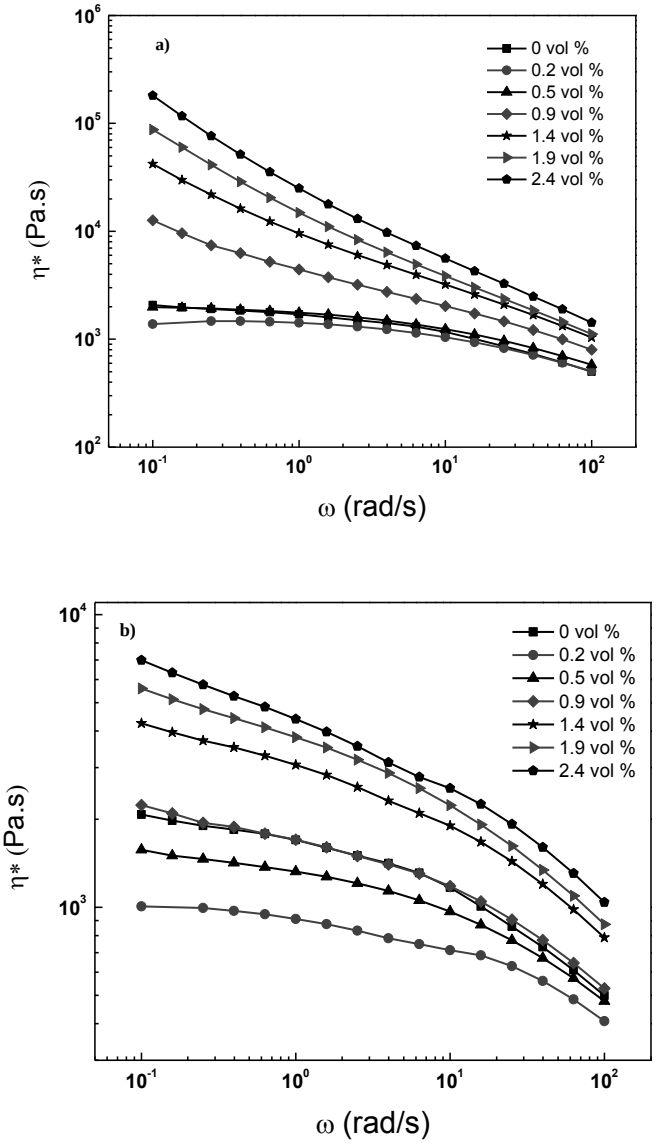

Figure 3. 6 - Complex viscosity of **a** PP / PR24LHTXT composites, and **b** PP / PR25PSXT composites as a function of frequency at 190 º C.

Summarizing the quantitative assessment of the experimental rheological analysis, depending on the type of carbon nanofiber substantial differences can be appreciated between the two composites. PP / PR 24 LHT XT composites, consistently with theoretical predictions and previous experimental reports in CNTs based polymer composites, show a transition between liquid-like and solid-like: as the nanofiber content increases, the creation of some interconnected structure leads to a solid-like behavior (G´ > G´´), which explain the plateaus

or independence behavior with frequency for G´ and G´´ at the lower frequencies [26] and [28].

3.3.4 Comparison of electrical and rheological behaviors in CNFs / PP nanocomposites

Electrical and rheological correlations may constitute a route to understand composites´ microstructure.

According to the electrical results, PR 24 LHT XT composites exhibit an abrupt transition from isolating to electrical conducting behavior, which can be described in the context of percolation theory, from contents of CNFs of ~ 0.42 vol %. In terms of microstructure, this fact is related to the formation of a 3D CNFs´ network which allows electrical transport. PR 25 LHT XT composites, on their hand, do not show isolating-to-conducting electrical transition.

First, in order to calculate the most appropriate rheological parameter to describe rheological thresholds, the normalized logarithm values of G´, G´´, G´ / G´´ and η* are plotted and compared with the normalized logarithm values of electrical conductivity for PR 24 LHT XT composites in Figure 3.7 [15]. Though G´ is commonly reported as the most adequate rheological parameter to describe rheological thresholds, up to now this question is still under discussion and different assumptions have been reported in the literature: power-law dependence based on G´ [15], [12] and [29], power-law dependence based on G´/ G´´ [14] and [15], and even on η* [30]. In Figure 3.7, apart the two first concentrations with negative values due to the reduced viscosity discussed above, the normalized logarithm values of G´´ and η* show a gradual increase with concentration when compared with G´ and mainly with G´/ G´´ which demonstrates to be the most sensitive parameter to the rheological thresholds and the most adequate parameter for comparing with electrical conducting values from 0.9 vol %. This is in accordance with the study by Kharchenko et. al, which uses the inverse of loss tangent to compare with electrical conductivity [14], and the study by Kota et. al, which concludes that η* and G´´, related to viscous response, are less sensitive than G´ and G´ / G´´ , related to the elastic response [15].

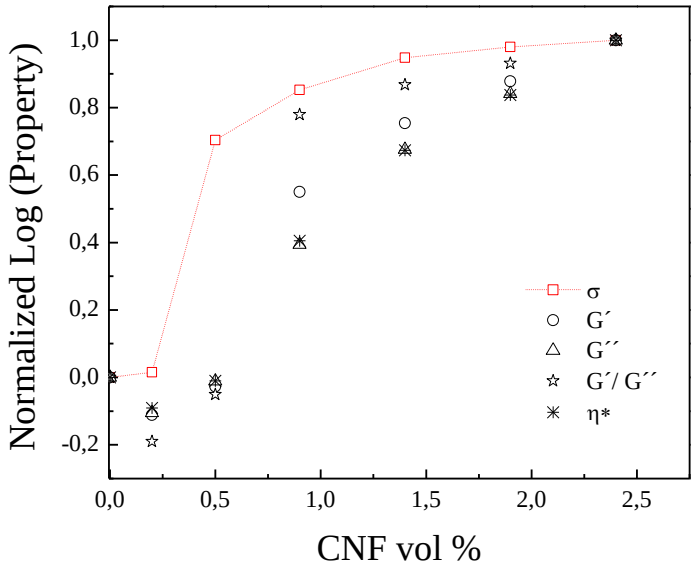

Figure 3. 7 - The normalized log values of electrical conductivity σ, storage modulus G´, loss modulus G´´, inverse loss tangent G´ / G´´ and complex viscosity η^* as a function of PR24LHTXT´s concentration. The rheological data corresponds to a frequency of 0.1 rad/s. The dashed line is to guide the eyes.

In order to compare the rheological and electrical thresholds, a power-law was fitted to G´/ G´´ and G´. The equations used and the two rheological parameters, together with the determined values of σ, are listed in Table 3.2. As it can be seen, the rheological threshold based on G´/ G´´ analysis is ~ 0.49 vol % whereas for G´ is ~ 0.47 vol %, which indicates that the rheological threshold occurs at a slight higher concentration than the electrical percolation threshold (0.42 vol % ± 0,07). The different values obtained for rheological and electrical thresholds in literature are cause of discussion. Some studies show that rheological threshold occurs after electrical percolation, referring that connectivity between fibers precedes rigidity percolation of the system [14]. Others studies, nevertheless, point out the opposite, on the basis of an adequate combination of alignment, dispersion of the fillers and molecular weight of polymer matrix [12].

Power-law relation	Percolation threshold, ϕc (vol %)	t	R2
$\sigma \alpha (\phi - \phi_c, \sigma)^t$	0.42	1.75	0.99
$G'/G'' \alpha (\phi - \phi_c, G'/G'')^t$	0.49	0.52	0.99
$G' \alpha (\phi - \phi_c, G')^t$	0.47	1.54	0.99

Table 3. 2 - Fitting results for power-law relations in electrical and rheological experiences for PP / PR 24 LHT XT composites.

The exponents calculated on the basis of a normal power law relation, were 0.52 for G´ / G´´ and 1.54 for G´. Even though for the electrical percolation theory the exponents are assumed to be universal with theoretical 3D values of ~ 2, a wide range of values have been reported for rheological thresholds based on G´ in polymer composites based on carbon nanotubes: 0.70 [12], 2.91 [30], 2.64 and 2.59 [31], which suggests that G´ or G´/ G´´ follow different scaling laws to describe their volume fraction dependence when compared with electrical conducting σ, [31].

3. 4 Conclusions

Two different CNFs were incorporated in in the same polypropylene matrix by twin-screw extrusion under the same processing conditions. Electrically, the two carbon nanofiber based polypropylene composites demonstrated to have different response: non-conducting and conducting as a function of volume fraction concentration. A large difference in the rheological behavior of both composites has been measured. Whereas the electrical conducting composites based on PR 24 LHT XT carbon nanofibers show liquid-like to solid-like transition which leads to the plateaus for G´, G´´ at low frequencies, the electrical isolating composites based on PR 25 PS XT carbon nanofibers remain practically unaltered in their rheological behavior when compared to the pure PP composites. This fact suggests that rheological analysis clearly differentiates electrical conducting from insulating performance for this particular type of systems. Furthermore, after comparing electrical conductivity and rheological analysis, it is concluded that G´/G´´ and in less extent G´ are the most appropriate rheological parameters for comparing with electrical behavior, which is consistent with previous works that identify elastic load rheological parameters as the best

candidates to compare to the onset of electrical percolation. The rheological threshold fitted from G´/ G´´ was found to be ~ 0.5 vol %, slightly higher than electrical percolation threshold ~ 0.4 vol %. Finally, the difference found between exponents in G´/ G´´ and G´ fittings, suggests different scaling laws to describe their volume fraction dependence when compared with electrical conductivity σ.

Acknowledgements

Financial support for this work has been provided by *Consellería de Educación e Ordenación Universitaria, Xunta de Galicia* through grant CN2011/008. The support of *Applied Sciences Inc.* for generously supplying the CNFs used. We would also like to thank Carla Leer and Patrick Lake for their assistance in the production of the CNF composites. A. J. Paleo wants to thank to IP-SME Pegasus through grant NMP2-CT-2006-026673.

References

1. Kang I, Heung YY, Kim JH, Lee JW, Gollapudi R, Subramaniam S, Narasimhadevara S, Hurd D, Kirikera GR, Shanov V, Schulz MJ, Shi D, Boerio J, Mall S, Ruggles-Wren M. Introduction to carbon nanotube and nanofiber smart materials. Composites Part B: Engineering 2006; 37 (6):382-394.

2. Burton DJ, Glasgow DG, Lake ML, Kwag C, Finegan JC. Influence of carbon nanofiber surface characteristics on composite properties. In: Repecka LSFF (ed) A Materials and Processes Odyssey, Books 1 and 2, vol 46. International Sampe Technical Conference Series 2001; pp 647-657.

3. Gordeyev SA, Macedo FJ, Ferreira JA, van Hattum FWJ, Bernardo CA. Transport properties of polymer-vapour grown carbon fibre composites. Physica B 2000; 279 (1-3):33-36.

4. Al-Saleh MH, Sundararaj U. A review of vapor grown carbon nanofiber/polymer conductive composites. Carbon 2009; 47 (1):2-22.

5. Tibbetts GG, Lake ML, Strong KL, Rice BP. A review of the fabrication and properties of vapor-grown carbon nanofiber/polymer composites. Compos Sci Technol 2007; 67 (7-8):1709-1718.

6. Das NC, Yamazaki S, Hikosaka M, Chaki TK, Khastgir D, Chakraborty A. Electrical conductivity and electromagnetic interference shielding effectiveness of polyaniline-ethylene vinyl acetate composites. Polymer International 2005; 54 (2):256-259.

7. Huang JC. Emi shielding plastics-a review. Advances in Polymer Technology 1995; 14 (2):137-150.

8. Lillehei PT, Kim J-W, Gibbons LJ, Park C. A quantitative assessment of carbon nanotube dispersion in polymer matrices. Nanotechnology 2009; 20 (32):325708-325714.

9. Gershon AL, Cole DP, Kota AK, Bruck HA. Nanomechanical characterization of dispersion and its effects in nano-enhanced polymers and polymer composites. Journal of Materials Science 2010; 45 (23):6353-6364.

10. Schadler LS, Giannaris SC, Ajayan PM. Load transfer in carbon nanotube epoxy composites. Applied Physics Letters 1998; 73 (26):3842-3844.

11. Fiedler B, Gojny FH, Wichmann MHG, Nolte MCM, Schulte K. Fundamental aspects of nano-reinforced composites. Compos Sci Technol 2006; 66 (16):3115-3125.

12. Du FM, Scogna RC, Zhou W, Brand S, Fischer JE, Winey KI. Nanotube networks in polymer nanocomposites: Rheology and electrical conductivity. Macromolecules 2004; 37 (24):9048-9055.

13. Wagener R, Reisinger TJG. A rheological method to compare the degree of exfoliation of nanocomposites. Polymer 2003; 44 (24):7513-7518.

14. Kharchenko SB, Douglas JF, Obrzut J, Grulke EA, Migler KB. Flow-induced properties of nanotube-filled polymer materials. Nat Mater 2004; 3 (8):564-568.

15. Kota AK, Cipriano BH, Duesterberg MK, Gershon AL, Powell D, Raghavan SR, Bruck HA Electrical and rheological percolation in polystyrene/MWCNT nanocomposites. Macromolecules 2007; 40 (20):7400-7406.

16. Zhu J, Wei S, Yadav A, Guo Z. Rheological behaviors and electrical conductivity of epoxy resin nanocomposites suspended with in-situ stabilized carbon nanofibers. Polymer 2010; 51 (12):2643-2651.

17. Evora MC, Klosterman D, Lafdi K, Li L, Abot JL. Functionalization of carbon nanofibers through electron beam irradiation. Carbon 2010; 48 (7):2037-2046.

18. Tessonnier J-P, Rosenthal D, Hansen TW, Hess C, Schuster ME, Blume R, Girgsdies F, Pfaender N, Timpe O, Su DS, Schloegl R. Analysis of the structure and chemical properties of some commercial carbon nanostructures. Carbon 2009; 47 (7):1779-1798.

19. Paleo AJ, van Hattum FWJ, Pereira J, Rocha JG, Silva J, Sencadas V, Lanceros-Mendez S. The piezoresistive effect in polypropylene-carbon nanofibre composites obtained by shear extrusion. Smart Mater Struct 2010; 19 (6): 065013-065019.

20. http://www.apsci.com

21. Bunde A, Havlin S. Fractals and disordered systems. In: Springer (ed), 2nd edition, New York, pp 27-8; 1996.

22. Heaney MB. Measurement and interpretation of nonuniversal critical exponents in disordered conductor-insulator composites. Physical Review B 1995; 52 (17):12477-12480.

23. Garboczi EJ, Snyder KA, Douglas JF, Thorpe MF. Geometrical percolation-threshold of overlapping ellipsoids. Physical Review E 1995; 52 (1):819-828.

24. Mutel MRK. Rheological properties of Fiber-Reinforced Polymer Melts. In: Utracki LA (ed) Chapter 12, Carl Hanser, Munich; 1991.

25. Ferry, JD. Viscoelastic Properties of Polymers. Wiley, New York; 1980.

26. Potschke P, Fornes TD, Paul DR. Rheological behavior of multiwalled carbon nanotube/polycarbonate composites. Polymer 2002; 43 (11):3247-3255.

27. Utracki LA. Flow and flow orientation of composites containing anisometric particles. Polymer Composites 1986; 7 (5):274-282.

28. Lozano K, Yang SY, Zeng Q. Rheological analysis of vapor-grown carbon nanofiber-reinforced polyethylene composites. Journal of Applied Polymer Science 2004; 93 (1):155-162.

29. Cipiriano BH, Kashiwagi T, Raghavan SR, Yang Y, Grulke EA, Yamamoto K, Shields JR, Douglas JF. Effects of aspect ratio of MWNT on the flammability properties of polymer nanocomposites. Polymer 2007; 48 (20):6086-6096.

30. Martins JN, Bassani TS, Barra GMO, Oliveira RVB. Electrical and rheological percolation in poly(vinylidene fluoride)/multi-walled carbon nanotube nanocomposites. Polymer International 2011; 60 (3):430-435.

31. Huang CL, Wang C. Rheological and conductive percolation laws for syndiotactic polystyrene composites filled with carbon nanocapsules and carbon nanotubes. Carbon 2011; 49 (7):2334-2344.

Chapter 4 - Piezoresistive effect in polypropylene - carbon nanofiber composites obtained by shear extrusion

This chapter is published on the following journal:

"***The piezoresistive effect in polypropylene-carbon nanofiber composites obtained by shear extrusion"*** A. J. Paleo, F. W. J. van Hattum, J. Pereira, J. G. Rocha, J. Silva, V. Sencadas, S. Lanceros-Méndez. Smart Materials and Structures 2010;19 (6) art. no. 065013

Abstract.

The piezoresistive effect on poly (propylene) - carbon nanofibre composites fabricated by twin screw extrusion and compression moulding has been investigated. The electrical and mechanical properties of PP/CNF composites have been obtained as a function of CNF concentration. Electrical conductivity exhibited low thresholds and values close to the required levels for EMI-shielding applications at 2.4 vol %. Meanwhile the elastic modulus showed an enhancement with a maximum up to 130 % for one of the composites at 0.9 vol % loading. Further, the piezoresisitive response has been evaluated in four point bending. Positive gauge factors between 2 and 2.5 have been obtained. The highest gauge factors are found within the percolation threshold. The characteristics of the materials and the production technique make them suitable for large scale applications.

4.1 Introduction

The rapid development of functional polymer nanocomposites, a new class of materials containing at least one filler dimension in the nanometer range, has opened up new perspectives for the design of smart materials: solid-state transducers which reproduce stable responses through variations of one property when subjected to external stimuli [1, 2].

Conventional smart materials such as electroactive ceramics, EACs, electroactive polymers, EAPs, and shape memory alloys, SMAs, namely, have shown several limitations: fragility and rigidity, EACs; low response speeds and high densities, SMAs; low actuation forces and mechanical energy density, and lack of robustness, EAPs, [3, 4]. Smart nanoscaled materials based on electrically conductive polymer nanocomposites, ECPNCs, may have the ability to meet these faults and represent a new chance to reproduce and measure motion, force and deformation.

Carbon nanofibres are important nanoscale materials, promising as effective fillers for polymer nanocomposites, due to their excellent electrical, thermal and mechanical characteristics, ease of incorporation and dispersion into polymers at lower cost compared to carbon nanotubes [5, 6].

To date, most of the studies on polymer systems based on CNFs have been focused on demonstrating percolation thresholds at only a few volume or weight percents of CNFs with the goal of explaining the role of dispersion in the conductivity values and the origin of the conduction mechanism [7, 8] . Because the conductive network dictates electrical properties, conductive behaviour of CNF composites can be expected to change when subjected to small mechanical deformations. In spite of the existing studies focused on piezoresistivity in polymer/CNT systems [9-11], little research has been focused on the piezoresistive properties of the composites enhanced by CNFs, which are discussed in this paper.

Poly (propylene) which is a thermoplastic polymer, with a large variety of applications such as packaging, textiles, automotive components among others, was chosen due to its broad use in melt extrusion and moulding plastic industry.

The poly (propylene) /CNF composites used in this study were fabricated by twin screw extrusion and compression moulding. Strain sensitivity effects on electrical resistance in PP composites with different volume fraction of CNFs were tested by standard tensile and four-point bending methods. Furthermore, electrical conductivity and mechanical properties were characterized with the goal to open up new routes to explain the electromechanical behaviour.

The ultimate objective of the present work is to obtain good piezoresistive performance of the composites that have been manufactured by reproducible production techniques that allow for large-scale applications.

4.2 Experimental

4.2.1 Materials

Two types of CNFs are used in this study, all Pyrograf III ™, supplied by Applied Sciences, Inc. (Cedarville, OH). The two types (PR19 LHT XT, PR24 LHT XT) differ mainly in graphitic structure and diameter. Furthermore, different heat- and debulking treatments were used on the fibres:

- PR24 adds a thin layer of disordered carbon. Fibre diameter around 100 nm.
- PR19 adds a thicker layer of turbostratic carbon. Fibre diameter around 150 nm.
- XT refers to an improved debulking method to lower the bulk density of fibre, enhancing its handling and dispersion in subsequent processing.
- LHT refers to a heat-treatment at 1500 ºC, converting any chemically vapour deposited carbon present on the surface of the fibre to a short range ordered structure, increasing the inherent electrical conductivity of the fibre.

An overview of the used fibres and their denominations is given in Table 4.1. The polymer used in this study is a powder polypropylene, Borealis EE002AE.

Composite Nr	CNF type	PP polymer	Extrusion temperature	Screw speed (rpm)	Screw configuration
1	PR19 LHT XT	Borealis EE002AE	190	50	High shear
2	PR24 LHT XT				

Table 4. 1 – Materials and processing conditions.

4.2.2 Fabrication of CNF/PP composites

Extrusion compounding was performed in a modular laboratorial mini co-rotating twin-screw extruder built in-house with an approximate L/D ratio of 26. A modular screw configuration was designed in order to apply high shear conditions during processing. The screw configuration was comprised of a special transport element with small pitch located in the solid conveying zone together with a block of kneading disks with a staggering angle of -30^{o}, located just before the melt conveying zone. The extrusion process was performed at a constant feed rate of 150 g/h of PP by means of a volumetric dosing unit Moretto DVM 18 L, while CNFs were fed downstream in the extruder to obtain fibre loadings between 0.2 to 2.4 vol %. The screw speed was kept constant at 50 rpm, all heating zones in extruder were set at 190 ºC. Extrusion conditions for the two composite samples are also summarised in Table 4.1.

The extruded PP/CNF nanocomposite material was then pelletised and pressed into compression moulded rectangular sheets, with an area of 185 x 120 mm^2 and 2 mm in thickness, in a hot press at 200 ºC, maintaining a pressure of 2 MPa for five minutes and during subsequent cooling. Subsequently, a labscale CNC mill Roland Modela MDX-20 was used to cut samples from the plate in dimensions required for tensile and electrical measurements. Tensile samples, 60 mm length, with a 15 mm (length) x 4 mm (width) x 2 mm (thickness) in parallel section were used in tensile and stress-strain piezoresistive tests. Rectangular samples 49 x 7 mm and 2 mm in thickness were used in volume resistivity experiments. Compression moulded (190 ºC, 5 MPa, 5 min) rectangular samples 49 x 10 mm and 1 mm in thickness were used in 4-point-bending tests.

4.2.3 Electrical conductivity measurement

The bulk resistance of rectangular samples were determined from the slope of I-V curves measured with an automated Keithley 487 picoammeter/voltage source, ten replicates of each sample were run to obtain an average and standard deviation. All measurements were performed at room temperature in direct current, DC, by using the two-probe method at the sample's rectangular extremities. Silver paste was used, after cleaning with acetone each of the extremities, to ensure good electrical contact. The volume resistivity ρ_V in Ω cm was calculated by equation (4.1):

$$\rho_v = \frac{RA}{d} \qquad (4.1) \qquad (1)$$

where R is the bulk resistance in Ω, A is the electrode area in cm^2 and d is the distance between electrodes in cm. Finally, electrical volume conductivity in S cm^{-1} was calculated from the inverse of ρ_V.

4.2.4 Electro-mechanical characterization of composites

4.2.4.1 Testing of mechanical and electrical properties

In order to investigate the effects of applied tensile strain on resistance, the piezoresistive effect by stretching the samples along the longitudinal direction, GF_L, was calculated by mechanical stress-strain tests performed in an AG-IS Shimadzu testing machine with a load cell of 500 N at a speed of 2 mm min^{-1}. These experiments were carried out on tensile samples described above. Silver paste was used as electrodes (4 mm wide, 10 mm distance) in the parallel section and copper wire was attached to the electrodes with the same paste. Three specimens were tested for each loading. Current versus time data were measured in a Keithley 487 picoammeter/voltage source simultaneously with strain until failure of the samples. The effective elastic modulus was derived from the stress - % strain curves and geometry of the samples. Resistance was calculated from voltage and current, and the GF_L is calculated using equation (4.2), where ε is strain and ΔR/R is the fractional resistance change with strain. Finally ΔR/R versus % ε curves were obtained and GF_L taken from the slope of these curves over the strain interval corresponding to the elastic part in stress-strain curves was calculated**.**

$$GF = \frac{\Delta R / R}{\varepsilon} \qquad (4.2)$$

4.2.4.2 Four - point bending tests

The piezoresistive gauge factor for transversal loading, GF_T, was measured by 4-point bending tests, as illustrated schematically in Figure 4.1. Again three samples for each condition were placed in a Shimadzu-AG-IS 500 N testing instrument at 4-cycles of 2 mm min^{-1} and 1 mm in z-displacement. Resistance change was captured at the same time with an Agilent 34401A digital multimeter. Two parallel rectangular gold electrodes of 4 mm width and 1 mm of distance between them were vacuum evaporated onto one of the sides for each one of the samples and copper wire was attached to the electrodes with silver paste.

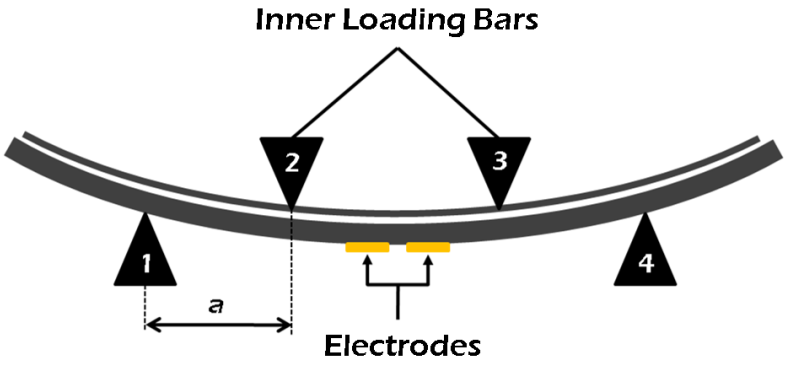

Figure 4. 1- Four-point bending testing configuration.

In this case, the strain, calculated from the theory of pure bending of a plate to a cylindrical surface valid between the inner loading points, is equal to $\varepsilon = \frac{3dz}{5a^2}$ where d is thickness, z is the displacement of the inner loading bars, and a is the distance between the first and second points of the 4-point bending load cell (a = 10 mm) [12]. The GF_T was calculated for the four upward cycles of the z-displacement vs. time and resistance curves experimentally acquired for each one of the samples. After this, GF_T average is calculated for each sample, and finally, the total average GF_T is obtained from the three samples. When the CNF loading approaches the percolation threshold, weak nonlinear piezoresistivity is observed. The piezoresistivity can be approximately regarded as linear under small strains so the GF was calculated taking for the fitting the points on the curves up to strains for which R^2 values larger than 0.96 in the linear regression were obtained.

4.3 Results and discussion

4.3.1 Electrical Conductivity

Representative I-V curves for PP composites with different PR19 LHT XT fiber loadings are shown in Figure 4.2 (the inset show the two lower CNF concentrations). The electrical volume conductivities of the neat PP and CNF/PP composites are represented in Figure 4.3 as a function of CNF concentration. The conductivity of the neat PP is close to 10^{-10} S cm^{-1}. With increasing CNF loading, the volume conductivity increases. In particular, the PR19 LHT XT composites (Nr 1) at 0.9 vol %. (≈ 2 wt. %) loading show a sharp increase in conductivity, reaching values above 10^{-3} S cm^{-1}; the PR24 LHT XT samples (Nr 2) show similar behaviour but at lower 0.5 vol %. (≈ 1 wt. %) loading, with values of conductivity of 10^{-4} S cm^{-1}. The combination of higher inherent fibre conductivity - due to the higher graphitisation index as compared to PR19 - with an outer layer that could prevent fibre breakage and improve fibre-matrix interaction, could be beneficial for obtaining higher conductive composites with PR24 LHT XT fibres.

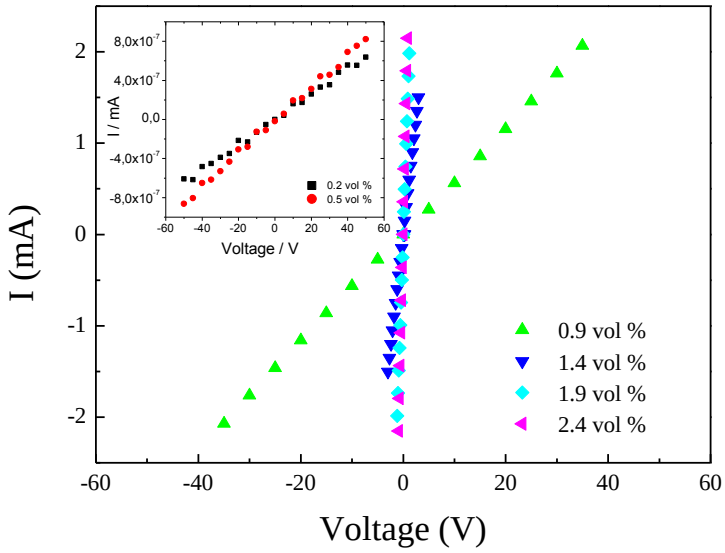

Figure 4. 2 - Typical I-V curves for the different concentrations of PR19 LHT XT samples. The inset shows the I-V curves for the two lower CNF concentrations. Similar trends were also observed for Composites PR24 LHT XT.

G. Sui et al. in their recent paper with PP and Pyrograf III® CNF composites fabricated by melt-compounding in a co-rotating twin screw extruder have reported sharp decrease in resistivity for 3 wt.% loading with values close to 10^6 ohm m, which are clearly less conductive than the values showed in this work at low loading of CNFs [13]. Furthermore, the review by M. Al-Saleh et al. represents a good reference to compare the values obtained in the present study in terms of conductivity with earlier studies [5]. From the comparison of the thresholds for different PP/CNFs composites, it is possible to observe only one previous study with similar values of thresholds, reported by Tibbets et al. for graphitized VGCFs 100-300 nm in diameter [14].

Though the variation of the electrical properties with concentration for CNF/polymer composites is usually understood in the framework of the percolation theory [15-17], recent studies point out the interparticle tunnelling and the formation of a percolation network with a mean tunnelling distance as the main mechanism responsible for the observed electrical behaviors [18] . On the other hand, models involving the formation of capacitor networks seem to be more suitable to explain low percolations thresholds [19].

As shown in Figure 4.2, the current-voltage I-V curves of the CNFs/PP nanocomposites show good linear relationship. M. Al-Saleh et al. in their review mention that investigating the current-voltage relationships gives an indication whether the composite conductivity is due to tunnelling or direct contact between particles [5, 20, 21]. Linear I-V relationships, point out the direct contact between fillers as the main conduction mechanism, whereas, for tunnelling mechanisms, a power law for I-V curves is expected. On the other hand, an early study by Chekanov et al. [22] shows that composites possessing the tunnelling type conductivity also obey Ohm´s law and therefore show linear IV relationships.

Overall the results show the possibility of tailoring electrical conductivity of these type of composites as a function of the desired applications. The bulk conductivity is well within the range of typically desired for the electrostatic painting of parts [$<10^{-6}$ S cm^{-1}] for all samples in the proximity of thresholds. Furthermore, both composites at 2.4 vol %. reach also the required levels for Radio Frequency Interference, RFI, applications [10^{-1} S cm^{-1}] [23].

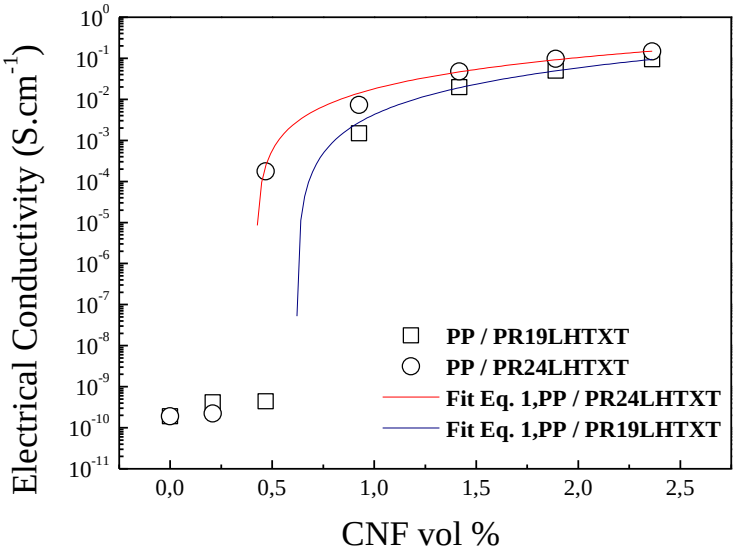

Figure 4. 3 - Electrical conductivity values vs. volume fraction loadings of CNFs for the various samples and the corresponding fit using equation 4. 3. The R^2 is 0.99 for the two fits.

As stated before, the behaviour of the conductivity can be described by the following power law relation, equation (4.3):

$$\sigma \, \alpha \, \sigma_0 \, (\phi - \phi_c)^{\,t} \qquad (4.3)$$

where σ is the composite and σ_0 the matrix conductivity, respectively, Φ_c the critical volume fraction and Φ the filler volume fraction. The t exponent is a critical exponent for the conductivity and depends only on the dimensionality of the system [15-17]. The critical exponent in Eq. 4.3 takes a value between 1.6-2.0 for a 3D system and has an universal value of 3 (exact) [17].

The major problem in analyzing these types of systems is the difficulty in characterizing the fillers' geometry. For fibres with a capped cylinder shape, the theoretical framework developed by Celzard [24] based on the Balberg model [25] provides the bounds for the percolation threshold or the critical volume fraction – the volume fraction where a giant cluster that spans the domain is formed. In general, the percolation threshold is defined in the following bounds:

$$1-e^{\frac{-1.4V}{\langle V_e \rangle}} \leq \phi_c \leq 1-e^{\frac{-2.8V}{\langle V_e \rangle}} \qquad (4.4)$$

Equation (4.4) links the average excluded volume, $\langle V_e \rangle$, the volume around an object in which the center of another similarly shaped object is not allowed to penetrate averaged over the orientation distribution and the critical concentration, Φ_c, where the value 1.4 corresponds to the lower limit – infinitely thin cylinders – and the value 2.8 to spheres. The values were obtained by simulation. The derivation of this equation and related discussion can be seen in [24]. The latter equation imposes a bound in the percolation threshold for the formation of the percolation cluster.

Using the average values from the supplier for the diameter and length, the following bounds, Table 4.2, are obtained:

CNF	Aspect Ratio	Percolation threshold
PR19LHTXT	433	$0{,}16 \leq \phi_c \leq 0{,}32$
PR24LHTXT	619	$0{,}11 \leq \phi_c \leq 0{,}23$

Table 4. 2 – Theoretical bounds for the percolation threshold for the two types of CNF.

In Figure 4.3 it is shown that the percolation threshold for the PR 19 LHT XT CNFs is bounded between ~ 0,5 % and ~ 1% . The percolation threshold is indicated by a change of 7 orders of magnitude in the conductivity. More precisely using Eq. 4.3 a value of 0.62 % ± 0,07 is obtained for the percolation threshold. These values are higher than the ones predicted by the theoretical bounds (Table 4.2). For the PR 24 LHT XT the experimental percolation threshold is bounded by 0,2 % and 0,5%, indicated by a change of 6 orders of magnitude in the conductivity. The calculated percolation threshold is 0,42 % ± 0,14. Again, a deviation from the theoretical prediction is observed. The intercept, which is related with the fibre conductivity, is a magnitude of 10^{-2} lower that the expected value for these types of CNF, indicating that the type of matrix influences the overall conductivity. Moreover the critical exponents are in accordance with the theoretical 3D values ~ 2,0 (PR19 - 2,04 ± 0,13; PR24 – 1,75 ± 0,21). These values point out that the conductivity is related with a formation of 3D network that spans the system. Nevertheless the higher values of the percolation thresholds,

for the two types of fibres, suggests the presence of small agglomerates as was previous discussed in a related work [18].

4.3.2 Mechanical Properties

The normalized elastic modulus of the neat PP and CNF nanocomposites obtained though strain-stress experiments, is listed in Table 4.3. As can be seen, CNF loading causes a reinforcing effect on the PP matrix, which increases with increasing CNF content. The tensile Young´s modulus of the nanocomposites is enhanced continuously with increasing CNF content until a certain loading content is reached, which stabilize and even worse mechanical properties. Nanocomposites with PR 19 LHT XT fibres reach that critical load at 0.9 vol %. with an enhancement in modulus of 130 % relatively with neat PP. The maximum enhancement for nanocomposites with PR24 LHT XT fibres is reached at 1.4 vol % loading with 121 % improvement of the mechanical characteristics, as compared to the neat PP. The lower aspect ratio of PR 19 LHT XT fibres could be the explanation for this stronger reinforcing effect on the Young´s modulus, it is known that nanofibers with high aspect ratios are more difficult to disperse, due to their high surface areas, resulting in a strong tendency to agglomerate and therefore causing a negative effect on the mechanical properties of the composites.

In terms of tensile strength, it should be noted that the strength is retained for both fiber types, relatively to the neat PP. While discussing the percolation threshold, the presence of small agglomerates was deduced. Such agglomerates limit the overall mechanical properties of the composite, ultimately leading to a decrease in strength, as they act as stress concentrators. The retaining of the tensile strength, seen in the current samples, indicates the presence of agglomerates only to a small extent, which is consistent with the limited increase in percolation threshold observed.

Loading	PR24 LHT XT	PR 19 LHT XT
Neat PP	1	1
PP + 0.2 vol %	1.19	1.07
PP + 0.5 vol %	1.15	1.12
PP + 0.9 vol %	1.10	1.30
PP + 1.4 vol %	1.21	1.28
PP + 1.9 vol %	1.13	1.23
PP + 2.4 vol %	1.21	1.24

Table 4. 3 – The normalized tensile´s Young modulus of PP and CNF / PP composites.

4.3.3 Electro-Mechanical Properties

The piezoresistive response was tested both under tensile and bending experiments by simultaneous measuring of the mechanical solicitation and the electrical response. Typical curves for the tensile piezoresistive stress-strain tests are represented in Figure 4.4. Representative curves for the bending piezoresistive tests are represented in Figure 4.5.

Samples with PR19 and PR24 LHT XT fibres showed not to be sensitive in terms of resistance under the small strains corresponding to the elastic part in mechanical strain-stress tests, with values of GF_T close to zero for all loadings above thresholds as can be noted in Figure 4.4 shows a typical stress-strain test performed simultaneously with electrical measurements for PP composites with 1.9 vol % loading of PR 19 LHT XT fibres.

The strain sensing performance of the PR 19 LHT XT composite at 2.4 vol % in Figure 4.5, shows the resistance change subjected to a cyclic 4-point-bending test. The resistance was measured over 4 cycles between 0 and 1 mm in displacement to ensure that the composite deformations were elastic. The plot shows that the composite resistance is reversible, which makes these materials potential candidates for strain gauges sensors with sensitivities that can be tuned by modifying the CNF loading.

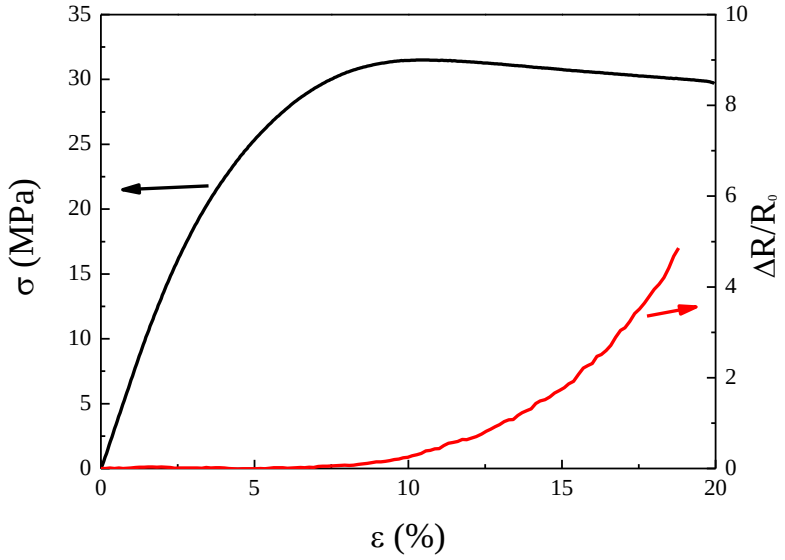

Figure 4. 4 - Longitudinal piezoresistive effect in stress-strain mechanical test simultaneously with total relative resistance change for PR19 LHT XT composites at 1.9 vol % loading.

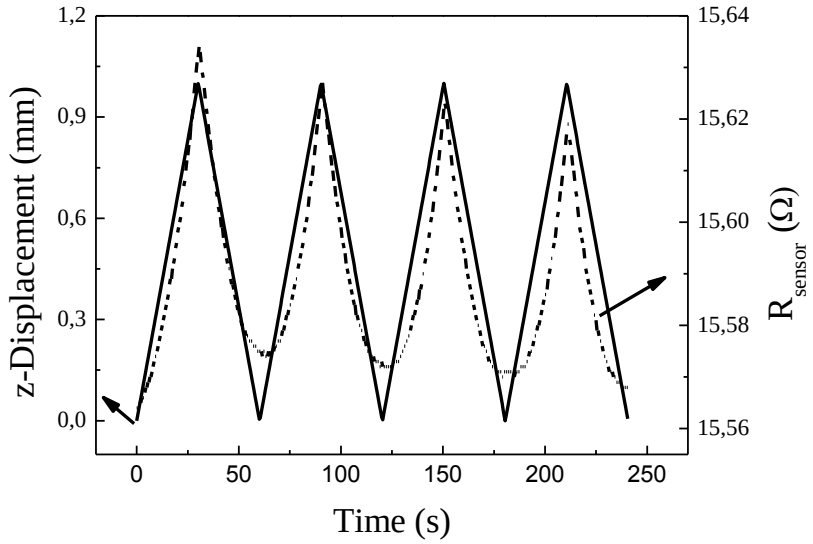

Figure 4. 5 - Sensing resistance of a rectangular sample PR19 LHT XT at 2.4 vol % as a function of time, during a four-point bending experiment consisting of 4 cycles at 1 mm in z-displacement.

In spite of the fact that the piezoresistivity of conducting particle-reinforced insulating matrix composites (CPICs) has been extensively studied, the fundamental understanding is still lacking. Carmona et. al, in their study with carbon black and short graphite fibres, suggests that the relationships between the relative concentration change and the pressure depends on the nature of the applied pressure [26]. Grimaldi et. al present a theory for GF in thick-film resistors (TFRs) based on elastic heterogeneity, when the conducting phase is stiffer than the insulating one, the local strains within the latter are enhanced with respect to averaged macroscopic strains, which induces higher GF values [27]. Again Grimaldi et. al in a further study assert that percolation networks based on interparticle tunnelling conduction show a logarithmic divergent piezoresistive response close to the threshold as far as the electrical conductivity becomes nonuniversal, they discuss this theory in relation to a carbon-black-polymer composites [28].

In this study, the experimental curves which are the result of the upward part for one of the 4 cycles of 4-point-bending tests, are noted in Figure 4.6 for PR24 LHT XT fibre composites for all vol % loadings. As it is proposed by Grimaldi et. al [28], when the CNF loading approaches the percolation threshold, weak nonlinear piezoresistivity is observed, however, with high CNF loading, the piezoresistivity can be approximately regarded as linear under small strains. As stated by Hu et al., who studied MWNTs in epoxy resin [29], the resistance change might be dominated by the breakup of the conductive network.

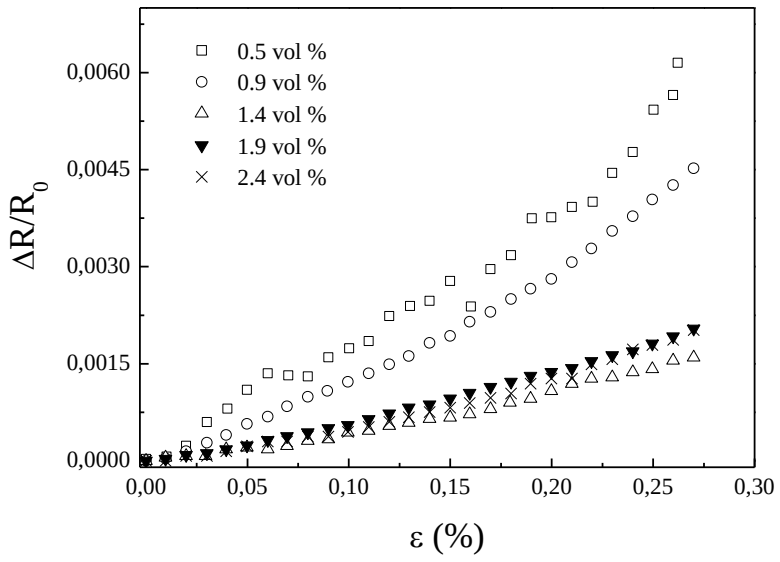

Figure 4. 6 - Experimental piezoresistivity of PR 24 LHT XT composites**.**

The transversal gauge factor values, GF_T, of PR19 and PR 24 LHT XT composites are plotted in Figure 4.7. It can be observed that these factors increase with decreasing CNFs concentration, consequently the composites with PR 19 LHT XT fibres showed a peak of 2.4 for 0.9 vol % loading, whereas for PR 24 LHT XT composites, the peak was produced at 0.5 vol % loading with a value of 2.0, these values are in the range of conventional resistance strain gauges, whose factors generally are between 2.0 and 3.2 [10]. The overall trend of the GF of the PR19 LHT XT sample is higher than that of PR24 LHT XT. This difference in the electro-mechanical response is to be ascribed to the main difference between both fibers: whereas the PR24 LHT XT fibers add a thin layer of disordered carbon, the PR19 LHT XT fibers adds a thicker layer of turbostratic carbon. In this way, the fiber diameter is around 100 nm for PR24 LHT XT and around 150 nm for PR19 LHT XT fibers. This fact leads to higher inherent fibre conductivity due to the higher graphitisation index for the PR24 LHT XT fibres as compared to the PR19 LHT XT ones. Further, higher conductivity for the same CNF concentrations leads to lower gauge factors.

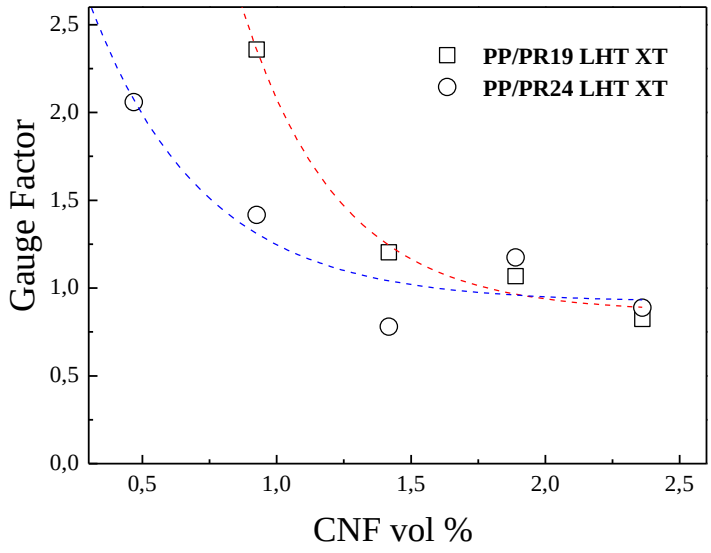

Figure 4. 7 - Gauge Factor values for PR19 LHT XT and PR24 LHT XT composites in function of volume loadings. The dashed-lines are to guide the eyes.

4.4 Conclusions

This paper presented the fabrication method, mechanical electrical and piezoresistive properties of poly (propylene) - carbon nanofiber composites with different CNF concentrations. The fabrication process was based on twin screw extrusion and compression moulding. The elastic modulus showed an enhancement with a maximum up to 23 % for one of the composites at 0.9 vol % loading. The electrical conductivity exhibits low thresholds and values close to the required levels for EMI-shielding applications at 2.4 vol %. Piezoresisitive gauge factors between 2 and 2.5 have been obtained within the percolation threshold. The characteristics of the materials and the production technique make them suitable for large scale applications as piezoresistive sensors.

Acknowledgments

We acknowledge the Foundation for Science and Technology through the *3º Quadro Comunitario de Apoio*, the *POCTI* and *FEDER* programs and the *NANO/NMed-SD/0156/2007 project*. JP, JS and VS thank the FCT grants SFRH/BD/66930/2009/, SFRH/BD/60623/2009 and SFRH/BPD/63148/2009, respectively. The support of *Applied Sciences Inc.* for generously supplying the CNFs used. We would also like to thank Carla Leer and Patrick Lake for their assistance in the production of the CNF composites. A. J. Paleo wants to thank to IP-SME Pegasus project through grant NMP2-CT-2006-026673.

References

1. Rogers C A 1993 Intelligent Material Systems -- The Dawn of a New Materials Age J. Intell. Mater. Syst. Struct. 4(1) 4-12

2. Newnham R E and Ruschau G R 1993 Electromechanical Properties of Smart Materials J. Intell. Mater. Syst. Struct. 4(3) 289-294

3. Vinogradov A, Su J, Jenkins C, Bar-Cohen Y 2006 State-of-the-art developments in the field of electroactive polymers Mater. Res. Soc. Symp. Proc. 51-56

4. Bag D S and Rao K U B 2006 Smart polymers and their applications J. Polym. Mater 23(3) 225-248

5. Al-Saleh M H and Sundararaj U 2009 A review of vapor grown carbon nanofiber/polymer conductive composites Carbon 47(1) 2-22

6. Tibbetts G G, Lake M L, Strong K L and Rice B P 2007 A review of the fabrication and properties of vapor-grown carbon nanofiber/polymer composites Compos. Sci. Technol. 67(7-8) 1709-1718

7. Prasse T, Cavaillé J-Y and Bauhofer W 2003 Electric anisotropy of carbon nanofibre/epoxy resin composites due to electric field induced alignment Compos. Sci. Technol. 63(13) 1835-1841

8. Hammel E, Tang X, Trampert M, Schmitt T, Mauthner K, Eder A and Pötschke P 2004 Carbon nanofibers for composite applications Carbon 42(5-6) 1153-1158

9. Park J M, Kim D S, Lee J R and Kim T W 2003 Nondestructive damage sensitivity and reinforcing effect of carbon nanotube/epoxy composites using electro-micromechanical technique Mater. Sci. Eng. C 23(6-8) 971-975

10. Pham G T, Park Y B, Liang Z, Zhang C, Wang B 2008 Processing and modeling of conductive thermoplastic/carbon nanotube films for strain sensing Compos. Pt. B-Eng 39(1) 209-216

11. Li C, Thostenson E T and Chou T W 2008 Sensors and actuators based on carbon nanotubes and their composites: A review Compos. Sci. Technol 68(6) 1227-1249

12. Timoshenko S P 1958 History of Strength of Materials, ed. R. E. Krieger Publ. Comp pp 93-218

13. Sui G, Jana S, Zhong W H, Fuqua M A and Ulven C A 2008 Dielectric properties and conductivity of carbon nanofiber/semi-crystalline polymer composites Acta Mater 56(10) 2381-2388

14. Tibbetts G G, Finegan I C and Kwag C 2002 Mechanical and electrical properties of vapor-grown carbon fiber thermoplastic composites Mol. Cryst. Liq. Cryst. 387 129 - 133

15. Stauffer D and Aharony A 1992 Introduction to Percolation Theory 2nd (London: Taylor and Francis)

16. Stroud D and Bergman D J 1982 Frequency dependence of the polarization catastrophe at a metal-insulator transition and related problems Phys. Rev. B: Condens. Matter 25(3) 2061

17. Nan C W 1993 Physics of inhomogeneous inorganic material Prog. Mater Sci. 37(1) 1-116

18. Cardoso P, Silva J, Paleo A J, Hattum F W, Simoes R and Lanceros-Méndez S 2009 The dominant role of tunneling in the conductivity of carbon nanofiber-epoxy composites Phys. Status Solidi A 1-4

19. Simoes R, Silva J, Vaia R, Sencadas V, Costa P, Gomes J and Lanceros-Méndez S 2009 Low percolation transitions in carbon nanotube networks dispersed in a polymer matrix: dielectric properties, simulations and experiments Nanotechnology 20 (3) 035703

20. Yui H, Wu G, Sano H, Sumita M and Kino K 2006 Morphology and electrical conductivity of injection-molded polypropylene/carbon black composites with addition of high-density polyethylene Polymer 47 (10) 3599-3608

21. Bar H, Narkis M and Boiteux G 2005 The electrical behavior of thermosetting polymer composites containing metal plated ceramic filler Polym. Compos. 26 (1) 12-19

22. Chekanov Y, Ohnogu R, Shigeo A and Sumita M 1999 Electrical properties of epoxy resin filled with carbon fibers J. Mater. Sci. 34 (22) 5589-5592

23. Miller B 1996 Plastics World 73

24. Celzard A, McRae E, Deleuze C, Dufort M Furdin G and Marêché J F 1996 Critical concentration in percolating systems containing a high-aspect-ratio filler Phys. Rev. B: Condens. Matter 53(10) 6209

25. Balberg I, Anderson C H, Alexander S and Wagner N 1984 Excluded volume and its relation to the onset of percolation Phys. Rev. B: Condens. Matter 30(7) 3933

26. Carmona F R, Canet R and Delhaes P 1987 Piezoresistivity of heterogeneous solid J. Appl. Phys. 61(7) 2550-2557

27. Grimaldi C, Ryser P and Strassler S 2001 Gauge factor enhancement driven by heterogeneity in thick-film resistors. J. Appl. Phys. 90(1) 322-327

28. Grimaldi, C, Maeder T, Ryser P and Strässler S 2003 Piezoresistivity and conductance anisotropy of tunneling-percolating systems Phys. Rev. B: Condens. Matter 67(1) 014205

29. Hu N, Karube Y, Yan C, Masuda Z and Fukunaga H 2008 Tunneling effect in a polymer/carbon nanotube nanocomposite strain sensor Acta Mater 56(13) 2929-2936.

Chapter 5 - Piezoresistive polypropylene-carbon nanofiber composites as mechanical transducers

This chapter is published on the following journal:

"*Piezoresistive polypropylene-carbon nanofiber composites as mechanical transducers*" A. J. Paleo, F. W. J. van Hattum, J. G. Rocha and S. Lanceros-Méndez. Microsystem Technologies 2012; 18(5), 592-597.

Abstract.

This paper describes a strain sensor based on a polypropylene-carbon nanofiber, PP-CNF, composite film, fabricated by twin screw extrusion and compression molding, which is an inexpensive industrial polymer production technique. Its working principle is based on the piezoresistive effect showed by this kind of composites. Strain sensing by variation of the electrical resistance of the sensor was tested by a four-point bending method. Furthermore, the dependence of the gauge factor as a function of the deformation and velocity of deformation was calculated. The reproducibility of the electrical response of the material was also tested by applying up to forty loading-unloading cycles. The experimental results showed that PP-CNF films have an overall appropriate response for being used as piezoresistive deformation sensors, with a small non-linear response, typical of composites within the percolation threshold. Finally, electrical equivalent model of the sensor was developed and the experimental data was tested against it, showing good agreement.

5.1 Introduction

The ability of a material to sense its own strain (self-sensing) is one of the most-wanted requisites for application of smart materials in solid-state transducers, which reproduce stable responses when subjected to external stimuli [1, 2]. Specific applications of strain sensors include structural deformation and vibration measurement, traffic monitoring, weighing, between many others.

In recent years, carbon nanotubes, CNTs, are the topic of many studies due to their mechanical, electrical and thermal properties. Also, due to their capability to change electronic properties when subjected to deformations, nanotubes have been considered for strain sensors [3]. Another promising nanoscale materials, similar to CNTs, are the carbon nanofibers, CNFs, which have excellent electrical, thermal and mechanical properties too [4, 5], but at a lower cost. Improved mechanical properties and unique electrical properties can be achieved by incorporating a relatively small loading of CNFs into a polymer matrix, which may offer a means of unlocking a number of new and exciting applications. An overall result of this is that the processing of CNF-based materials can represent a new route to fabricate smart composites at relatively low-cost.

To date, most of the studies about polymer systems based on CNFs focus on demonstrating percolation thresholds, at only a few volume or weight percent of CNFs, with the goal of explaining the role of dispersion in the electrical properties and the origin of the conduction mechanism [6, 7]. Some other studies report on the variations of the resistivity of the composites in the presence of external deformations [8-11], effect reported as piezoresistivity.

The first studies on piezoresistive response of particle modified polymers were performed in carbon black rubber systems [12-16]. These studies reveal that the piezoresistive behavior can deliver further details on the network structure of the composites. In the last decade, Flandin et al., studied in situ the AC electrical properties under large strain of nanocomposites of electrically conductive fillers dispersed in a thermoplastic insulating matrix, as a mean of monitoring microstructural evolution of such composites [17]. More recently, Knite et al., correlated the piezoresistive of nanoscaled carbon black/polyisoprene systems to the change in interparticle distances [18]. Other studies reporting on different

systems, e. g., polypropylene/graphite [19], epoxy/graphite [20], and PE, PS epoxy based metal particle composites [21], reveal different piezoresistive behavior. In spite of the existing studies focused on the fundamentals of piezoresistive properties in polymer/CNT systems [22-24], research on the real performance as strain self-sensing sensors of CNT or CNF based composites, which is the main objective of this study, is still in its early stage. For instance, very recently, Wichmann et al., studied the electrical behavior of nanocomposites based on multiwall carbon nanotubes and carbon black particles, for strain sensing applications, by applying an analytical model. The study showed that piezoresistivity may contribute to understand the network structure and the charge carrier transport mechanism [25].

In this sense the ultimate goal of the present work is to investigate the piezoresistive performance of composites based on CNFs for transducer applications. The composites have been processed by common-use industrial techniques, and thus bridge the gap from nanoscience to technology for a large-scale production of smart self-sensing materials with reliable and reproducible properties for real-use applications.

5.2 Experimental

5.2.1 Processing of materials

Carbon nanofibers PR19 LHT XT, Pyrograf III^{TM}, supplied by Applied Sciences, Inc. (Cedarville, OH) were used in this study. The polymer used was a powder polypropylene, Borealis EE002AE. Extrusion compounding was performed in a modular laboratorial mini co-rotating twin-screw extruder with an approximate L/D ratio of 26. The extrusion process was performed at a constant feed rate of 150 g/h of PP by means of a volumetric dosing unit (Moretto DVM 18 L), while CNFs were fed downstream in the extruder to obtain fiber loadings between 0.2 to 2.4 vol % (0.5 to 5 wt %). The screw speed was kept constant at 50 rpm and all heating zones in the extruder were set at 190 ºC. The extruded PP/CNF nanocomposite material was then pelletised and subsequently compression moulded (190 ºC, 5 MPa, 5 min) into rectangular samples of 49 mm x 10 mm and 1 mm of thickness. Morphology and CNF dispersion were investigated by Scanning Electron Microscopy, SEM, in a Phillips X230 FEG apparatus. Surface and cross section images were taken after coating the samples with a gold layer by magnetron sputtering. A more detailed description of the fabrication of fibers and their mechanical response is presented in a previous article [11].

5.2.2 Electro-mechanical characterization

In 4-point-bending experiments, the strain, calculated from the theory of pure bending of a plate to a cylindrical surface placed between the inner loading points, is given by:

$$\varepsilon = \frac{3dz}{5a^2}, \quad (5.1)$$

where d is the distance from the neutral plane to the plane of the sample, which in this case is the thickness of the sample (1 mm), z is the displacement of the composite at point $y = a$ (Figure 5.1), and a is the distance between the first and second points of the 4-point bending load cell (10 mm) [26].

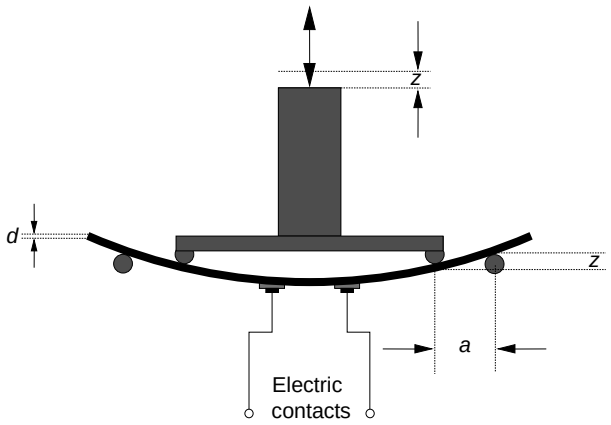

Figure 5. 1 - Diagram of the 4-point bending jig used in the present study. ($d = 1$ mm and $a = 10$ mm).

The piezoresistive gauge factor for the 4 point bending experiment, GF, is given by:

$$GF = \frac{\Delta R/R}{\varepsilon}, \quad (5.2)$$

where ε is the strain, given by equation (5.1), and $\Delta R/R$ is the fractional electrical resistance that changes with strain.

The GF was measured in three samples in a Shimadzu-AG-IS 500 N testing instrument, at different conditions: the first set of experiences were developed in order to determine the dependence of GF with deformation. They consist of 4 load cycles at deformation speed of 2 mm min^{-1} and maximum deformation ranging from 0.25 mm up to 2 mm in z direction. A second set of experiments, performed with the aim of testing the stability of the response, consisted in 40 load cycles at speed of 2 mm min^{-1} and displacement of 1 mm in z direction.

Finally, the dependence of GF with deformation speed was tested by applying the same z-displacement (1 mm) at different velocities (1, 2 and 3 mm min^{-1}).

In order to measure the resistance changes, two parallel rectangular gold electrodes, of 4 mm width and 1 mm of distance between them, were vacuum evaporated onto one side of the samples. Copper wires were attached to the electrodes with silver paste. The resistance change $(\Delta R/R)$ was calculated from the resistance vs. time curves of four upward cycles in the z direction. After this procedure, the mean value of GF was calculated for each sample for the three samples. The GF in the second set of experiments was directly calculated from the fourth, eighth, sixteenth, twenty fourth, thirty second and fortieth upward cycle in each of the three samples and the final mean value was calculated.

Although the calculations for GF are presented for the upward cycles, there are no differences in the results obtained from the downward cycles.

5.3 Results and discussion

Figure 5.2 shows two SEM cross sectional images of the films. A good dispersion is achieved as no large CNF agglomerates are observed in the composites (Figure 5.2a and Figure 5.2b).

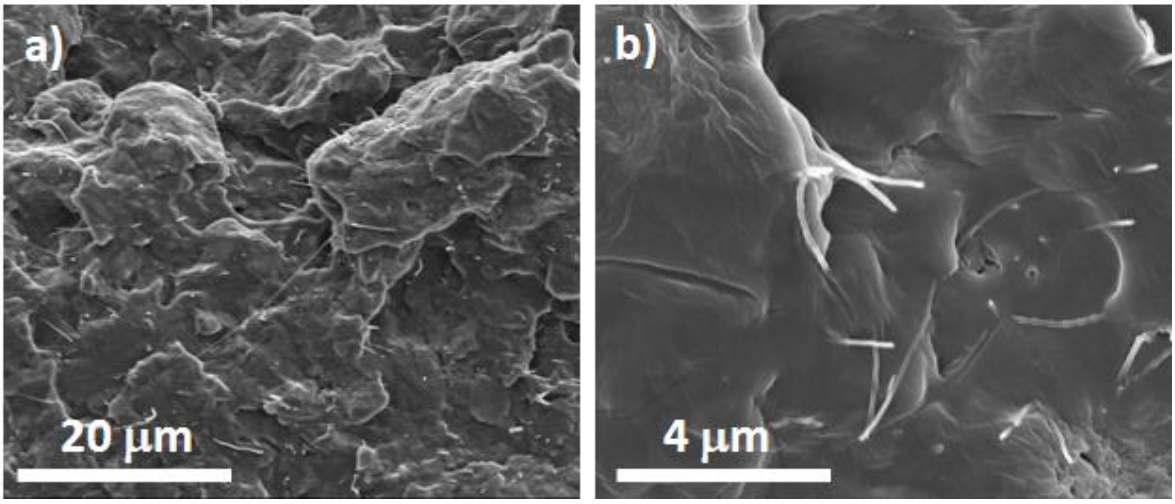

Figure 5. 2 - SEM pictures of the PP / CNF composites with 0.9 vol %.

The piezoresistive response was tested under bending experiments by simultaneous measuring of the mechanical solicitation and the electrical response.

As it was demonstrated in a previous study [11], the highest gauge factor ($GF = 2.4$) was found just below the percolation threshold (0.9 vol %. loading). Therefore, the present study is focused in this concentration.

A typical cyclic loading experiment and the corresponding electrical response for the composites are shown in Figure 5.3. For this sample, the initial electrical resistance value, before the application of external forces is 3500 Ω.

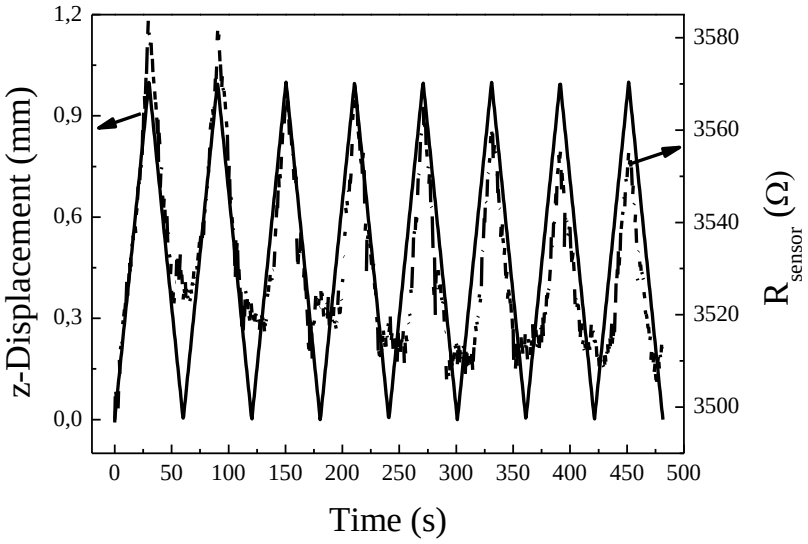

Figure 5. 3 - Resistance of the PP/CNF composites with 0.9 vol % as a function of time, during a four-point bending experiment, consisting of displacement cycles of 1 mm in z direction.

Figure 5.4 shows the relative resistance variation as a function of deformation for several cycles. From these plots, by applying equation (5.2), the gauge factor for each cycle was calculated. Due to the small delay in the sensor response in the loading cycles (Figure 5.3), the gauge factor was calculated in the linear region, once the resistance variation accompanied the variation of the mechanical response (Figure 5.4). It is interesting to notice that this delay does not occur in the unloading cycles.

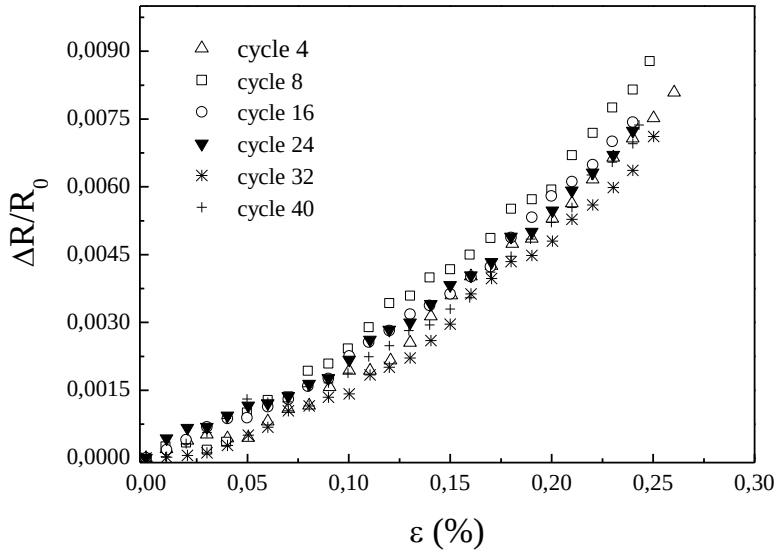

Figure 5. 4 - Relative resistance change, ΔR/R, as a function of applied strain, ε, by 4-point bending of PP/CNF nanocomposites.

It has been previously observed that when the CNF loading approaches the percolation threshold, a weak nonlinear piezoresistivity is observed [11, 27]. This is the case of the samples in the present study. The piezoresistivity can be regarded as approximately linear under small strains. So the GF was calculated from the points on the curves for which R^2 values larger than 0.96 were obtained in the linear regression.

5.3.1 Gauge factor dependence with deformation

Figure 5.5 shows the strain sensing performance of the composites. Here, GF was calculated when the films were subject to cyclic 4-point-bending tests with displacements in the range from 0.25 to 2 mm in z direction. The plot shows a positive linear relationship between deformation and GF. This linearity is limited by the loss of mechanical resistance in the composites and the peak is reached before 2 mm, with a maximum GF of 4.3.

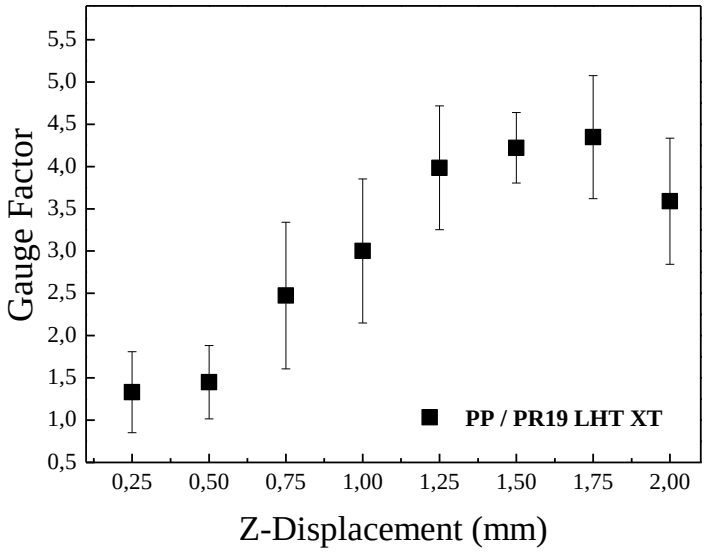

Figure 5. 5 - GF as a function of z-displacement in the four-point bending experiments consisting of 4 cycles.

As mentioned before, the experimental data revealed that the resistance exhibited a non-linear relationship with the applied strain. This implies that the piezoresistive stress coefficient is not a constant value, but depends on the applied stress level [28]. This phenomenon occurs in carbon-black-polymer systems, where the rate of the change in resistivity decreases significantly with increasing the applied stress [29-35]. However, with CNFs, the increasing GF with increasing deformation is inherent to the mechanism behind the electrical response of the composites. As previously observed [4, 5], close to the percolation threshold, increasing deformations result in stronger variations of the fiber network topology as well as in the effective local CNF concentration. This originates stronger variations in resistance and therefore in GF.

5.3.2 Gauge factor dependence on long-cycle-series

With the aim of testing the sensing stability and reliability for these materials for sensor applications, a second set of bending experiences were performed. In these experiments, the materials were subject to a series of 40 loading-unloading cycles, all of them with peak deformations of 1 mm in z direction and velocity of 2 mm min^{-1}. The calculated values of GF

as a function of the number of cycles (Figure 5.6) show a large dispersion, therefore no definite conclusion can be drawn. On the other hand, it can be generally stated that GF does not suffer strong variations and remains practically constant with the number of applied cycles.

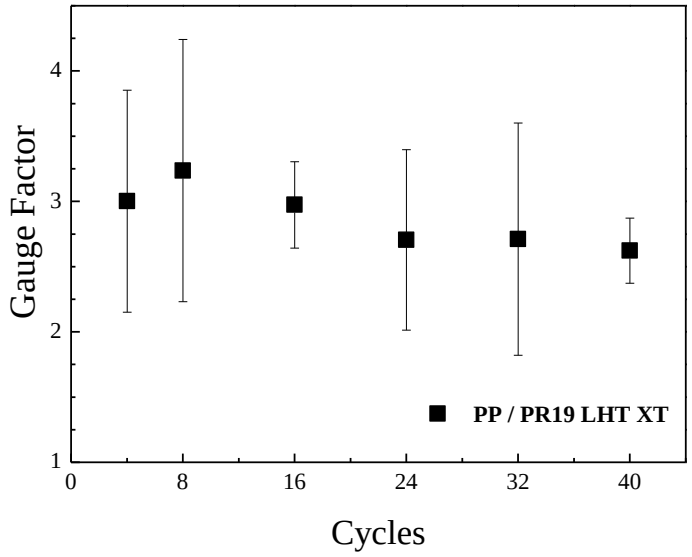

Figure 5. 6 - GF as a function of the number of loading-unloading cycles in the four-point bending experiments.

5.3.3 Gauge factor dependence with velocity

Finally the time response of the material was tested by applying the same deformation (1 mm in z direction) but at different velocities. It was observed that GF is independent of the deformation velocity for velocities from 1 mm min^{-1} to 3 mm min^{-1}.

5.3.4 Electrical equivalent model

In order to explain the observed results, an electrical model was developed to represent the behavior of the piezoresistive nanocomposite (Figure 5.7). R_1 models the fixed electrical resistance of the film, R_2 $d_i(t)$, models the linear change in electrical resistance with

displacement, that is, it is the linear approximation of the resistance changes with displacement, $d_i(t)$, for small displacements. Finally, C, models the energy storage capacity of the film structure, i.e. irreversible reconfigurations or slow varying reconfiguration with respect to the time-scale of the sensor response.

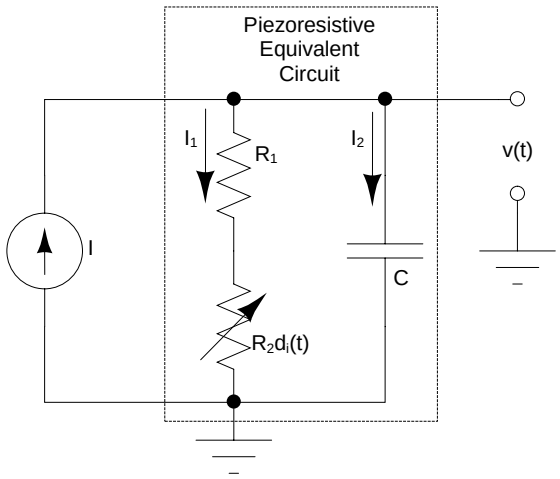

Figure 5. 7 - Electrical circuit model of the piezoresistive sensor. R1 and R2 represent the fixed and variable contributions to the resistance and C represents the capacitance.

The piezoresistive element can be tested by applying a constant current, I, changing the displacement, $d_i(t)$, and measuring the output voltage v(t).
The voltage v(t) can be calculated from:

$$I = I_1 + I_2 = \frac{v(t)}{R_1 + R_2 d_i(t)} + C\frac{dv(t)}{dt}, \tag{5.3}$$

which can be regrouped to:

$$\frac{dv(t)}{dt} = \frac{IR_1 + R_2 d_i(t) I - v(t)}{C\left(R_1 + R_2 d_i(t)\right)}. \tag{5.4}$$

In order to test the dynamical model, a single ramp displacement function $d_i(t)$ was used both in the simulations as well as for obtaining the experimental results. Figure 5.8 shows the measured resistance at the output of the sensor, when it is excited with a constant current of 100 μA and it is subjected to the displacement ramp. Overlapped to the experimental measurement, a simulated response of the circuit of Figure 5.7 is also plotted. In order to obtain the simulated curve, equation (5.4), which is an Initial Value Problem, IVP, was

solved numerically using Euler's method. Table 5.1 shows the parameters used in the model to obtain the best fit of the experimental data.

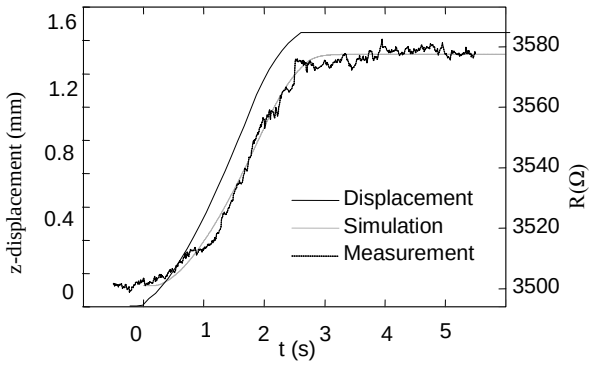

Figure 5. 8 - Simulated and measured responses of the piezoresistive sensor for a ramp displacement waveform.

Parameter	Value
R1	3500 Ω
R2	50 Ω/mm
C	200 µF

Table 5. 1 - Parameters of the electrical equivalent model of the piezoresistive sensor.

In a further step, the model applied to the dynamical experiments reported in Figure 5.3 The experimental and simulation results presented in Figure 5.9 support the suitability of the model.

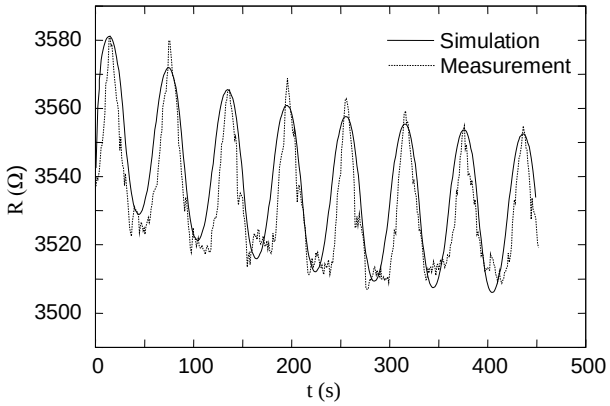

Figure 5. 9 - Application of the piezoresistive model of Figure 5.7 to the data reported in Figure 5.3.

In this way, it can be concluded that the piezoresistive sensor can then be modeled by two resistors (a fixed one and a variable one) and a capacitor. In this way, the fixed resistors represent the intrinsic contribution to the electrical characteristics of the nanocomposite due to the carbon nanofiber loading and the variable part is due reversible nanofiber network reconfiguration (variations of the nanofiber relative distance) due to the applied loading and consequent deformation of the sample. Finally, the energy storage capacity will represent irreversible or slow variations, compared to the sensor response, due to reconfigurations of the carbon nanofiber network [36, 37].

5. 4 Conclusions

This work demonstrates that piezoresistive Poly(propylene)/CNF composites can be fabricated by twin screw extrusion and compression molding, allowing the composites to be produced industrially. Strain sensitivity effects on electrical resistance in the composites were tested by four-point bending methods. The obtained gauge factor increases with increasing deformation from ~1.5 up to 4 for deformations from 0.25 to 1.5 mm. On the other hand, the gauge factor is independent of the strain velocity and is stable for up to 40 four-point bending cycles, at least. In this way, it was demonstrated that the composites can be used as self-sensing materials. Finally, it was shown that an electrical circuit consisting in two resistors, a fixed and a variable one, and one capacitor can be used to model the behavior of the piezoresistive transducer.

Acknowledgments

We acknowledge the Foundation for Science and Technology through the *3º Quadro Comunitario de Apoio*, the *POCTI* and *FEDER* programs and the *NANO/NMed-SD/0156/2007 project*. The support of *Applied Sciences Inc.* for generously supplying the CNFs used. We would also like to thank Carla Leer and Patrick Lake for their assistance in the production of the CNF composites. J. G. Rocha thanks the *FCT* for the Grant SFRH/BSAB/1014/2010. A. J. Paleo wants to thank to IP-SME Pegasus project through grant NMP2-CT-2006-026673.

References

1. C A Rogers, Intelligent Material Systems, The Dawn of a New Materials Age, J. Intell. Mater. Syst. Struct. 4(1) (1993) 4-12.

2. R E Newnham and G R Ruschau, Electromechanical Properties of Smart Materials, J. Intell. Mater. Syst. Struct. 4(3) (1993) 289-294.

3. Z Li, P Dharap, S Nagarajaiah, E V Barrera, J D Kim, Carbon nanotube film sensors, Adv. Mater. 16(7) (2004) 640-643.

4. M H Al-Saleh and U Sundararaj, A review of vapor grown carbon nanofibre/polymer conductive composites, Carbon 47(1) (2009) 2-22.

5. G G Tibbetts, M L Lake, K L Strong and B P Rice, A review of the fabrication and properties of vapor-grown carbon nanofibre/polymer composites, Compos. Sci. Technol. 67(7-8) (2007) 1709-1718.

6. T Prasse, J-Y Cavaillé and W Bauhofer, Electric anisotropy of carbon nanofibre/epoxy resin composites due to electric field induced alignment, Compos. Sci. Technol. 63(13) (2003)1835-1841.

7. E Hammel, X Tang, M Trampert, T Schmitt, K Mauthner, A Eder and P Pötschke ,Carbon nanofibres for composite applications, Carbon. 42(5-6) (2004) 1153-1158.

8. J M Park, D S Kim, J R Lee and T W Kim, Nondestructive damage sensitivity and reinforcing effect of carbon nanotube/epoxy composites using electro-micromechanical technique, Mater. Sci. Eng. C 23(6-8) (2003) 971-975.

9. G T Pham, Y B Park, Z Liang, C Zhang, B Wang, Processing and modeling of conductive thermoplastic/carbon nanotube films for strain sensing, Composites B 39 (2008) 209-216.

10. C Li, E T Thostenson and T W Chou, Sensors and actuators based on carbon nanotubes and their composites: A review, Compos. Sci. Technol. 68(6) (2008) 1227-1249.

11. A J Paleo, F W J van Hattum, J Pereira, J G Rocha, J Silva, V Sencadas, S Lanceros-Méndez, Piezoresistive effect in polypropylene - carbon nanofibre composites obtained by shear extrusion, Smart Mater. Struct. 19(6) (2010) 065013.

12. P E Wack, R L Anthony, and E Guth, Electrical Conductivity of GR-S and Natural Rubber Stocks Loaded with Shawinigan and R-40 Blacks, J. Appl. Phys. 18 (5) (1947) 456-469.

13. A Voet and F R Cook, Investigation of carbon chains in rubber vulcanizates by dynamic electrical conductivity, Rubber Chem. Technol. 41(5) (1968) 1207-1214.

14. A Voet, A K Sircar and T J Mullens, Electrical properties of stretched carbon black loaded vulcanizates, Rubber Chem Technol 42 (1969) 874-894.

15. P K Pramanik, D Khastagir, and T N Saha, Effect of extensional strain on the resistivity of electrically conductive nitrile-rubber composites filled with carbon filler, J. Mater. Sci. 28(13) (1993) 3539-3546.

16. J Kost, A Foux, and M Narkis, Quantitative model relating electrical resistance, strain, and time for carbon black loaded silicone rubber, Polym. Eng. Sci. 34 (21) (1994) 1628-1636.

17. L Flandin, J Y Cavaille, Y Brechet, and R Dendievel, Characterization of the damage in nanocomposite materials by a.c. electrical properties: experiment and simulation, J. Mater. Sci. 34 (8) (1999) 1753-1759.

18. M Knite, V Teteris, B Polyakov, and D Erts, Electric and Elastic Properties of Conductive Polymeric Nanocomposites on Macro- and Nanoscales,Mater. Sci. Eng., C 19 (1-2) (2002) 15-19.

19. V G Shevchenko, A T Ponomarenko, and C Klason, Strain sensitive polymer composite material, Smart Mater. Struct. 4 (1) (1995) 31-35.

20. A Celzard, E McRae, J F Mareche, G Furdin and B Sundqvist, Conduction mechanisms in some graphite–polymer composites: Effects of temperature and hydrostatic pressure, J. Appl. Phys. 83 (1998) 1410-1419.

21. X W Zhang, Y Pan, Q Zheng, and X S Yi, Time dependence of piezoresistance for the conductor-filled polymer composites, J. Polym. Sci., Part B: Polym. Phys. 38 (21) (2000) 2739-2749.

22. J M Park, D S Kim, J R Lee and T W Kim, Nondestructive damage sensitivity and reinforcing effect of carbon nanotube/epoxy composites using electro-micromechanical technique, Mater. Sci. Eng. C 23 (2003) 971–975.

23. G T Pham, Y B Park, Z Liang, C Zhang and B Wang, Processing and modeling of conductive thermoplastic/carbon nanotube films for strain sensing, Composites B 39 (2008) 209-216.

24. C Li, E T Thostenson and T W Chou, Sensors and actuators based on carbon nanotubes and their composites: a review, Compos. Sci. Technol 68 (2008) 1227-1249.

25. M H G Wichmann, S T Buschhorn, J Gehrmann and K Schulte, Piezoresistive response of epoxy composites with carbon nanoparticles under tensile load, Physical Review B 80 (2009) 245437.

26. S P Timoshenko, History of Strength of Materials, ed. R. E. Krieger Publ. Comp (1958) 93-218.

27. C Grimaldi, T Maeder, P Ryser and S Strässler, Piezoresistivity and conductance anisotropy of tunneling-percolating systems, Phys. Rev. B: Condens. Matter 67(1) (2003) 014205.

28. Y Wang, L Zhang, Y Fan, D Jiang, L An, Stress-dependent piezoresistivity of tunneling-percolation systems, J Mater Sci 44 (11) (2009) 2814-2819.

29. B Lundberg and B Sundqvist, Resistivity of a composite conducting polymer as a function of temperature, pressure, and environment: Applications as a pressure and gas concentration transducer, J Appl Phys 60 (1986) 1074-1079.

30. Carmona F, Canet R, Delhaes P, Piezoresistivity of heterogeneous solids, J Appl Phys 61(7) (1987) 2550-2557.

31. A Celzard, E McRae, J F Marêché, G Furdin and B. Sundqvist, Conduction mechanisms in some graphite–polymer composites: Effects of temperature and hydrostatic pressure, J Appl Phys 83 (1998) 1410-1419.

32. M Hussain, Y-H Choa, K Niihara, Fabrication process and electrical behavior of novel pressure-sensitive composites, Composites Part. A: Applied Science and Manufacturing, 32(12) (2001) 1689-1696.

33. Wang L, Ding T, Wang P, Effects of conductive phase content on critical pressure of carbon black filled silicone rubber composite, Sens Actuators A 135 (2007) 587-592.

34. D T Beruto, M Capurro, G Marro, Piezoresistive behaviour of silicone- graphite composites in the proximity of the electric per- colation threshold, Sens. Actuators A 117 (2005) 301-308.

35. M B Heaney, Resistance-expansion-temperature behavior of a disordered conductor–insulator composite, Appl Phys Lett 69 (1996) 2602-2604.

36. P Cardoso, J Silva, A J Paleo, F W Hattum, R Simoes and S Lanceros-Méndez, The dominant role of tunneling in the conductivity of carbon nanofibre-epoxy composites, Phys. Status Solidi A 207(2) (2010) 407-410.

37. R Simoes, J Silva, R Vaia, V Sencadas, P Costa, J Gomes and S Lanceros-Méndez, Low percolation transitions in carbon nanotube networks dispersed in a polymer matrix: dielectric properties, simulations and experiments, Nanotechnology. 20 (3) (2009) 035703.

General Conclusions

Four different Pyrograf®-III VGCNFs were systematically incorporated in the same polypropylene matrix and with the same processing conditions by twin-screw extrusion under relatively high shear mixing regime.

The nanocomposites fabricated with highly graphitic outer wall layers (PR 19 LHT XT and PR 24 LHT XT carbon nanofibers) revealed to have good electrical response with a significant increase in volume conductivity for 0.5 % vol, with CNFs which have the shortest diameter (PR 24 LHT XT). Nanocomposites fabricated with disordered pyrolitically stripped layer type of CNFs (PR 25 PS XT), in contrast, revealed to have good mechanical performance with an increase of 32 % in Young´s modulus for 2.4 % vol and enhanced thermal stability, which may be the result from the better adhesion between PP and this particular nanofiber´s type whereas at the same time revealed no relevant increase of the electrical conductivity for all filler loadings. The heat treatment at temperatures of 1500 ºC of PR 24 and PR 19 fibres (LHT grade) with a more ordered structure on the fiber´s surface and better intrinsic conductivity, together with the higher bulk density which allows better distribution and dispersion in the PP, unlike PR 25 fibers, demonstrate superior electrical conducting results for this particular polymer and processing method.

Thermogravimetric analysis showed shift to higher temperatures of the main thermal degradation of the polymer with the addition of CNFs. Differential scanning calorimetry indicated a strong enhancement of the degree of crystallinity with the inclusion of the filler, being practically independent on the filler content and type, which could be correlated with the global enhancement of Young´s modulus in all composites.

A quantitative method based on transmitted light optical microscopy by means of greyscale analysis, GSA, was used to determine the dispersion of PP / CNFs composites. The results indicated a good correlation between variance, a parameter which measures quantitatively the dispersion: the lower the variance, the better the cluster´s dispersion, and filler concentration. Furthermore, the analysis by GSA suggests that a dispersion limit, (related to the dispersions´ capacity in processing by twin-screw extrusion, TSE), was attained at 1.4 vol %. Above this limit a majority of fiber clustering, possibly correlated with only slight changes in Young´s modulus, was observed. Besides, the analysis by GSA demonstrates to be a possible method to correlate with conductivity, if cluster distribution seems to be more important than nanofibers´ dispersion for obtaining low percolation thresholds and high conductivity values, then this method which quantifies clusters dispersion at resolutions of approximately 1 µm

(1000 nm) may be helpful to correlate with conductivity, when the appropriate structured CNF for the electrical property is used.

A large difference in the rheological behavior between electrically non-conducting and conducting composites as function of volume fraction has been measured. Whereas the electrical conducting composites based on PR 24 LHT XT carbon nanofibers show liquid-like to solid-like transition which leads to the plateaus for G´, G´´ at low frequencies, the electrical isolating composites based on PR 25 PS XT carbon nanofibers remain practically unaltered in their rheological behavior when compared to the pure PP composites. This fact suggests that rheological analysis clearly differentiates electrical conducting from insulating performance for this particular type of systems. After comparing electrical conductivity and rheological analysis, it is concluded that G´ / G´´ (inverse of loss tangent) and in less extent G´ are the most appropriate rheological parameters for comparing with electrical behavior. The rheological threshold fitted from G´/ G´´ was found to be ~ 0.5 % vol, slightly higher than electrical percolation threshold ~ 0.4 % vol.

Finally, the piezoresistive response of the CNFs / PP composites was investigated. The piezoresistive response was analysed by the Gauge Factor, GF, and it is proved to be strongly dependent on carbon nanofibers´ concentration, with maximum values of GF between 2 and 2.5 within the percolation threshold. Furthermore, the dependence of Gauge factor as a function of the deformation and velocity of deformation was calculated. The obtained gauge factor increases with increasing deformation from ~1.5 up to 4 for deformations from 0.25 to 1.5 mm. On the other hand, the gauge factor is independent of the strain velocity and is stable for up to 40 four-point bending cycles, at least. In this way, it was demonstrated that the electrical conducting composites fabricated by twin screw extrusion and compression molding, allowing the composites to be produced industrially, analysed in this study can also be used as self-sensing materials.